Technische Universität München

Fakultät für Medizin

The influence of TCR avidity on the fate decisions of single T cells

Justin Christopher Leube

Vollständiger Abdruck der von der Fakultät für Medizin der Technischen Universität München zur Erlangung des akademischen Grades eines

Doktors der Naturwissenschaften (Dr. rer. nat.)

genehmigten Dissertation.

Vorsitzender: Prof. Dr. Marc Schmidt-Supprian

Prüfer der Dissertation:

1. TUM Junior Fellow Dr. Veit Buchholz
2. Prof. Dr. Vigo Heissmeyer

Die Dissertation wurde am 16.05.2022 bei der Fakultät für Medizin der Technischen Universität München eingereicht und durch die Fakultät für Medizin am 08.11.2022 angenommen.

Parts of the data used in this thesis have been generated and submitted as a Master's Thesis (Leube, 2017). This is indicated in the corresponding figure legends.

Table of Contents

Index of Figures

Abbreviations

ACT	Ammonium chloride-Tris
APC	Antigen presenting cell
APL	Altered peptide ligand
BSA	Bovine serum albumin
CFU	Colony forming units
DC	Dendritic cell
DMEM	Dulbecco's Modified Eagle Medium
DMSO	Dimethyl sulfoxide
EDTA	Ethylenediaminetetraacetic acid
FACS	Fluorescence activated cell sorting
FCS	Fetal calf serum
Gy	Gray
HCl	Hydrochloride
HSC	Hematopoietic stem cell
i.p.	Intraperitoneal
i.v.	Intravenous
IFN-γ	Interferon-γ
IL	Interleukin
KDE	Kernel density estimate
LCMV	lymphocytic choriomeningitis virus
L.m.	*Listeria monocytogenes*
MHC	Major histocompatibility complex
mIL-3	Murine IL-3
mIL-6	Murine IL-6
mSCF	Murine SCF
PBS	Phosphate buffered saline
PFA	Paraformaldehyde
PI	Propidium iodide
pMHC	Peptide MHC
RT	Room temperature
scRNA-seq	Single cell RNA sequencing
SD	Standard deviation
SEM	Standard error of the mean
SPF	Specific pathogen-free
TCR	T cell receptor

1 Introduction

1.1 T cell mediated immune responses

T cells are a critical component of the adaptive immune system. As such, they fulfill a broad range of functions. $CD8^+$ T cells, also known as killer T cells, provide direct protection against a diverse set of viruses and intracellular bacteria by eliminating infected cells. Although $CD4^+$ T cells can also fulfill direct effector functions, they most commonly act as regulators of innate and adaptive immunity and are therefore referred to as helper T cells.

T cells recognize pathogens by binding of their T cell receptor (TCR) to short, foreign, peptides presented on major histocompatibility complex (MHC) molecules. To recognize a highly diverse set of threats ranging from viruses, bacteria, and fungi to malignant cells, an equally diverse set of receptors is necessary. The TCR, comprised of an alpha and a beta chain, is generated by genetic recombination of DNA segments during T cell development. By this process, referred to as V(D)J recombination, it is estimated that up to 10^{20} unique TCR sequences can be generated (Laydon et al., 2015). The random nature of these recombination events would inevitably lead to the recognition of self-antigens and autoimmunity. Therefore, T cell precursors (thymocytes) are subjected to thymic selection to ensure that their TCR affinity for self-peptide MHC ligands lies within an optimal range to mediate functionality while ensuring immunological tolerance.

To show the general capacity of TCR binding to peptide MHC (pMHC) complexes, the affinity of the TCR toward self-peptide MHC complexes must exceed a particular minimal threshold (positive selection) (Klein et al., 2014). In contrast, thymocytes that bind too strongly to self-peptide MHC complexes undergo apoptosis to prevent the development of autoimmunity (negative selection) (Klein et al., 2014).

In the late stages of positive selection thymocytes undergo lineage commitment to become $CD8^+$ or $CD4^+$ T cells. After downregulation of the CD8 coreceptor in $CD4^+$ $CD8^+$ thymocytes, those cells that continuously receive stimulatory signals through their TCR retain CD4 coreceptor expression due to the recognition of self-peptide MHCII molecules. Thymocytes receiving insufficient signals at this stage again upregulate CD8 while silencing CD4 expression (Taniuchi, 2018).

After thymic selection mature, naive T cells are released from the thymus to the periphery. In mice it has been estimated that a pool of approximately 80-1200 $CD8^+$ T cells and 20-400 $CD4^+$ T cells recognizes a given foreign pMHC (Jenkins & Moon, 2012; Moon et al., 2007; Obar et al., 2008). Importantly, the T cells belonging to such an epitope-specific T cell

population vary considerably in their binding strength toward their cognate antigen (Nikolich-Žugich et al., 2004).

Naive T cells circulate between the blood and secondary lymphoid organs (Lewis et al., 2008). They probe the pMHC complexes on professional antigen-presenting cells (APCs) within the secondary lymphoid organs. Generally, antigens of intracellular origin are presented on MHCI, while extracellularly derived antigens are presented on MHCII to $CD8^+$ and $CD4^+$ T cells, respectively. Importantly, certain APCs can additionally present antigens taken up by phagocytosis on MHCI molecules (cross-presentation) (Embgenbroich & Burgdorf, 2018). This process is important for the priming of $CD8^+$ T cells in tumor immunity, certain viral infections, and vaccinations (Embgenbroich & Burgdorf, 2018).

While the recognition of the cognate pMHC complex with the TCR and CD4 or CD8 coreceptor (signal 1) activates T cells, two additional signals are necessary for full activation. The binding of costimulatory receptors upregulated on activated APCs constitutes signal 2, while cytokines secreted by the APCs or bystander cells constitute signal 3. Upon full activation T cells are recruited into the immune response, meaning that they begin to vigorously proliferate and differentiate into effector and memory subsets. After pathogen clearance, the majority of the expanded T cell population contracts leaving behind a pool of long-lived memory T cells (Badovinac et al., 2002; Sprent & Surh, 2003). How the signals of T cell activation influence T cell differentiation and response characteristics will be described in the following chapters.

1.2 The TCR is a critical determinant of T cell behavior

The binding characteristics of a TCR to its cognate pMHC have been shown to influence the expansion, differentiation, and function of T cells (Bhattacharyya & Feng, 2020; Busch & Pamer, 1999; Savage et al., 1999; Snook et al., 2018; Tubo & Jenkins, 2014; van Panhuys, 2016; Zehn et al., 2009). The binding characteristics can be defined and measured in multiple ways. While the interaction affinity describes the monomolecular interaction strength of a TCR and pMHC, the aggregate binding strength of multiple TCR and pMHC molecules is described as TCR avidity (Campillo-Davo et al., 2020). Coreceptors such as CD8 further increase the binding avidity (Wooldridge et al., 2005). Additionally, TCR pMHC interaction strength has been characterized as functional avidity, which is defined as the peptide concentration that stimulates a half-maximal biological outcome (Cytokine production, activation marker upregulation). It thus defines the sensitivity of a given TCR for its pMHC antigen while taking affinity, avidity, and the contribution of other receptors into account (Viganò et al., 2012). As TCR pMHC interaction between T cells and APCs typically involve coreceptors, the binging strength of this interaction will generally be referred to as TCR avidity throughout this thesis.

Furthermore, a distinction between signal quality and quantity can be made. While TCR signal quality describes the structurally hardwired characteristics of a TCR, such as affinity and avidity, signal quantity is dependent on the antigen dose, i.e. pMHC density on an APC (Tubo & Jenkins, 2014).

How these factors translate into T cell activation has been studied by both the modulation of signal quality and quantity and several models have been proposed to explain this process. Generally, two main models have been proposed, namely the receptor occupancy and the kinetic proofreading model (several versions of this model exist) (Lever et al., 2014). In brief, the receptor occupancy model proposes that T cell activation is proportional to the number of TCRs bound to pMHC, which immediately enter a signaling competent state (Lever et al., 2014). This model predicts that low-affinity ligands can achieve identical T cell activation if they are present in a high enough concentration and thus that the maximum response is independent of TCR-pMHC binding parameters, which contradicts experimental findings (Dushek et al., 2011). In contrast, the kinetic proofreading model suggests that the TCR pMHC interaction must be of a certain minimal duration to reach a state capable of signal transduction (Lever et al., 2014). This model allows T cells to discriminate between low- and high-affinity ligands based on the dissociation time of the receptor-ligand interaction (Lever et al., 2014).

Mechanistically it is interesting how structurally hardwired differences in binding strength translate to graded levels of T cell activation and ultimately an influence on T cell fate. In general, signaling events can lead to digital or analog outcomes. Digital processes lead to an all-or-nothing response. Inputs into such pathways change the population frequency distribution between the on and the off state. In a digital process, there is no population in an intermediate state. Thus, differences in activation strength cannot be passed on in a graded manner. In contrast, analog processes shift the entire population in proportion to the input signal (Conley et al., 2016), leading to a heterogeneous cell population with differing activation states.

Signals from the TCR are transmitted by the MAPK, NFκB and the calcium signaling pathways (Brownlie & Zamoyska, 2013). While the initial signaling events of the MAPK pathway are graded, a positive feedback loop is rapidly activated, leading to digital activation (Das et al., 2009). As downstream targets of the MAPK pathway are critical cell cycle regulators such as Ras, digital activation allows for robust proliferation of cells that have crossed a minimal activation threshold (Conley et al., 2016). Similarly, the NFκB pathway is also activated in a digital manner (Kingeter et al., 2010).

In contrast, the calcium signaling pathway has been shown to be strongly influenced by TCR pMHC affinity (J.-L. Chen et al., 2010; Christo et al., 2015; Rosette et al., 2001) and leads to

graded regulation of transcription factors such as IRF4 and Nur77 (Conley et al., 2020; Woronicz et al., 1994).

In summary, TCR signaling regulates T cell activation in both a digital and analog manner. The MAPK and NFκB pathways show digital features, which can be seen downstream in the digital expression of CD69, for example (Das et al., 2009). In contrast, the calcium signaling pathway translates stimulation strength into analog responses, such as the regulation of the transcription factors IRF4 or Nur77 (Conley et al., 2016, 2020; Woronicz et al., 1994). Together, a graded influence of TCR binding strength on T cell fate is achieved by a change in balance of transcription factors and further transcriptional feedback loops (Bhattacharyya & Feng, 2020; Conley et al., 2016).

1.3 Regulation of T cell clonal selection by TCR avidity

The magnitude and diversification of the $CD8^+$ T cell response is dependent on many factors such as the precursor frequency (Moon et al., 2007; Obar et al., 2008), nature and dose of the antigen (Wherry et al., 1999), signals by APCs (Marchingo et al., 2014), competition between T cells (Kedl et al., 2003; Oberle et al., 2016) and the binding characteristics of the TCR (Busch & Pamer, 1999; Savage et al., 1999; Zehn et al., 2009). Antigen-specific T cells are selected to expand from the naive repertoire in a process known as clonal selection. As mentioned before, T cells need three signals for full activation and participation in the immune response. Importantly however, the signal received by TCR stimulation is the most crucial as without it signals 2 and 3 do not lead to T cell activation. T cells are thereby recruited into the immune response by exit from their naive state and initiation of proliferation after sufficient stimulation.

Surprisingly, very little is known about the regulation of T cell recruitment by TCR avidity. In an elegant study by Van Heijst et al., T cell recruitment in systemic infection was studied using genetic barcoding. The study showed that recruitment of transferred high-avidity T cells was very efficient and largely independent of infection dose or vector. It did not, however, investigate the recruitment efficiency of T cells with low avidity to the priming antigen (van Heijst et al., 2009). It has been shown that the initiation of T cell proliferation is controlled by a sharp (digital) signaling threshold (Au-Yeung et al., 2014). Given the digital nature of this process, the TCR avidity of a T cell should influence its probability of crossing this activation threshold upon stimulation, thus leading to a recruitment probability dependent on TCR binding characteristics. In this regard, it has been shown that $CD4^+$ T cells below a certain avidity threshold are not clonally selected, in other words recruited (Malherbe et al., 2004).

It is unknown what the fate of unrecruited T cells is. In theory two fates could be adopted. First, sub-threshold stimulation could lead to induction of anergy, where T cells enter a non-functional state as a mechanism of peripheral tolerance (Chappert & Schwartz, 2010;

Schwartz, 2003). It has been shown for $CD4^+$ T cells that anergy can be induced by low-affinity ligands as well as low ligand doses (Korb et al., 1999; Mirshahidi et al., 2004). In the other case unrecruited T cells would not be affected by sub-threshold stimulation, which has been described as clonal ignorance in the context of autoimmune and tumor diseases (Ochsenbein, 2005; Salaman & Gould, 2020). As these cells would essentially remain in a naive state, the question arises whether initially unrecruited low-avidity T cells could contribute during a second infection with the same pathogen or in an antigenic drift situation, where the cognate antigen has acquired increased affinity to the respective TCR.

1.4 $CD4^+$ T cell diversification

Owing to their regulatory role of adaptive and innate immunity, $CD4^+$ T cells diversify into many functional lineages with equally diverse functions. How differentiation into the helper cell lineages is regulated is described by two models. The qualitative model proposes that differentiation is regulated by the cytokine environment present during T cell activation, the quantitative model attributes a more important role to the strength of TCR stimulation (Bhattacharyya & Feng, 2020). Most likely, the integration of both signals together acts to instruct the $CD4^+$ T cell response. In the following, I will give a brief overview of different $CD4^+$ T cell subsets followed by a more detailed introduction to $CD4^+$ T cell differentiation in the viral models studied in this thesis.

While Type 1 helper T cells (Th1 cells) fulfill an important role in the response to intracellular bacteria, viruses and antitumor responses, aberrant responses are often seen in inflammatory autoimmune responses. The function of Th1 cells is to activate macrophages, aid $CD8^+$ T cell responses and induce a general antiviral state (Saravia et al., 2019; Zhu & Zhu, 2020). Th1 differentiation is induced by strong TCR and costimulatory signals and IL-12 and IFN-γ (Ruterbusch et al., 2020). The lineage-defining transcription factor is Tbet (Szabo et al., 2000). Th1 cells secrete TNF-α and IFN-γ as signature cytokines (Mosmann et al., 1986)

Type 2 helper T cells (Th2 cells) are induced upon parasitic infections and play a role in allergy and asthma. The signature cytokines secreted by Th2 cells are IL-3, IL-5 and IL-13 which lead to IgE class switching of B cells and the recruitment of Eosinophils (Mosmann et al., 1986; Ruterbusch et al., 2020). Th2 differentiation is induced rather by low TCR avidity or antigen dose in contrast to Th1 differentiation. IL-4 and IL-5 induce Th2 differentiation and its master transcription factor Gata3. (Ouyang et al., 2000).

The helper cell subset implicated in the defense against fungi and extracellular bacteria as well as autoimmune disorders is Th17 cells (Harrington et al., 2005; Park et al., 2005). Th17 cells produce the pro-inflammatory cytokines IL-17A, IL-17F and IL-22 and express the lineage-defining transcription factor retinoic acid-related orphan receptor-γt (Rorγt) (Ivanov et al., 2006;

Saravia et al., 2019). Differentiation is induced by TGFβ, IL-6 and IL-23 together with relatively strong TCR signals (Saravia et al., 2019).

Importantly, regulatory T cells keep the balance between immunity and tolerance by counteracting excessive inflammation. These cells are characterized by the expression of Foxp3 and can be induced during thymic selection as well as in the periphery (Fu et al., 2004; Hori et al., 2003; Sakaguchi et al., 1995; Williams & Rudensky, 2007). Induction of a regulatory phenotype in the periphery is mediated by retinoic acid, IL-10 and TGFβ as well as weak TCR stimulation. The immunosuppressive effect of these cells is mediated by cell surface receptors (CD25, CTLA4, and TIGIT) as well as anti-inflammatory cytokines such as IL-10 and TGFβ. (Bhattacharyya & Feng, 2020; Bilate & Lafaille, 2012; Schmitt & Williams, 2013; Vignali et al., 2008).

Arguably one of the most important discovered functions of $CD4^+$ T cells is their role in the induction of humoral immunity. Follicular helper T cells (Tfh) are essential for the formation of germinal centers and B cell affinity maturation (Breitfeld et al., 2000; C. H. Kim et al., 2001; Schaerli et al., 2000). Tfh cells home to B cell follicles where they direct humoral immunity by secretion of IL-4 and IL-21 as well as providing stimulatory signals through surface receptors such as CD40L and ICOS (Crotty, 2019). Tfh differentiation is a multistep process that requires DC as well as B cell interactions. Mature Tfh cells are characterized by the expression of Bcl6 as well as CXCR5 and high levels of PD1 (Y. S. Choi et al., 2013; Johnston et al., 2009; Schaerli et al., 2000; Vinuesa et al., 2016).

1.5 TCR avidity and differentiation of $CD4^+$ T cells in viral infection

$CD4^+$ T cell differentiation into Th1, Th2, Th17 subsets is described as a continuous process that is reinforced by positive feedback loops (Saravia et al., 2019). While also the differentiation into fully mature Tfh cells is a multistep process relying on signals provided by DCs as well as B cells for full commitment (Crotty, 2019; Vinuesa et al., 2016), it has been shown that the decision between Tfh and Th1 fate is taken very early within the first two cell divisions after T cell activation (Y. S. Choi et al., 2013; Ditoro et al., 2018). Such early fate bifurcation implies a strong significance of the early priming conditions such as TCR signal strength (Ditoro et al., 2018; Fazilleau et al., 2009; Tubo et al., 2013). Indeed, studies have shown *in vitro* that TCR signaling mainly modulates T cell responses during the first two days of stimulation (Jelley-Gibbs et al., 2000). The early fate decision between the Tfh and other T helper subsets is mainly attributed to the balance of the transcription factors BCL6 and BLIMP1. These act upon each other as reciprocal antagonists (J. Choi & Crotty, 2021; Johnston et al., 2009).

The balance between BCL6 and BLIMP1 can be regulated by cytokine signaling. IL-6 and TGFβ induce BCL6 expression through STAT3 signaling. In contrast IL-2 signaling through CD25 induces BLIMP1 expression by STAT5 signaling (Sheikh & Groom, 2020). Recently, DiToro and colleagues showed that T cells receiving stronger TCR signals produced IL-2 and were biased toward a Tfh fate, while those receiving weaker TCR signals upregulated CD25 and became non-Tfh effectors (Ditoro et al., 2018). This implies a feedback mechanism which aids in the enforcement of divergent cellular fates between these two subsets.

Importantly, the strength of TCR signaling also influences the T helper cell fate decisions. It is well described that high antigen doses (Constant et al., 1995; Hosken et al., 1995) and high-affinity TCR ligation favor the differentiation of Th1 over Th2 cells (Blander et al., 2000; Brogdon et al., 2002; Jorritsma et al., 2003; Kumar et al., 1995; Tao et al., 1997). With regard to the Th1 vs. Tfh fate decision, the influence of TCR avidity is still debated. While one study showed biased differentiation of high-avidity T cells into Th1 cells (Kotov et al., 2019) another showed biased differentiation into Tfh cells (Fazilleau et al., 2009). A third study could show a differential effect of antigen affinity and antigen dose on this fate decision. In this study, Th1 generation was dependent on high-affinity ligands but independent of antigen dose, whereas Tfh generation was independent of ligand affinity but was increased with antigen dose (Keck et al., 2014). By generating APL versions of the lymphocytic choriomeningitis virus (LCMV) Armstrong and LCMV Clone 13 (LCMV CL13) strains, Künzli et. al could show different effects of T cell signal strength in acute and chronic infection. While increasing signal strength correlated positively with Th1 differentiation in acute infection, it correlated with Tfh differentiation in chronic infection (Künzli et al., 2021). It has been described that chronic LCMV infection favors the generation of Tfh cells (Fahey et al., 2011; Vella et al., 2017), while Th1 cells become exhausted (Crawford et al., 2014; Parish et al., 2014). This mechanism is conserved in other chronic viral infections such as HIV (Lindqvist et al., 2012; Oxenius et al., 2001) and HCV (Raziorrouh et al., 2016; Schulze zur Wiesch et al., 2012) infections.

Taken together the influence of TCR signal strength on Tfh vs Th1 differentiation seems to be dependent on the experimental system studied. This warrants, further investigation especially to discern the influence of TCR avidity and antigen persistence.

1.6 Single-cell fate mapping

Typically, T cell immune responses are studied by transfer of monoclonal transgenic T cell populations or by the analysis of the polyclonal endogenous responses identified by pMHC tetramer or activation marker staining. Both approaches study T cell responses on a population level, meaning that the observed response is composed of multiple T cell clones with unique characteristics. While these experiments have been pivotal for our understanding of T cell

immune responses, they do not allow the assessment of the underlying response heterogeneity. Specifically, the clonal composition of these responses remains unresolved. During clonal selection, individual antigen-specific T cells are recruited and vigorously expand during the response. By single-cell fate mapping, the unambiguous relationship between the characteristics of the original single T cell and its daughter cells is maintained. The progeny of a single T cell is also referred to as a T cell family to avoid confusion with the term clonal, which can also describe a response that originates from multiple T cells harboring the same TCR (Buchholz et al., 2016; Buchholz & Flossdorf, 2018).

Single-cell fate mapping has revealed many insights into T cell responses. Pioneering studies have shown that a single T cell can give rise to phenotypically distinct progeny (Stemberger et al., 2007), as well as that the contribution of a T cell family to the ongoing immune response is drastically variable (Buchholz et al., 2013; Cho et al., 2017; Tubo et al., 2013). Furthermore, the efficiency of antigen-specific T cell recruitment was studied for the first time (van Heijst et al., 2009). This study showed that recruitment of high-avidity T cells was highly efficient and largely independent of antigen dose or vector. Lastly, single-cell fate mapping has also been used to show that central memory T cells possess stem-like properties (Graef et al., 2014).

Regarding memory development, these studies have shed light on the developmental hierarchy of this process. Our group could show that memory precursor T cells most likely arise early during the immune response and subsequently give rise to effector cell subsets, while the differential expansion of these subsets can be explained by differences in cell cycle speed (Buchholz et al., 2013; Kretschmer et al., 2020). Additionally, the early differentiation of memory cells programs clonal dominance upon murine cytomegalovirus infection (Grassmann et al., 2020).

Importantly single-cell fate mapping has also been used to assess a deterministic influence of the TCR on $CD4^+$ T cell fate. By limiting dilution transfer, Tubo et. al. compared single-cell (endogenous and transgenic) to population-derived T cell responses. The authors found substantial variability in the phenotypic response patterns generated by single T cells derived from the endogenous TCR repertoire. (Tubo et al., 2013). As single T cells from the endogenous repertoire should possess unique TCRs, these findings are often interpreted as a strong deterministic influence of the TCR on single T cell fate. However, it remained unclear to what extent the response variability of single T cells could indeed be explained by differences in TCR signal strength.

In disagreement to the hypothesis that the TCR has a strong deterministic influence on $CD4^+$ T cell fate, single-cell derived response of monoclonal T cells showed a similarly high degree of phenotypic variability (Cho et al., 2017). While population-derived responses toward high- or low-affinity APLs showed robust avidity-dependent differences in the resulting response

patterns, single-cell derived responses to high affinity stimulus showed both phenotypic response patterns (Cho et al., 2017). Together these data showed a probabilistic- rather than a deterministic influence of TCR signal strength on $CD4^+$ T cell differentiation, as a large part of response variability could not be explained by differences in TCR signal strength (Cho et al., 2017).

In summary, the influence of TCR avidity on T cell recruitment remains unclear. Furthermore, the influence of TCR avidity on single $CD4^+$ T cell fate has not been studied using unique characterized TCRs specific for the same epitope and thus, also the influence of TCR avidity on single cell fate remains incompletely understood in this regard.

1.7 Cellular barcoding to facilitate single-cell fate mapping

To establish an unambiguous relationship between a single cell and its offspring, a unique heritable marker is needed. In general, markers (also called barcodes) used for fate mapping can be grouped into two categories. DNA based markers are not expressed and must be analyzed by sequencing while protein markers are expressed and can be analyzed for example by flow cytometry. Both approaches come with certain advantages and disadvantages. While DNA barcodes allow for extreme barcode diversity and the simultaneous analysis of many cellular families, the barcode readout requires disruption of the analyzed cells. In contrast, protein markers allow the identification of cell families in living cells, enabling their use in functional assays and retransfer experiments at the expense of barcode diversity and the number of cellular families that can be analyzed within the same recipient. (Buchholz et al., 2016; Buchholz & Flossdorf, 2018)

1.7.1 DNA-based barcoding

In 2008, Schepers et al. pioneered a barcoding approach in which they transduced T cells with a retroviral library encoding GFP and a semi-random 98-bp DNA barcode (Schepers et al., 2008). After expansion of these individual clones, their lineage relationships could be analyzed by microarray (Schepers et al., 2008) or next-generation sequencing(Gerlach et al., 2013). This approach was also used to study T cell recruitment by Van Heijst et al (van Heijst et al., 2009).

A different DNA based barcode approach has been used to study hematopoietic stem cell fate *in vivo*. This approach, called Polylox barcoding, relies on Cre-mediated recombination of several loxP-flanked segments, generating a theoretical barcode diversity of over 1 million unique recombination products (Pei et al., 2017). The Polylox barcode was introduced into the

Rosa26 locus, while CreERT2 was expressed from a ubiquitous or stem cell-specific promoter and Polylox recombination induced by Tamoxifen administration (Pei et al., 2017).

1.7.2 Protein-based barcoding

A protein-based strategy to track the families of individual T cells in vivo is the use of congenic markers. Congenic mice are inbred mouse strains that possess different alleles only for one gene (Rogner & Avner, 2003). In mice strains bearing versions of CD45 (CD45.1 or CD45.2) and CD90 (CD90.1 and CD90.2) have been used. Importantly, the expression of these alleles can be distinguished by staining with monoclonal antibodies. However, the differences in these proteins do not lead to altered protein function. As these alleles are expressed codominantly, nine distinct congenic phenotypes (congenic matrix) can be achieved by intercrossing these four variants. With one phenotype reserved for the recipient mice (CD45.2/.2 and CD90.2/.2) up to eight populations or single cells can be distinguished from each other and the recipients (Buchholz et al., 2013, 2016). For T cells, specificity of the T cells can be achieved by crossing TCR transgenic mice to this diverse congenic background (Buchholz et al., 2013; Cho et al., 2017). As mentioned before, one advantage of these congenic markers is that analysis can be performed on living cells. Therefore, the congenic matrix allows for phenotypic characterization, functional assays, retransfer to secondary/tertiary recipients and RNA sequencing (Buchholz et al., 2013; Graef et al., 2014; Grassmann et al., 2020; Stemberger et al., 2007). However, this approach makes it difficult to study rare clonal events and cannot be transferred to other leucocytes such as NK cells, since CD90 as one essential component of the congenic matrix, is not reliably expressed in non-T-cells. For these reasons the approach of retroviral color-barcoding was developed in our lab (Grassmann et al., 2019, 2022).

For retroviral color-barcoding, the hematopoietic stem cells (HSCs) of a mouse strain of interest are isolated and retrovirally transduced with fluorescent proteins of the GFP family. This approach allows the tracking and isolation of larger numbers of single-cell families by flow cytometry in comparison to congenic methods (Grassmann et al., 2019). After the co-transduction of stem cells with GFP, YFP, Ametrine (or T-Sapphire), CFP and BFP these are transferred into irradiated recipient mice. During the next weeks, the immune system (myeloid and lymphoid) of the irradiated recipients is reconstituted from the transduced stem cells yielding mature immune cells that express stable and unique combinations of fluorescent proteins. From these retrogenic mice, single-uniquely labeled cells can be sorted and transferred to recipient mice for subsequent fate-mapping experiments. (Flommersfeld et al., 2021; Grassmann et al., 2019, 2020, 2022)

By using HSCs isolated from a TCR transgenic mouse, naive T cells with a known specificity can be equipped with such barcodes. This thesis uses retrogenic color-barcoding in two ways. By a combination of retrogenic color- and congenic barcoding up to 85 T cell families can be tracked longitudinally in a single recipient mouse, which allows for high-throughput analysis of single-cell fate mapping experiments. Furthermore, it will be combined with retrogenic TCR expression (Holst et al., 2006) to generate barcoded T cell populations with known TCR characteristics.

1.8 Experimental models to study influence of TCR signal strength on T cell fate

1.8.1 Altered peptide ligands to study the influence of T cell avidity on recruitment

To study the influence of TCR affinity on T cell recruitment we will make use of OT1 (Hogquist et al., 1994) and OT3 (Enouz et al., 2012) TCR transgenic mice recognizing the model antigen chicken ovalbumin, in combination with different *Listeria monocytogenes* (*L.m.*) strains expressing APLs. While OT1 T cells recognize chicken ovalbumin with very high avidity, OT3 T cells possess a low avidity for this antigen (Enouz et al., 2012). As an intracellular pathogen, *L.m.* elicits strong $CD8^+$ T cell responses and is a well-studied infection model of $CD8^+$ T cell immunity. Additionally, *L.m.* has been engineered to express model antigens. For example, the strain *L.m.*-OVA expresses the well-characterized SIINFEKL epitope recognized by OT1 T cells (Condotta et al., 2012).

Such recombinant *L.m.* strains have been used elegantly to investigate the influence of TCR-pMHC affinity on the $CD8^+$ T cell response. Zehn and colleagues engineered *L.m.* to express APLs of the native OT1 epitope SIINFEKL (N4). APLs harbor single amino acid substitutions in this epitope and bind to the OT1 TCR with decreasing affinity. Importantly, they are presented on the H-2Kb MHC molecule with the same efficiency as the wildtype peptide (Zehn et al., 2009). Two APLs will be used in this study, SIYNFEKL (Y3), which has an isoleucine to tyrosine substitution in position 3, and SIITFEKL (T4), which possesses an asparagine to threonine substitution in position 4. While Y3 shows a slight reduction in affinity, T4 is ligand on the threshold between positive and negative selection of OT1 thymocytes (Daniels et al., 2006; Zehn et al., 2009).

The study by Zehn and colleagues revealed that the strength of the TCR-pMHCI interaction correlates positively with T cell expansion, sustained proliferation, and delayed contraction. T cells stimulated with low-avidity ligands resembled high-avidity stimulated cells phenotypically,

besides showing slightly lower surface levels of CD25 and CCR7 at early time points (Zehn et al., 2009). Taken together, this study, among others, indicated that the T cell repertoire undergoes a form of avidity maturation during a response (Busch & Pamer, 1999; Savage et al., 1999; Zehn et al., 2009): While T cells with a broad range of avidities are initially recruited, only high avidity T cells undergo sustained proliferation and expansion (Zehn et al., 2009). However, it was shown that even very low-avidity stimulation is sufficient to generate functional memory (Zehn et al., 2009).

1.8.2 TCRs and viral strains to study CD4$^+$ T cell fate

To study the influence of TCR avidity on CD4$^+$ T cell differentiation we aimed to use TCRs of distinct functional avidity in combination with viral strains which establish an acute or chronic infection.

To this end, we chose LCMV as a well-studied model pathogen that can elicit acute and chronic viral infections (Zhou et al., 2012). While the LCMV Armstrong strain causes an acute infection the LCMV CL13 strain (derived from LCMV Armstrong) leads to persistent infection of the host. These viral strains only differ in a single amino acid in their viral polymerase and glycoprotein respectively, leading to acute versus chronic infection (Matloubian et al., 1993). Importantly the immunodominant CD4$^+$ T cell epitope GP66-77 originally described by Oxenius et al. remains unchanged between these two viral strains (Matloubian et al., 1993; Oxenius et al., 1995).

Previously TCRs for this epitope had been isolated from T cells bearing a fixed TCR alpha chain after infection with LCMV Armstrong (C. Kim et al., 2013). In contrast, we aimed to isolate TCRs from the naive repertoire to draw from a structurally unreduced spectrum of an immune repertoire that had not been subjected to selective pressure. By studying T cells bearing TCRs of unique characteristics and their response in acute and chronic infection we aimed to segregate the influence of TCR signal strength and antigen persistence on CD4$^+$ T cell differentiation.

2 Aims of this thesis

T cells are a critical arm of adaptive immunity. While $CD8^+$ T cells convey immunity by killing infected or malignant cells, $CD4^+$ T cells play a role in connecting and regulating the interplay between innate, humoral and T cell mediated immunity. Both T cell subsets have in common that they recognize foreign peptides presented on MHC molecules with their TCR which is the pivotal receptor regulating T cell activation. The strength with which a TCR binds to its cognate pMHC complex has been described to influence the expansion, differentiation, and function of T cells (Bhattacharyya & Feng, 2020; Busch & Pamer, 1999; Snook et al., 2018; Tubo & Jenkins, 2014; van Panhuys, 2016; Zehn et al., 2009). The general aim of this thesis is to analyze the influence of TCR binding strength on T cell fate decisions.

It has been shown that recruitment of a high avidity T cells was remarkably efficient and largely independent of antigen dose or vector (van Heijst et al., 2009). However, the recruitment efficiency of low avidity T cells has not been assessed. To initiate proliferation T cells must cross a digital threshold of activation(Au-Yeung et al., 2014). The probability of a T cell to be recruited should be dependent on its TCR avidity as this parameter will influence the probability of crossing this digital activation threshold. The first part of this thesis will revolve around the question in how far T cell recruitment is regulated by TCR binding strength and the implications of this regulation for secondary immune responses.

The functional diversification of $CD4^+$ T cells has been shown to be dependent on TCR avidity. Previously, these influences have been studied by varying antigen dose, the use of APLs or with TCRs of limited numbers or structural diversity. Furthermore, the extent to which signals mediated by the TCR instruct $CD4^+$ T cell fate at the single-cell level is still debated. The second part of this thesis will revolve around the question how TCR avidity shapes the $CD4^+$ T cell response to acute and chronic viral infection. To address this question, we isolated TCRs with a broad spectrum of functional avidities for the well-studied LCMV GP66-77 epitope. After characterization of these TCRs we investigated the responses of T cells bearing these TCRs *in vivo* by use of retrogenic mice. By transferring populations of T cells bearing a TCR of interest and analyzing the phenotypic composition of the response to acute and chronic infection aimed to separate the influence of TCR avidity and antigen persistence on differentiation. Furthermore, we studied the clonal heterogeneity of these responses by single-cell transfers. By this we sought to elucidate how probabilistic TCR-avidity-independent factors vs. deterministic TCR-avidity-dependent factors influences the fate decisions of single $CD4^+$ T cells.

3 Materials and Methods

3.1 Materials

3.1.1 Devices

Device	Model	Supplier
10x Instrument	Chromium Controller	10x Genomics, Pleasanton, USA
Balance	EG 2200-2NM	Kern & Sohn GmbH, Balingen, Germany
	ACJ 320-4M	Kern & Sohn GmbH, Balingen, Germany
Centrifuge	Biofuge fresco	Heraeus, Hanau, Germany
	Pico 17	Heraeus, Hanau, Germany
	Multifuge 3 S-R	Heraeus, Hanau, Germany
	Multifuge X3R	Heraeus, Hanau, Germany
	Mega Star 3.OR	VWR, Darmstadt, Germany
Counting chamber	Neubauer improved	Paul Marienfeld & Co. KG, Lauda-Königshofen, Germany
Flow cytometer/ cell sorter	CytoFLEX LX	Beckman Coulter, Fullerton, USA
	CytoFLEX S	Beckman Coulter, Fullerton, USA
	Cyan ADP	Beckman Coulter, Fullerton, USA
	FACS Aria II	Becton Dickinson, Heidelberg, Germany
	MoFlo Astrios	Beckman Coulter, Fullerton, USA
Incubator	HERAcell 240	Heraeus, Hanau, Germany
Laminar flow hood	HERAsafe	Heraeus, Hanau, Germany
Microscope	Primovert	Carl Zeiss, Jena, Germany
pH-meter	766	Knick, Berlin, Germany
Sequencer	NovaSeq6000	Illumina, San Diego, USA
	MiSeq	Illumina, San Diego, USA
Water bath		GFL, Burgwedel, Germany

3.1.2 Chemicals and reagents

Reagent	Supplier
2X DMEM	Sigma-Aldrich, Taufkirchen, Germany
Ammonium chloride (NH_4Cl)	Carl Roth, Karlsruhe, Germany
BamHI restriction enzyme	Thermo Fisher, Darmstadt, Germany
BHI	In house MIH, Klinikum rechts der Isar
Bovine serum albumin (BSA)	Sigma-Aldrich, Taufkirchen, Germany
Calcium chloride ($CaCl_2$)	Merck, Darmstadt, Germany
Chromium Single Cell 3' GEM v3 kit	10x Genomics, Pleasanton, USA
Chromium Single Cell 3′ Feature Barcode Library Kit	10x Genomics, Pleasanton, USA
Dimethyl sulfoxide (DMSO)	Sigma-Aldrich, Taufkirchen, Germany
Disodium phosphate (Na_2HPO_4)	Carl Roth, Karlsruhe, Germany
Dulbecco's Modified Eagle Medium (DMEM)	Life Technologies, Carlsbad, USA
E. coli Stbl3	Thermo Fisher, Darmstadt, Germany
Ethanol	Klinikum rechts der Isar, München, Germany
Ethylenediaminetetraacetic acid (EDTA)	Carl Roth, Karlsruhe, Germany
Fetal calf serum (FCS)	Sigma-Aldrich, Taufkirchen, Germany
Gentamycin	Life Technologies, Carlsbad, USA
Heparin-sodium (5000 IU/mL)	Ratiopharm, Ulm, Germany
HEPES	Carl Roth, Karlsruhe, Germany
Herculase II fusion DNA polymerase	Agilent Technologies, Santa Clara, USA
High sensitivity DNA Kit	Agilent Technologies, Santa Clara, USA
Ionomycin	Sigma-Aldrich, Taufkirchen, Germany
L-Glutamine	Sigma-Aldrich, Taufkirchen, Germany
LB Ampicillin media	In house MIH, Klinikum rechts der Isar
LB Ampicillin plates	In house MIH, Klinikum rechts der Isar

Reagent	Supplier
LCMV GP61-80 peptide	Peptides and Elephants, Henningsdorf, Germany
NotI restriction enzyme	Thermo Fisher, Darmstadt, Germany
Paraformaldehyde (PFA)	Sigma-Aldrich, Taufkirchen, Germany
PBS solution	Life Technologies, Carlsbad, USA
Penicillin	Life Technologies, Carlsbad, USA
Phosphate buffered saline (PBS)	Carl Roth, Karlsruhe, Germany
Potassium chloride (KCl)	Carl Roth, Karlsruhe, Germany
PureLink HiPure Plasmid Filter Maxiprep Kit	Thermo Fisher, Darmstadt, Germany
PureYield plasmid Miniprep	Promega, Madison USA
Qubit dsDNA hs assay kit	Life Technologies, Carlsbad, USA
Recombinant murine IL-3	PeproTech, Hamburg, Germany
Recombinant murine IL-6	PeproTech, Hamburg, Germany
Recombinant murine SCF	PeproTech, Hamburg, Germany
RetroNetin	Takara Biotech. Kusatsu, Japan
RPMI 1640	Life Technologies, Carlsbad, USA
Skim milk powder	Sigma-Aldrich, Taufkirchen, Germany
Sodium chloride (NaCl)	Carl Roth, Karlsruhe, Germany
ß-Mercaptoethanol	Life Technologies, Carlsbad, USA
Streptomycin	Life Technologies, Carlsbad, USA
Tris-Hydrochloride (Tris-HCl)	Carl Roth, Karlsruhe, Germany
Trypan Blue solution	Carl Roth, Karlsruhe, Germany
Trypsin-EDTA	Life Technologies, Carlsbad, USA

3.1.3 Antibodies and staining reagents

All antibodies have been titrated to the optimal dilutions.

Antibody	Supplier	Identifier
Anti-mouse CD27	BioLegend, San Diego, USA	LG.3A10
Anti-mouse CD27	Thermo Fisher, Darmstadt, Germany	LG7.F9
Anti-mouse CD62L	BioLegend, San Diego, USA	MEL-14
Anti-mouse CD62L	Becton Dickinson, Heidelberg, Germany	MEL-14
Anti-mouse CD3e	Becton Dickinson, Heidelberg, Germany	145-2C11
Anti-mouse CD3e	BioLegend, San Diego, USA	145-2C11
Anti-mouse TCR beta	Becton Dickinson, Heidelberg, Germany	H57-597
Anti-mouse CD4	Thermo Fisher, Darmstadt, Germany	RM4-5
Anti-mouse CD8a	BioLegend, San Diego, USA	53-6.7
Anti-mouse CD19	Becton Dickinson, Heidelberg, Germany	1D3
Anti-mouse Sca-1	BioLegend, San Diego, USA	D7
Anti-mouse CD16/32	BioLegend, San Diego, USA	93
Anti-mouse CD69	BioLegend, San Diego, USA	H1.2F3
TotalSeq™-B0301 anti-mouse Hashtag 1	BioLegend, San Diego, USA	M1/42; 30-F11
TotalSeq™-B0302 anti-mouse Hashtag 2	BioLegend, San Diego, USA	M1/42; 30-F11
TotalSeq™-B0304 anti-mouse Hashtag 4	BioLegend, San Diego, USA	M1/42; 30-F11
TotalSeq™-B0305 anti-mouse Hashtag 5	BioLegend, San Diego, USA	M1/42; 30-F11
TotalSeq™-B0306 anti-mouse Hashtag 6	BioLegend, San Diego, USA	M1/42; 30-F11
TotalSeq™-B0307 anti-mouse Hashtag 7	BioLegend, San Diego, USA	M1/42; 30-F11
TotalSeq™-B0307 anti-mouse Hashtag 8	BioLegend, San Diego, USA	M1/42; 30-F11
Anti-mouse CXCR5	Thermo Fisher, Darmstadt, Germany	SPRCL5
Streptavidin-PE/APC/BV421	Thermo Fisher, Darmstadt, Germany BioLegend, San Diego, USA	n.a.

Antibody	Supplier	Identifier
Anti-mouse CD44	BioLegend, San Diego, USA	IM7
Anti-mouse PD1	Thermo Fisher, Darmstadt, Germany	J43
Anti-mouse CXCR6	BioLegend, San Diego, USA	SA051D1
Anti-mouse CCR7	BioLegend, San Diego, USA	4B12
Anti-PE biotin	BioLegend, San Diego, USA	PE001
Anti-mouse CXCR3	BioLegend, San Diego, USA	CXCR3-173
Anti-mouse Tim3	BioLegend, San Diego, USA	RMT3-23
Anti-mouse TCRbeta	BioLegend, San Diego, USA	H57-597
Anti-mouse Ly108	BioLegend, San Diego, USA	330-AJ
Anti-mouse CD11c	BioLegend, San Diego, USA	N418
Propidium iodide (PI)	Thermo Fischer, Darmstadt, Germany	n.a.
Fixable Viability Dye eFluor-780	Thermo Fischer, Darmstadt, Germany	n.a.
Zombie UV™ Fixable Viability Kit	BioLegend, San Diego, USA	n.a.
I-A(b) LCMV GP 66-77	NIH Tetramer Core Facility, Atlanta, USA	n.a.
Anti-mouse CD28	BioLegend, San Diego, USA	37.51
Anti-mouse CD45.1	BioLegend, San Diego, USA	A20
Anti-mouse CD45.2	BioLegend, San Diego, USA	104
Anti-mouse CD90.1	Becton Dickinson, Heidelberg, Germany	OX7
Anti-mouse CD90.1	Thermo Fisher, Darmstadt, Germany	HIS51
Anti-mouse CD90.2	BioLegend, San Diego, USA	53-2.1
CellTrace violet proliferation kit	Thermo Fisher, Darmstadt, Germany	n.a.

3.1.4 Buffers and media

Buffer	Composition
Ammonium chloride-Tris (ACT)	90 % (v/v) 0.17 M NH_4Cl 10 % (v/v) 0.17 M Tris HCl, pH 7.2
FACS Buffer, pH 7.5	1x PBS 0.5 % (w/v) BSA 2 mM EDTA
Complete DMEM (cDMEM)	1x DMEM 10 % (v/v) FCS 0.12 % (w/v) HEPES 0.02 % (w/v) L-Glutamine 1 % (v/v) Penicillin/Streptomycin 0.1 % (v/v) Gentamycin 0.1 % (v/v) ß-Mercaptoethanol
Complete RPMI (cRPMI)	1x RPMI 1640 10 % (v/v) FCS 0.12 % (w/v) HEPES 0.02 % (w/v) L-Glutamine 1 % (v/v) Penicillin/Streptomycin 0.1 % (v/v) Gentamycin 0.1 % (v/v) ß-Mercaptoethanol
Freezing Medium	FCS 10 % (v/v) DMSO
Transfection Buffer, pH 6.76	ddH_20 1.6 % (w/v) NaCl 0.074 % (w/v) KCl 0.05 % (w/v) Na_2HPO_4 1 % (w/v) HEPES

3.1.5 Cell lines

Cell line	Organism	Origin
Platinum-E (Plat-E)	Human	Cell Biolabs, San Diego USA
RD114	Human	ATCC, Manassas, USA
Jurkat TRP	Human	Peter Steinberger, Vienna
Vero	African green monkey	ATCC, Manassas, USA
BHK21	Syrian golden Hamster	ATCC, Manassas, USA

3.1.6 Plasmids and recombinant DNA

Plasmid/recombinant DNA	Origin
pMP71	Wolfgang Uckert, MDC Berlin, Germany
EGFP	MIH, TU Munich, Germany
EYFP	MIH, TU Munich, Germany
CFP	MIH, TU Munich, Germany
Ametrine	MIH, TU Munich, Germany
EBFP2	MIH, TU Munich, Germany
T-sapphire	MIH, TU Munich, Germany
Murine CD4	MIH, TU Munich, Germany

3.1.7 Oligonucleotides

Oligonucleotide	Sequence	Supplier
CD4 BamHI fwd	5'ATTAGGATCCGCCACCATGTGC CGAGCCATCTCTC3'	Sigma-Aldrich, Taufkirchen, Germany
CD4 NotI rev	5'TAATGCGGGCCGCTCAGATGAG ATTATGGCTC3'	Sigma-Aldrich, Taufkirchen, Germany

3.1.8 Mice

Mouse strain	Official name	Origin
C57BL/6	C57BL/6JOlaHsd	Envigo, Indianapolis, USA
OT1 x Rag1 $^{-/-}$ Matrix	C57BL/6-Tg(TcraTcrb)1100Mjb/J x B6.129S7-Rag1tm1Mom/J x (B6.SJL-Ptprca Pepcb/BoyJ x B6.PL-Thy1a/CyJ)	The Jackson Laboratory, Bar Harbor, USA
OT3 TCRα$^{-/-}$	n.a.	Prof. Dietmar Zehn (TUM)
CD45.1	B6.SJL-Ptprca Pepcb/BoyJ	The Jackson Laboratory, Bar Harbor, USA
CD11c-DTR-GFP	B6.FVB-Tg(Itgax-DTR/EGFP)57Lan/J	The Jackson Laboratory, Bar Harbor, USA
Smart x Great x Vert-X (SGX)	B6.129S4-Il17atm1.1Lky/J x C.129S4(B6)-Ifngtm3.1Lky/J x B6(Cg)-Il10tm1.1Karp/J	The Jackson Laboratory, Bar Harbor, USA
SMARTA x Rag1$^{-/-}$ Matrix	B6;D2-Tg(TcrLCMV)Aox/J x (B6.129S7-Rag1tm1Mom/J x (B6.SJL-Ptprca Pepcb/BoyJ x B6.PL-Thy1a/CyJ))	The Jackson Laboratory, Bar Harbor, USA
Rag1 $^{-/-}$ Matrix	B6.129S7-Rag1tm1Mom/J x (B6.SJL-Ptprca Pepcb/BoyJ x B6.PL-Thy1a/CyJ)	The Jackson Laboratory, Bar Harbor, USA

C57BL/6 mice were purchased from Envigo. OT3 TCRα$^{-/-}$ mice were kindly provided by Prof. Dietmar Zehn (Technical University of Munich). Other mouse strains were bred and maintained under specific pathogen-free (SPF) conditions at the mouse facility at the Technical University of Munich. All animal experiments were approved by local authorities and performed in accordance with national guidelines.

3.1.9 Software

Software	Supplier
FlowJo V10	FlowJo LLC, Ashland, USA
Prism 9	Graphpad, La Jolla, USA
SCANPY (v 1.6)	Theis lab (GitHub) (Wolf et al., 2018)
Affinity Designer (v1.10.1)	Serif Europe Ltd., Nottingham, Great Britain
Microsoft Office (v16.60)	Microsoft, Redmond, USA
FlowSOM (v 3.0.13)	FlowJo exchange (van Gassen et al., 2015)
V-quest	www.imtg.org (Brochet et al., 2008)
Cellranger (v 5.0.0)	10x Genomics, Pleasanton, USA
Hashsolo	https://github.com/calico/solo (Bernstein et al., 2020)

3.2 Methods

3.2.1 Molecular biology

pMP71 plasmid DNA was purified from overnight cultures of transformed *E. coli* Stbl3 clones selected on LB Ampicillin plates, and purified by maxiprep (HiLink, Invitrogen). Plasmids were verified by sequencing before use.

Murine CD4 was amplified from the cDNA of C57BL/6 mice by PCR with the primers listed above containing restriction sites for cloning into pMP71. After digest with BamHI and NotI, the CD4 construct was ligated into pMP71 and transformed into *E.coli* Stbl3. The plasmid was purified from liquid cultures by PureYield Plasmid miniprep system (Promega) and verified by sequencing.

3.2.2 Tissue culture

Plat-E, RD114, Vero and BHK21 cells were grown in cDMEM in tissue-culture treated cell culture flasks. Jurkat TRP cells were grown in cRPMI in tissue-culture treated cell culture flasks. Cell lines were incubated at 37 °C and 5 % CO_2 in humidified atmosphere and were split every 2-4 days depending on their confluence. Adherent cells were treated with Trypsin-EDTA (5 min, 37 °C) prior to splitting.

3.2.2.1 Transfection of virus-producing cell lines

Retroviral packaging cell lines were transfected with retroviral vectors encoding for the fluorescent proteins GFP, YFP, CFP, BFP, Ametrine and T-sapphire or TCRs via calcium phosphate precipitation. Plat-E (ecotropic) or RD114 cells (amphotropic), were seeded in 6-well plates and grown until they reached 70 % confluence. 18 µg of the retroviral plasmid dissolved in 135 µl ddH_2O was mixed with 15 µl of a 3,3 M $CaCl_2$ solution. For precipitation, this mixture was added dropwise to an equal volume of transfection buffer while vortexing. The precipitate was incubated for 10-15 minutes at room temperature (vortex after 10 minutes) and then carefully distributed onto the cells. After 6 hours, the medium was exchanged. After 48 and 72 hours, viral supernatants were collected and purified from remaining cells by centrifugation (1500 rpm, 4 °C, 7 min). Viral supernatants were stored at 4 °C for up to 4 weeks.

3.2.2.2 Transduction of Jurkat TRP

Jurkat triple reporter (TRP) cells stably expressing TCRs of interest and or murine CD4 were generated by retroviral transduction. Therefore, 400 µl of the respective RD114 supernatant (cRPMI) was added per well of a tissue-culture treated 48-well plate and centrifuged at 3.000 xg and 32 °C for 2 hours. Jurkat TRP cells were counted and the cell density was adjusted to $5x10^5$ cells/ml in cRPMI. Then, 50 µl of the cell suspension (25.000 cells) was added carefully to the viral supernatant and the plate was centrifuged again at 800 xg and 32 °C for 1,5 hours. Transduction efficacy was determined after 2 days by flow cytometry. Transduced cells were purified by fluorescence activated cell sorting for comparable levels of TCR and CD4 expression.

3.2.2.3 Jurkat functional avidity assay

For peptide stimulation experiments $1.5*10^5$ splenocytes were seeded in 100 µl cRPMI containing 2x the final GP61-80 peptide dilution in technical triplicates. As a positive control 1 µg of anti-CD3e and 2 µg anti-CD28 antibodies were added. As a negative control just cRPMI containing no peptide was used. After 1 hour incubation at 37 °C $3*10^4$ Jurkat TRP cells were added per well in 100 µl cRPMI. After 18 hours of incubation reporter expression was assessed by flow cytometry. Responses were normalized to the positive control and EC50 values determined by fitting with log(agonist) vs. normalized response function in Graphpad Prism.

3.2.3 Mice and infection experiments

3.2.3.1 Generation of retrogenic mice

Femorae and tibiae of 8-15 weeks old OT1 $Rag1^{-/-}$ Matrix, SMARTA $Rag1^{-/-}$ Matrix or $Rag1^{-/-}$ Matrix mice were removed and freed from tissue. The epiphyses were cut off and bone marrow cells were flushed out with cDMEM using a 10 mL syringe with a 26G needle. Bone marrow

cells were harvested by centrifuged at 1500 rpm for 6 minutes and resuspended in 3 mL ACT buffer for red blood cell lysis. Red blood cell lysis was stopped after 3 minutes by the addition of 7 mL cDMEM. Afterwards, bone marrow cells were centrifuged again, and resuspended in 500 µl FACS buffer containing, anti-mouse CD19 and anti-mouse Ly6A/E (Sca-1) antibodies and incubated for 30 minutes at 4 °C protected from light. After staining, cells were washed with 10 mL FACS buffer and resuspended in 500 µl cDMEM for cell sorting. PI was added 1/100 for live/dead discrimination. $CD19^-$ $Sca\text{-}1^+$ hematopoietic stem cells (HSCs) were sorted into 15 mL tubes containing 1 mL FCS. Sorted cells were washed with 10 mL PBS and resuspended in cDMEM, supplemented with 2 ng/mL murine IL-3 (mIL-3), 50 ng/mL murine IL-6 (mIL-6) and 50 ng/mL murine SCF (mSCF). HSCs were seeded in a tissue-culture treated 48-well plate (250.000-350.000 cells/400 µl). After 3 days, cells were split 1:1 or 1:2 depending on their confluency.

For retroviral transduction, a tissue-culture untreated 48-well plate was coated with 10 µg/mL RetroNectin in PBS (150 µl per well) overnight at 4 °C. HSCs were transduced after 4 days of culture. Retroviral supernatants were pooled accordingly to achieve combinatorial transduction of the HSCs. After removal of RetroNectin 400 µl of the pooled supernatants were added per well and centrifuged at 3.000 xg and 32 °C for 2 hours. Stem cells were collected and washed once with cDMEM after which they were resuspended in fresh cDMEM, supplemented with 2 ng/mL mIL-3, 50 ng/mL mIL-6 and 50 ng/mL mSCF (final cell density: 300.000 cells/400 µl). Viral supernatants were removed from the plate and 400 µl of the prepared HSCs were added per well. The plate was centrifuged at 800 xg and 32 °C for 1,5 h and cultured for two days before measurement of transduction efficacies by flow cytometry.

Two days after HSC transduction, C57BL/6 recipient mice were irradiated in a cesium irradiator. The mice were irradiated with total dose of 9 grays (Gy) that were delivered in two equal doses 4 hours apart. Subsequently, transduced stem cells were collected and washed with PBS. For adoptive transfer the cells were resuspended in FCS at a final density of $1\text{-}3x10^6$ cells/recipient. Adoptive transfer of transduced stem cells was performed by intravenous injection (i.v.) into the irradiated hosts. After 4 weeks, chimerism of the retrogenic mice was determined in peripheral blood samples via flow cytometry.

3.2.3.2 Measurement of T cell recruitment

Splenocytes of OT1 $Rag1^{-/-}$, OT3 $TCR\alpha^{-/-}$ (both $CD45.1^+$ $CD90.1^-$) and P14 ($CD45.1^+$ $CD90.1^+$) mice were stained with cell trace violet (CTV, Invitrogen) according to manufacturer instructions and stained with monoclonal antibodies as described above. Respectively, $2.5x10^4$ $CD8^+$ $CD44^{low}$ CTV^{high} OT1 or OT3 cells were co-transferred with P14 cells into C57BL/5 ($CD45.1^-$ $CD90.1^-$) recipients by i.p. injection. At the indicated time points post infection, spleen, lymph nodes (inguinal, axillary, mesenterial, iliac), blood and bone marrow were harvested and

CD45.1$^+$ cells enriched by speed enrichment after red blood cell lysis. After enrichment cells were stained and analyzed as described. Recruitment was calculated as:

$$Recruitment\ P14\ corrected\ [\%] = \left(1 - \frac{\frac{OT1}{P14} infected}{\frac{OT1}{P14} naive}\right) * 100$$

or $Recruitment\ [\%] = \left(1 - \frac{OT1\ count\ infected}{OT1\ count\ naive}\right) * 100$

3.2.3.3 Retransfer of CD4$^+$ T cell families

On day 8 p.i. with LCMV Armstrong the T cell families derived from transfer of single color-barcoded SMARTA T cells were speed enriched (shared CD45.1 expression) and sorted from 4/5 of total splenocytes isolated from primary recipients. Cells enriched from one primary recipient were retransferred into one secondary recipient (C56BL/6-CD11c-DTR-GFP) by i.v. injection. Secondary recipients were infected with LCMV Armstrong as described three weeks after retransfer. C56BL/6-CD11c-DTR-GFP mice were used for this experiment to avoid the rejection of color-barcoded cells.

3.2.3.4 Hemisplenectomy

Hemisplenectomy was performed as described by Grassmann et al., 2020. Briefly, laparotomy was performed on anesthetized mice at day 8 p.i. with *L.m.*-N4/T4 by a left subcostal incision of the skin and the peritoneum. The spleen was mobilized and approximately one-third of the spleen was ligated and removed. The remaining spleen was cauterized. Peritoneum and skin were closed by surgical stitches. The obtained spleen sample was placed in RPMI (10% FCS, 0.025% L-glutamine, 0.1% HEPES, 0.001% gentamycin and 0.002% streptomycin) with Heparin to prevent coagulation until further processing.

3.2.4 Pathogens

3.2.4.1 LCMV

The LCMV Armstrong and LCMV CL13 strains were propagated in BHK21 cells as described by Welsh & Seedhom, 2008. LCMV titers were determined by immunological focus assay as described by Battegay et al., 1991. For adoptive transfer experiments mice were infected one day after cell transfer with $2*10^6$ PFU of LCMV CL13 i.v. or $2*10^5$ PFU of LCMV Armstrong i.p. in PBS. For intermediate dose LCMV CL13 infection mice were infected i.v. with $8*10^4$ LCMV CL13 and 200 PFU LCMV CL13 for acute LCMV CL13 infection.

3.2.4.2 Listeria monocytogenes

Glycerol stocks of the recombinant *L.m.* APL strains were stored at -80 °C and subjected to a maximum of 3 freeze-thaw cycles. 5 ml Brain- Heart-Infusion broth (BHI) were inoculated with 20 µl of the bacterial stock. The bacteria were cultured at 37 °C in a shaking incubator (90 rpm) for about 4 hours. Colony forming units (CFU) were determined by OD_{600} measurement and the following formula: CFU = OD_{600} *12 *10^8. Mice were infected with 5000 CFU i.v. one day after cell transfer. The infectious dose was checked by plating 1:5 dilutions of the final solution on BHI plates (technical triplicates). CFU were counted after incubation (37 °C) over night.

3.2.4.3 Modified Vaccinia Ankara

MVA-OVA was kindly provided by Andreas Muschaweckh. The virus was homogenized by sonication prior to dilution. Mice were infected with 10^8 PFU i.p. one day after cell transfer unless otherwise indicated.

3.2.5 Generation of single-cell suspensions

3.2.5.1 Spleen and lymph nodes

Spleens and lymph nodes were harvested and mashed through a 40 µm cell strainer in a petri dish containing 5 mL cRPMI. Cells were harvested by centrifugation and red blood cell lysis performed with ACT buffer for 3 minutes at RT. Red blood cell lysis was stopped by adding 7 mL cRPMI. Cell numbers were determined using a Neubauer counting chamber.

3.2.5.2 Blood

50-100 µl blood were collected in heparinized tubes by punction of the *vena facialis* using a lancet. 10 mL ACT buffer were added to the samples and incubated for 10 minutes at RT to lyse erythrocytes. Blood cells harvested by centrifugation and pellets were resuspended in 5 mL ACT buffer for another 5 minutes at RT. The reaction was stopped by the addition of 5 ml cRPMI.

3.2.5.3 Bone marrow

The femorae and tibiae were removed and freed from tissue. The epiphyses were cut off and bone marrow cells were flushed out with cDMEM using a 10 mL syringe with a 26G needle. Bone marrow cells were harvested by centrifuged at 1500 rpm for 6 minutes and resuspended in 3 mL ACT buffer for red blood cell lysis. Red blood cell lysis was stopped after 3 minutes by the addition of 7 mL cDMEM.

3.2.6 Flow cytometry and cell sorting

3.2.6.1 Flow cytometric speed enrichment of cells

Spleens of naive, retrogenic donor, or primary recipient mice were harvested and brought into single-cell suspension as described. Splenocytes were stained in FACS buffer (1 mL per $1x10^8$ cells) with an anti-mouse CD45.1 antibody for 30 minutes at 4 °C protected from light for the detection of transferred cells. For the isolation of T cells from the naive repertoire splenocytes were stained with IA(b) GP66-77 tetramer for 45 minutes at 37° C in cRPMI. Cells were washed with 10 mL FACS Buffer and resuspended in FACS Buffer. $CD45.1^+$ cells were enriched by speed enrichment on a MoFlo Astrios cell sorter. For speed enrichment a fluorescence trigger is set instead of a scatter trigger, cutting of particles negative for the enrichment marker. This trigger limits analysis complexity of the detected events to one parameter, thereby reducing consumption of electronic hardware resources and enabling dramatically increased sample flow rates in comparison to other flow cytometric approaches. Collected samples were then subjected to purity sorting for further use.

3.2.6.2 Cell sorting and adoptive transfer

Single cell suspensions were stained with respective antibodies for 30 minutes at 4 °C in the dark. Cells were washed with 10 mL PBS and resuspended in FACS buffer (final cell density: $5x10^7$ cells/mL). PI was added 1/100 for live/dead discrimination. Cell sorting was performed on a BD FACSAria III (Becton Dickinson), MoFlo XDP or MoFlo Astrios cell sorter (Beckman Coulter). For adoptive transfers cells were sorted into 96-well V-bottom plates containing 200 µl FCS and cell pellet of $4*10^5$ feeder cells (splenocytes of the recipient mouse strain).

For adoptive transfer of $CD8^+$ T cells, peripheral blood mononuclear cells or splenocytes from retrogenic or congenic donor mice were stained following red blood cell lysis with antibodies directed against CD8 and CD44 (and CD45.1/CD90.1 when sorting from retrogenic mice). Single naive T cells (Living $CD8^+$ $CD44^{low}$) of distinct congenic phenotype or distinct color-barcode were sorted. Cells were injected i.p. into C57BL/6 or C57BL/6-CD11c-DTR-GFP mice. Adoptive transfers for single T cell fate mapping were performed in a multiplexed fashion. This means that up to 8 × 1 T cells harboring distinct congenic marker profiles or up to 85 × 1 distinctively color-barcoded T cells were sorted into the same well and transferred in parallel into the same recipients. For population experiments 100 naive OT1 cells were transferred.

For adoptive transfer of $CD4^+$ T cells expressing a given TCR, peripheral blood mononuclear cells or splenocytes from retrogenic mice were stained following red blood cell lysis with antibodies directed against CD4, CD44, TCRb CD8, CD19 and a congenic marker. Single naive T cells (Living congenic $marker^+$ $CD4^+$ $TCRb^+$ $CD44^{low}$) of distinct congenic phenotype or distinct color-barcode were sorted. Importantly, $CD4^+$ T cells expressing the same TCR

levels as the endogenous $CD4^+$ T cell population were sorted, to ensure comparable TCR expression between populations and experiments. Cells were injected i.p. into C57BL/6 or C57BL/6-CD11c-DTR-GFP mice. Adoptive transfers for single T cell fate mapping were performed in a multiplexed fashion. This means that up to 25 × 1 distinctively color-barcoded T cells were sorted into the same well and transferred in parallel into the same recipients. For population experiments 500 naive $CD4^+$ cells were transferred unless indicated otherwise.

3.2.6.3 Flow cytometry

Lymphocytes were isolated from respective organs as described and stained in a v-bottom 96-well plate. A maximum of 10^7 cells were added per well and centrifuged at 1500 rpm and 4 °C for 3 minutes. Pellets were resuspended in 100 µl FACS buffer anti-mouse CD16/CD32 1/500 for blocking of Fc receptors to avoid unspecific binding of antibodies and incubated for 20 minutes. Afterwards, cells were washed 1.5 times with FACS buffer and stained with the respective antibodies – diluted in 100 µl FACS buffer per well – for 30 minutes at 4 °C in the dark. Cells were washed 2.5 times with FACS buffer and analyzed by flow cytometry.

Staining of CXCR5 was performed in three successive steps separated by 1.5x wash steps. First samples were stained with anti-CXCR5 PE for 30 minutes, followed by staining with a biotinylated-anti-PE secondary antibody for 20 minutes and then by Streptavidin-PE in combination together with other surface staining antibodies. These staining steps were performed at RT.

Staining for CCR7 and IA(b) GP66-77 were performed at 37 °C unless otherwise indicated.

After washing infectious samples were fixed with 1 % PFA for 60 minutes. Samples were analyzed on CytoFLEX LX (Beckman Coulter), CytoFLEX S (Beckman Coulter) or Cyan ADP (Beckman Coulter) flow cytometers.

3.2.7 Single cell RNA sequencing

In the LCMV Armstrong experiment, we co-transferred 500 naive color-barcoded T cells expressing TCR 1, 5, 15, 11, 14, and 9 per recipient mouse. C56BL/6-CD11c-DTR-GFP mice were used for this experiment to avoid the rejection of color-barcoded cells. In the LCMV CL13 experiment we transferred 5000 T cells of TCR 1, 11, and 9 into separate recipient mice. For single cell RNA-seq (scRNA-seq), transferred or endogenous T cells were speed enriched from pooled splenocytes of the recipient mice based on CD45.1/CD90.1 expression or IA(b) GP66-77 tetramer binding at the indicated timepoints. In the LCMV Armstrong experiment tetramer staining was performed at 37 °C, whereas it was performed at 4 °C in the LCMV CL13 experiment. In the LCMV Armstrong experiment the sample was split after speed enrichment according to the frequencies of transferred TCR populations and labeled with Hashtag

antibodies to allow for demultiplexing by TCR in the sequencing sample. In the LCMV CL13 experiment the different TCR populations were similarly labeled by hashtag antibodies. In addition to the hashtag antibodies the cells were stained with anti CD4, anti CD8, anti CD19, anti CD11c, and antibodies for the respective congenic marker. Cells for sequencing were sorted as live $CD4^+$ congenic $marker^+$ $CD8^-$ $CD19^-$ $CD11c^-$. In the LCMV Armstrong experiment TCR populations were sorted by their additional expression of a fluorescent protein whereas they were identified by congenic marker expression in the LCMV CL13 experiment. T cells were sorted into an FCS-coated v-bottom 96-well plate containing 200 µl FACS buffer (without EDTA) per well.

Sorted T cells applied to droplet-based sc-RNA seq using the Chromium Single Cell 3′ Library & Gel Bead Kit (10x genomics). Preparation of antibody feature barcode libraries was performed with a Chromium Single Cell 3′ Feature Barcode Library Kit (10x genomics). QC was performed with a High sensitivity DNA Kit on a Bioanalyzer 2100 and libraries were quantified with the Qubit dsDNA hs assay kit. Libraries were pooled according to their minimal required read counts (20.000 reads/cell for gene expression libraries; 5.000 reads/cell for Feature Barcode Libraries). Illumina paired end sequencing was performed with 150 cycles on a NovaSeq 6000. Single cell partitioning, barcoding, RNA extraction and library preparation were performed by Sebastian Jarosch, Monika Hammel and Anton Mühlbauer at the Institute for Medical Microbiology, Immunology and Hygiene (TUM).

Annotation was performed using cellranger (V5.0.0, 10x Genomics) against the murine reference genome GRCm38 release 84, with manual addition of the genes for GFP, YFP, CFP, BFP, T-sapphire, and Ametrine. All subsequent analysis has been performed using SCANPY V1.6 (Wolf et al., 2018). After general preprocessing according to good practice in scRNA seq analysis (<15% mitochondrial genes, regessing out cell cycle, mitochondrial genes and total counts), Hashtag demultiplexing and doublet removal as described by Bernstein et al., the data was count normalized per cell and logarithmized, Hashtag barcodes and fluorescent proteins, as well as variable TCR chains were removed from the variables for analysis. SCANPY was also used for dimensionality reduction and clustering. The neighborhood graphs were based on n = 10 principal components and 20 neighbors. Clustering was performed using the Leiden algorithm with resolution r = 0.7. UMAP dimensionality reduction was computed using SCANPY's default parameters.

3.2.8 Isolation of TCRs from the naive repertoire

For the isolation of TCRs from the naive repertoire the splenocytes of three C57BL/6 mice were co-stained with IA(b) GP66-77 PE and BV421 (1:2000; $2*10^7$ cells/ml) in cRPMI for 45 minutes at 37 °C. After washing the splenocytes were speed enriched on IA(b) GP66-77 PE.

The enriched cells were then stained with anti-CD44, anti-CD4, anti-CD8 and anti-CD19 antibodies and PI was added before purity sorting for live dead discrimination. Gates for double tetramer positivity were set up with an unenriched splenocyte sample spiked with SMARTA T cells. From this sample SMARTA^{+} and tetramer negative controls were sorted for expansion. Single live CD4^{+} CD44^{low} double tetramer^{+} CD8^{-} CD19^{-} were sorted into a 384 well plate containing 25 µl/well cRMPI supplemented with 25 U/ml IL-2 and Expamer. After 13 days of expansion 0.5 µl D-Biotin (1 mM) was added 12 hours before restaining to stop stimulation. Half of the cells from each expanded clone were used for tetramer restaining, the other half was used for TCR sequencing. The expanded clones were co-stained with IA(b)-GP66-77 PE and BV421 to confirm tetramer specificity. TCR-alpha and beta chains were amplified by TCR-SCAN RACE polymerase chain reaction as described in Dössinger et al., 2013. and subsequently sequenced on the Illumina MiSeq platform. Second TCR alpha chains were excluded from the sequencing results by low count number or unproductive rearrangement (stop/frameshift). The alpa and beta chain sequences were analyzed with IMGT/V-Quest (Brochet et al., 2008). TCR expression constructs were designed *in silico* and synthesized and cloned into pMP71 by Twist Bioscience. The TCR expression constructs had the following structure: Kozak-Sequence followed by TCR beta chain followed by a porcine teschovirus-1 2A self-cleaving peptide (P2A), followed by the TCR alpha chain. Full sequences of the expression constructs can be found in the attachment.

3.2.9 Statistical analysis

Quantification and statistical analysis was performed with the Prism (GraphPad). A detailed description of each statistical test is given in the respective figure legend. Significance is defined as * $p < 0.05$, ** $p < 0.01$, *** $p < 0.001$, **** $p < 0.0001$. Normality tests were performed to decide whether to use parametric or nonparametric tests, where applicable.

4 Results

4.1 Influence of TCR avidity on the recruitment of CD8$^+$ T cells

4.1.1 TCR avidity influences expansion, phenotype, and recovery of CD8$^+$ T cells

Upon infection antigen-specific T cells undergo massive proliferation and phenotypic diversification. To assess the influence of TCR avidity on these processes, we utilized OT1 T cells in combination with APL-expressing *Listeria monocytogenes* strains as a model system. OT1 transgenic T cells recognize a chicken Ovalbumin epitope (SIINFEKL) presented on H2-Kb. By the expression of the native SIINFEKL epitope or versions with single amino acid substitutions, the binding strength of the TCR to its cognate peptide MHC complex can be modified. The OT1 TCR has a high binding strength to the native SIINFEKL epitope, which is reduced 4-fold for the SIYNFEKL (Y3) and about 70-fold for the SIITFEKL (T4) epitope (Zehn et al., 2009). We transferred 100 or 8x1 naive OT1 T cells, bearing unique congenic markers into naive C56BL/6 recipients to study single-cell- (8x1 cell) or population-derived responses (100 cells) to these ligands. After infection with the respective *L.m.*-APL strains, we analyzed the T cell responses on day 8 post infection (p.i.) in the spleen (Figure 2A). Population- and single-cell derived responses where distinguished by their congenic markers and phenotypically analyzed for the expression of CD27 and CD62L (Figure 1). Central memory precursor (TCMp) cells co-express CD27 and CD62L whereas effector memory precursor (TEMp) cells lose CD62L expression and terminal effector cells (TEF) are negative for both markers (Figure 1).

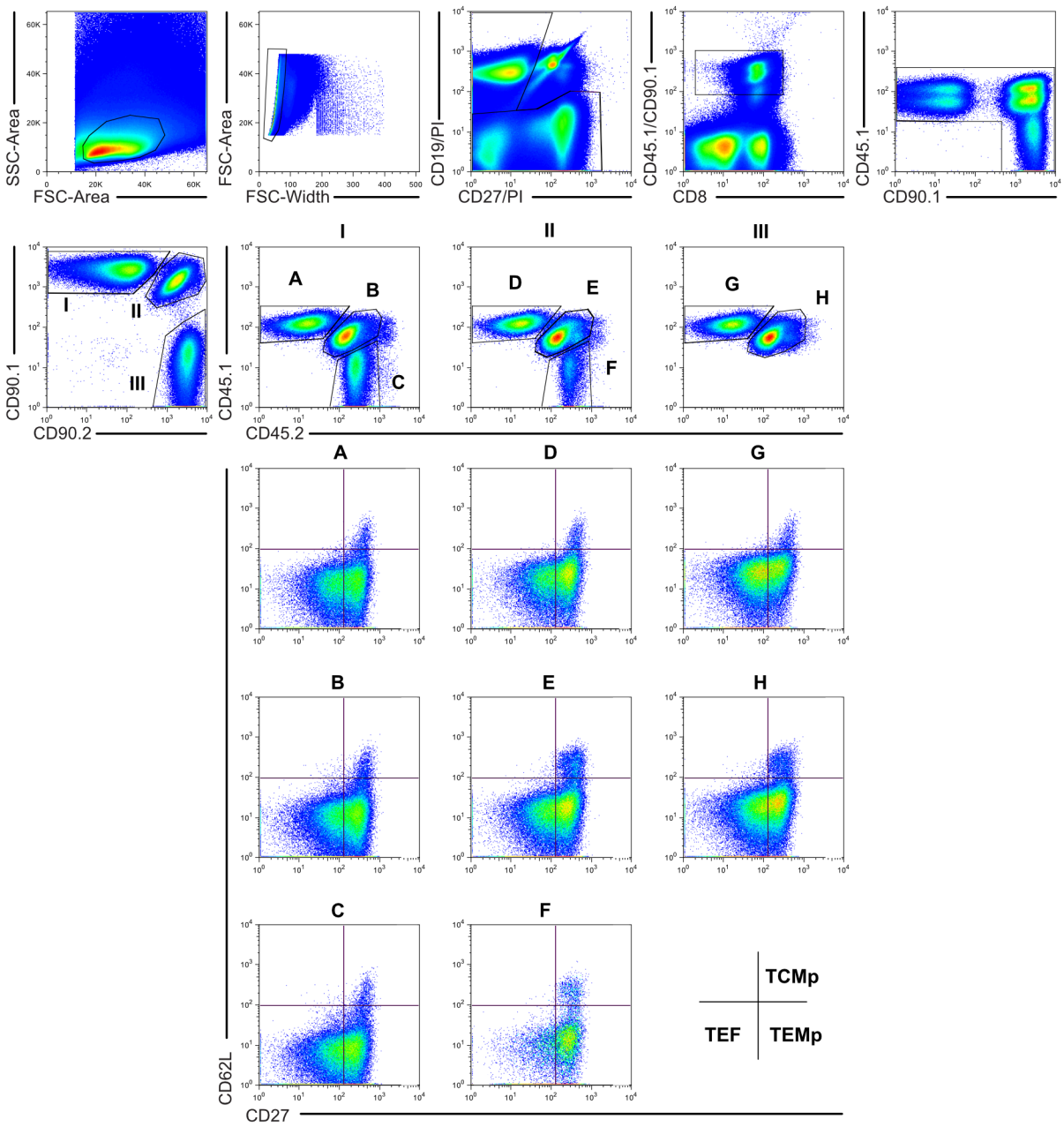

Figure 1: Identification and phenotyping of T cell families by congenic barcoding

Full gating strategy for the detection and phenotyping of single-cell derived T cell responses. A gating control of a representative mouse transferred with 8x100 OT1 T cells and *L.m.*-N4 infection is shown. Modified from (Leube, 2017).

We found that T cell expansion is strongly influenced by TCR avidity, with population-derived responses toward *L.m.*-N4 reaching a 155-fold greater absolute size than responses to *L.m.*-T4 (Figure 2B left panel). In contrast to the population-derived responses, single-cell derived responses to the APLs displayed extreme size variability (Figure 2B right panel): While 100-cell derived responses against *L.m.*-Y3 or *L.m.*-T4 were predictably smaller, single-cell derived responses against *L.m.*-Y3 or *L.m.*-T4 could be larger than single-cell responses against *L.m.*-N4. The expansion differences found on the population level were accompanied by a

difference in the correlation between response size and frequency of TCMp cells (Figure 2C). Population derived responses to *L.m.*-N4 are large and have a lower frequency of TCMps, whereas responses to *L.m.*-Y3/T4 are smaller, show higher variability and a higher frequency of TCMps (Figure 2C). In contrast the correlations between size and frequency of TCMp cells were largely overlapping for single-cell derived responses, showing that the principle differentiation pathway was not altered in between *L.m.*-APL infection (Figure 2C, right panel).

100 cell-derived responses constitute the averages of multiple single cell-derived responses and are therefore reliable in their size and phenotypic composition. However, population derived responses to lower avidity APLs appeared less reliable and showed a higher degree of variability than their high-avidity counterparts (Figure 2B). Moreover, we were surprised to find a large discrepancy in the expansion differences induced by high- and low-avidity ligands of 155-fold vs. 17-fold for population- vs. single-cell derived responses, respectively (Figure 2B). These findings could be explained if fewer individual T cells are recruited to participate in the responses against *L.m.*-Y3 and *L.m.*-T4 compared to *L.m.*-N4. This would affect only the sizes of population-derived responses but not that of the detected T cell families. Indeed, we found that the efficiency with which we could recover T cell families responding *L.m.*-Y3 and *L.m.*-T4 was significantly reduced compared to *L.m.*-N4 infection, hinting at decreased T cell recruitment upon low avidity TCR stimulation (Figure 2D, E).

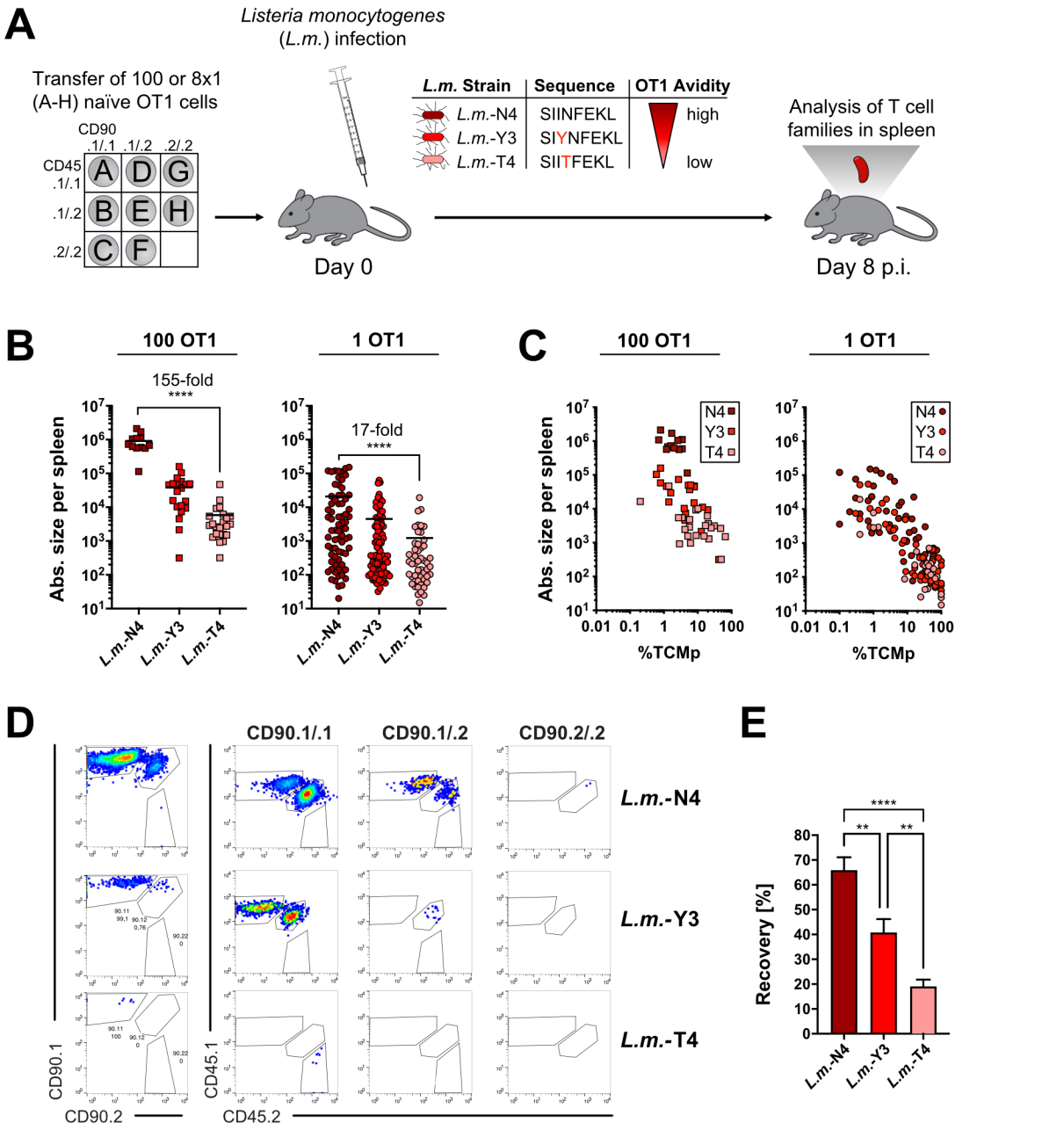

Figure 2: TCR avidity influences expansion, phenotype, and recovery of CD8⁺ T cells

(A) 100 or 8x1 naive OT1 T cells were transferred into C57BL/6 mice followed by infection with 5000 CFU *L.m.*-N4, *L.m.*-Y3 or *L.m.*-T4. Analysis of expanded T cell populations was performed at day 8 post infection. (B) Absolute cell numbers of 100 cell (left panel) and single-cell derived responses (right panel) in the spleen of recipient mice. (C) Correlation between absolute cell numbers and percentage of TCMp cells for immune responses derived from 100 (left panel) or single naive OT1 T cells (right panel). (D) Representative pseudo color plots showing the detection of single-cell-derived T cell responses after *L.m.*-N4, *L.m.*-Y3 and *L.m.*-T4 infection. (E) Corresponding bar graph depicts the percentage of recovered single cell-derived T cell families. 100 cell derived data are compiled from at least 3 experiments with at least n=4 mice per group. Single-cell transfer data are compiled from 4-5 independent experiments with at least n=5 mice per group. Lines indicate the mean, error bars the SEM. Significances in are calculated using one-way ANOVA (Kruskal-Wallis) and Dunn's multiple comparison test. **P* < 0.05, ***P* < 0.01, ****P* < 0.001, *****P* < 0.0001. Modified from (Leube, 2017).

4.1.2 The avidity of the priming stimulus modulates T cell recruitment into the immune response

The failure to recover single-T-cell derived progeny could be due to two factors: 1) T cells could proliferate not at all, which would mean that they were not recruited into the immune response. 2) T cells could proliferate insufficiently, leaving their progeny so small that it was not detected despite successful recruitment. To discern if the detected differences in recovery efficiency are best explained by technical challenges to detect small progenies or if they correspond to differential T cell recruitment, we developed a flow cytometric assay to detect unrecruited T cells directly. We defined that unrecruited T cells should possess a naive (undivided, $CD44^{low}$) phenotype. To measure recruitment efficiency, we transferred equal numbers of CellTrace Violet (CTV) labeled OT1 and antigen-unspecific P14 T cells, sharing one congenic marker (CD45.1) for enrichment while being distinguishable by a second (CD90.1). As antigen-unspecific T cells are not recruited during infection, we used them as an internal control for antigen-specific T cell recruitment. Inherently, unrecruited T cells are exceedingly rare; therefore, efficient enrichment of this population is needed. On day 8 p.i. we harvested spleen, lymph nodes (inguinal, axillary, mesenteric, iliac), blood and bone marrow and enriched $CD45.1^{+}$ cells by flow cytometric speed enrichment. For speed enrichment, a fluorescence trigger is set instead of a scatter trigger, by which particles with a fluorescence below this value are ignored by the cytometer, thereby reducing the consumption of electronic hardware resources and enabling dramatically increased sample flow rates compared to other flow cytometric approaches. Achievable enrichment factors are dependent on the target cell frequencies, being especially high for low target cell frequencies (Figure 3A, B).

Upon infection with *L.m.*-N4 OT1 T cells are efficiently recruited into the immune response, as described by van Heijst et al. (Figure 3C, D, E). Of note, the number of recovered undivided antigen unspecific T cells is also reduced after infection (Figure 3C and D). This highlights the importance of using an internal control to reliably measure T cell recruitment. By calculating the recruitment efficiency factoring in this internal control we measure slightly reduced but comparable OT1 recruitment to the published results (Figure 3E) (van Heijst et al., 2009).

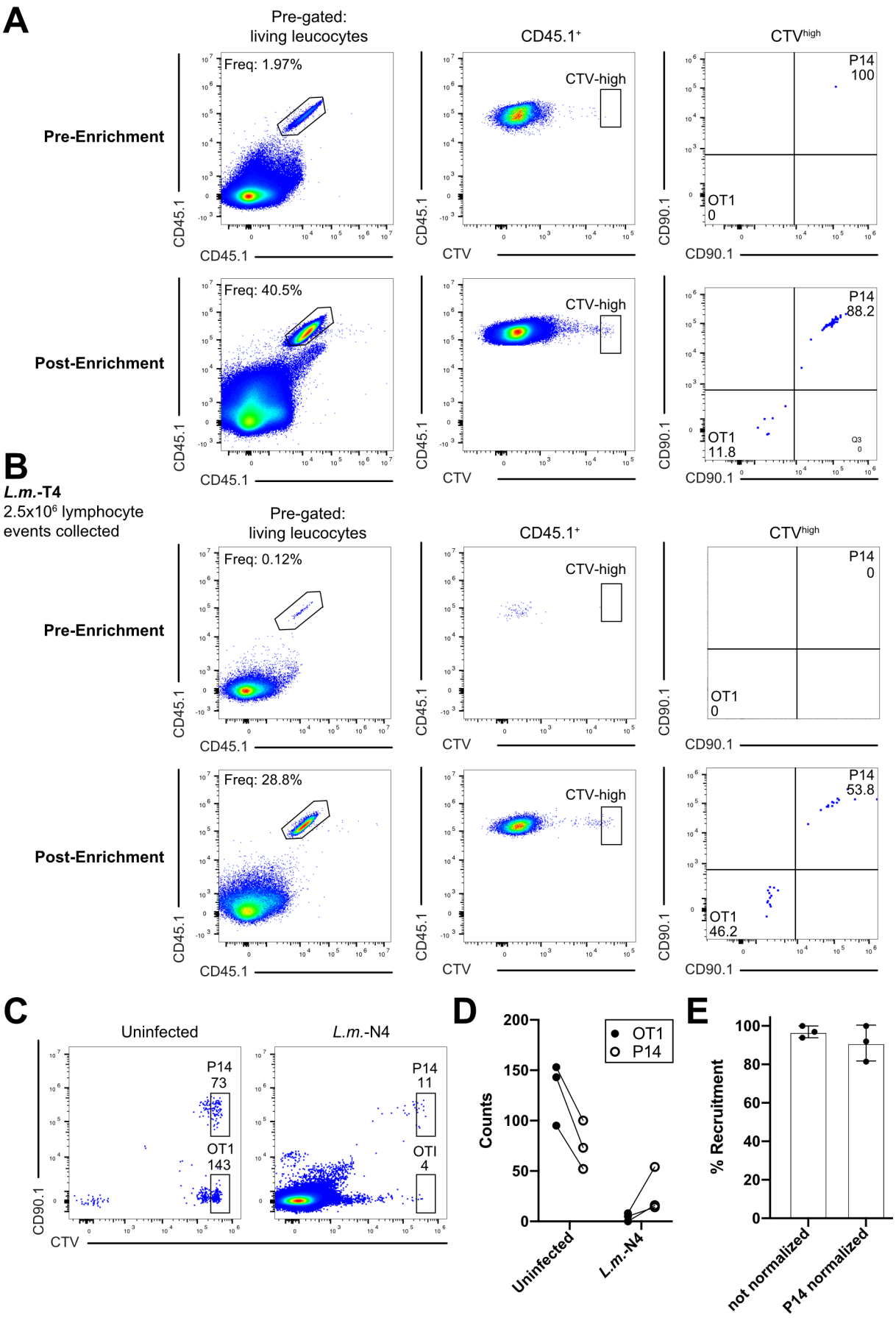

Figure 3: Establishment of a flow cytometric assay to measure T cell recruitment

Detection of undivided T cells before and after speed enrichment. Equal cell numbers of *L.m.*-N4 (A) and *L.m.*-T4 (B) enriched and unenriched samples were collected. The enrichment efficiency is indicated by the frequency of $CD45.1^+$ cells among live leucocytes in the pre-enrichment (upper row) and post-enrichment (lower row) setting. (C) Pseudo color plots show the counts of undivided OT1 and P14 cells in an exemplary uninfected (left) and *L.m.*-N4 infected mouse (right). (D) Quantification of undivided OT1 and P14 cells in uninfected and *L.m.*-N4 mice, values obtained from the same mouse are connected by a line. (E) Calculated recruitment efficiencies with and without taking into account normalization to the P14 control population as described in the methods section. Data are representative of two experiments with n=2-3 mice per group. The bar graph shows the mean, error bars represent the SD.

Using the described method, we analyzed the recruitment efficiency upon *L.m.*-N4/Y3/T4 infection (Figure 4A). While the ratio of undivided $CD44^{low}$ OT1 and P14 cells remained unchanged in uninfected mice, OT1 T cells were efficiently recruited after infection with *L.m.*-N4. With decreasing avidity of the priming stimulus, higher frequencies of undivided $CD44^{low}$ OT1 cells could be found (Figure 4B, D). Crucially, undivided OT1 and P14 cells showed similar levels of CD44 expression and were $CD44^{low}$ in comparison to divided OT1 T cells, highlighting that these cells had not been activated (Figure 4C). Using the transferred P14 cells as an internal control, we determined the efficiency of OT1 recruitment to be 85 % after infection with L.m.-N4. This recruitment efficiency was decreased to roughly 70 % after L.m.-Y3 and 40 % after L.m-T4 infection (Figure 4E). We could thus confirm that T cell recruitment is dependent on TCR avidity, and that the discrepancy in recovery of single-T-cell-derived progenies between *L.m.*-N4, -Y3 and -T4 infected mice can largely be explained by this difference.

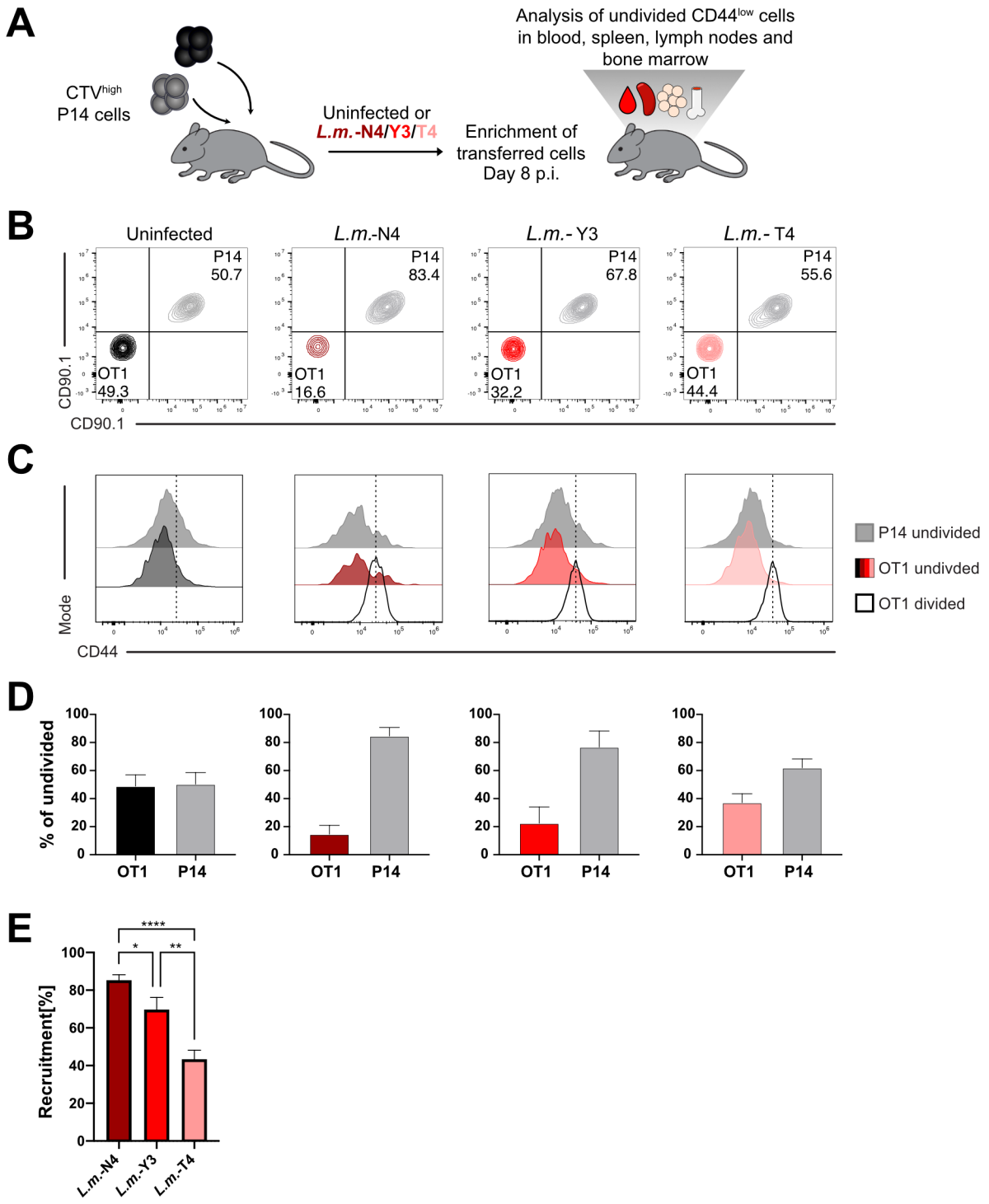

Figure 4: Low avidity T cell priming leads to impaired recruitment of antigen-specific CD8⁺ T cells

(A) 2.5 x 10^4 CTV labeled naive OT1 (CD45.1⁺ CD90.1⁻) and P14 (CD45.1⁺ CD90.1⁺) cells were co-transferred into C57BL/6 mice followed by infection of recipients with 5000 CFU *L.m.*-N4, *L.m.*-Y3 or *L.m.*-T4. On day 8 p.i. blood, spleen, lymph node and bone marrow cells were enriched for CD45.1⁺ cells and analyzed for the presence of unrecruited (undivided CD44^{low}) cells. (B) Representative contour plots showing the frequency of OT1 and P14 cells among undivided CD45.1⁺ CD44^{low} live CD8⁺ T cells. (C) Histograms depict CD44 expression among undivided P14, undivided OT1 and divided OT1 T cells. The dotted line indicates the CD44 geo-MFI of the OT1 divided population. For the uninfected setting, the CD44 geo-MFI values

of the N4 setting was used. (D) Bar graphs show the percentage of OT1 and P14 cells among undivided CD44^{low} live CD8^{+} T cells. (E) Bar graphs depicts the efficiency of T cell recruitment, calculated from the measured OT1 to P14 ratios from infected and uninfected mice shown in B-D. Data are compiled from 4 independent experiments with n=3 mice per group. Lines indicate the mean, error bars the SD (D) or SEM (E). Significances in are calculated using one-way ANOVA (Kruskal-Wallis) and Dunn's multiple comparison test. *P < 0.05, **P < 0.01, ***P < 0.001, ****P < 0.0001.

4.1.3 T cells harboring TCRs of unique avidity are differentially recruited into the primary response

Since amino acid exchanges in epitopes affect the interaction toward a given TCR as well as the MHC molecule, they could also lead to differences in antigen presentation efficiency, thus contributing to changes in signal strength independent of TCR binding strength. We consolidated our finding with two TCRs with unique avidities toward the wildtype SIINFEKL epitope to circumvent this potential drawback. In addition to the OT1 transgenic line, we made use of OT3 mice. The OT3 TCR was isolated as a TCR that escapes negative selection in Vβ5xRip-mOva mice. It shows similar functional avidity as OT1 T cells responding to the T4 APL (Enouz et al., 2012).

We again transferred equal numbers of CTV labeled OT1 or OT3 and P14 T cells into naive recipients. We isolated and enriched these cells on day 8 p.i. from *L.m.*-N4 or uninfected mice by speed enrichment as described (Figure 5A). The expansion differences between OT1 and OT3 cells were within the observed range of the population-derived responses of OT1 T cells to *L.m.*-N4 or *L.m.*-T4 (Figure 5B). Again, OT1 T cells were recruited efficiently into the immune response (Figure 5C). In comparison, recruitment of OT3 T cells was substantially lower and mirrored the recruitment efficiency of OT1 T cell in response to *L.m.*-T4 infection (Figure 5C, E and F). Additionally undivided OT1 and OT3 cells showed a CD44^{low} phenotype compared to their divided counterparts confirming their naive phenotype (Figure 5D).

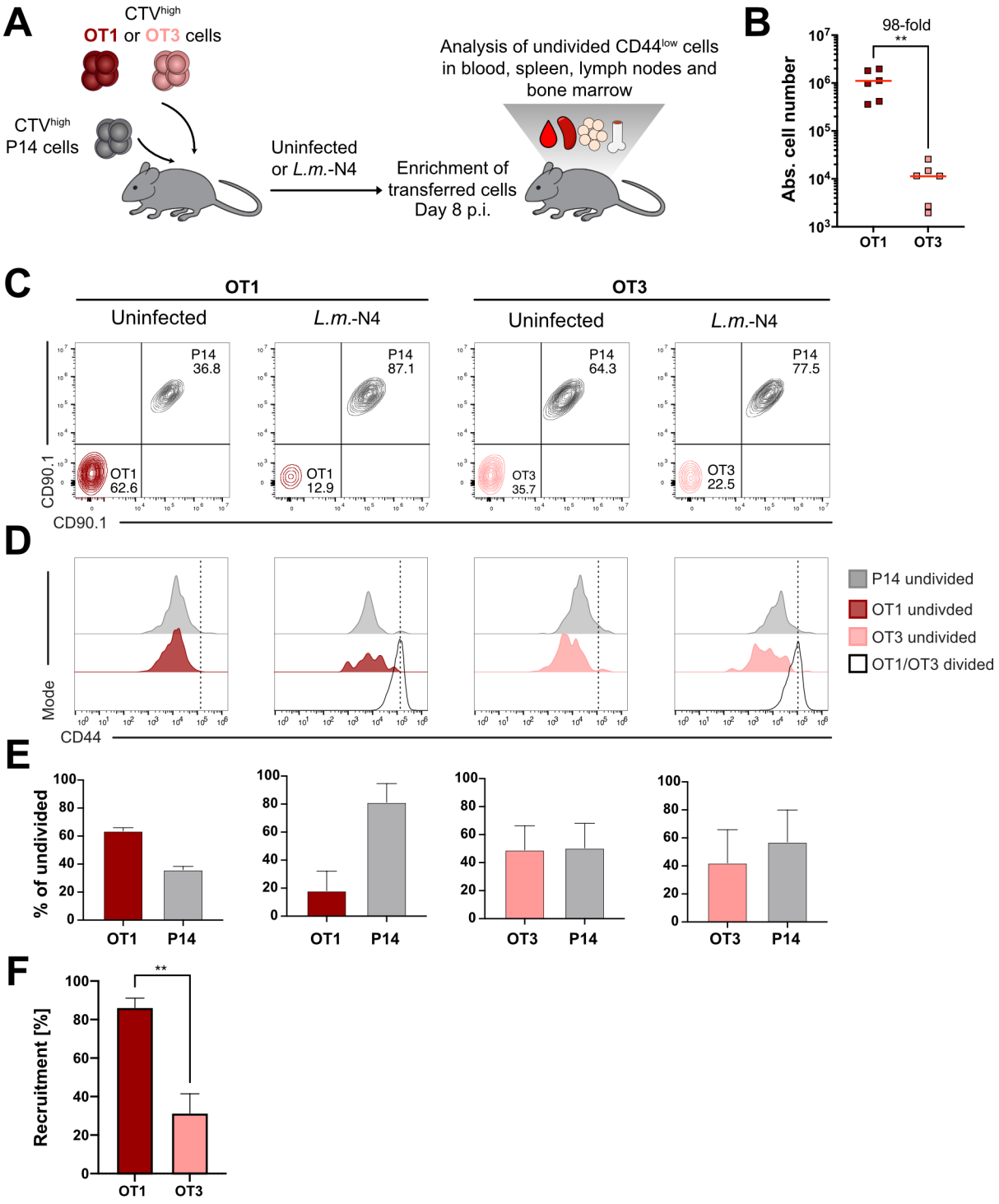

Figure 5: T cells harboring TCRs of unique avidity are differentially recruited into the primary response

(A) 2.5 x 10^4 CTV labeled naive OT1 or OT3 (CD45.1$^+$ CD90.1$^-$) were co-transferred with 2.5 x 10^4 CTV labeled naive P14 (CD45.1$^+$ CD90.1$^+$) cells into C57BL/6 mice followed by infection of recipients with 5000 CFU *L.m.*-N4. On day 8 p.i. blood, spleen, lymph nodes and bone marrow cells were enriched for CD45.1$^+$ cells and analyzed for the presence of unrecruited (undivided CD44^{low}) cells. (B) Absolute cell numbers of recovered OT1 and OT3 cells after enrichment. (C) Representative contour plots showing the frequency of OT1, OT3 and P14 cells among undivided CD45.1$^+$ CD44^{low} live CD8$^+$ T cells. (D) Histograms depict CD44 expression among undivided P14, undivided OT1 or OT3 and divided OT1 or OT3 T cells. The dotted line indicates the CD44 geo-MFI of the OT1 or OT3 divided population. For

the uninfected setting, the CD44 geo-MFI values of the corresponding OT1 or OT3 divided setting was used. (E) Bar graphs show the percentage of OT1, OT3 and P14 cells among undivided $CD44^{low}$ live $CD8^{+}$ T cells. (F) Bar graphs depicts the efficiency of T cell recruitment, calculated from the measured OT1 or OT3 to P14 ratios from infected and uninfected mice shown in C-E. Data are compiled from 2 independent experiments with n=3 mice per group. Lines indicate the mean, error bars the SD (E) or SEM (F). Significances in (F) are calculated using t-Test (Mann-Whitney). *P < 0.05, **P < 0.01, ***P < 0.001, ****P < 0.0001.

4.1.4 T cell clones left unrecruited during the primary response can enter the response to heterologous high-avidity secondary infection

We found that the majority of low-avidity T cells was left unrecruited during a primary response. Naturally, the question arose if these cells were functional and capable of participation in a secondary response. For $CD4^{+}$ T cells it had been shown that subthreshold stimulation can led to the induction of anergy (Korb et al., 1999; Mirshahidi et al., 2004). However, the lack of proliferation and maintenance of a $CD44^{low}$ phenotype suggested that these cells had retained a naive phenotype, akin to clonal ignorance which had previously been described in the context autoimmunity and tumor diseases (Ochsenbein, 2005; Salaman & Gould, 2020). To distinguish between these two possible fates, we aimed to determine if T cells that remained unrecruited during a primary response could enter a response to a heterologous secondary infection with a high-avidity antigen.

To answer this question, we needed to efficiently track the clonality of an antigen specific T cell population longitudinally during primary and secondary infection. To ensure the efficiency of this analysis we combined the congenic- (Buchholz et al., 2013) and retrogenic color-barcoding (Grassmann et al., 2019, 2022) approaches. In brief, we introduced a retrogenic color-barcode in the HSCs of five OT1 strains expressing different combinations of congenic markers. This yielded 10-20 unique color-barcodes in each of the resulting congenically distinct chimeras. By use of these congenic color-barcoded OT1 retrogenic mice we were able transfer up to 85 uniquely barcoded OT1 T cells into one recipient. The gating strategy to detect the transferred clones can be seen in Figure 6A and 6B for one *L.m.*-N4 and one *L.m.*-T4 infected mouse, respectively.

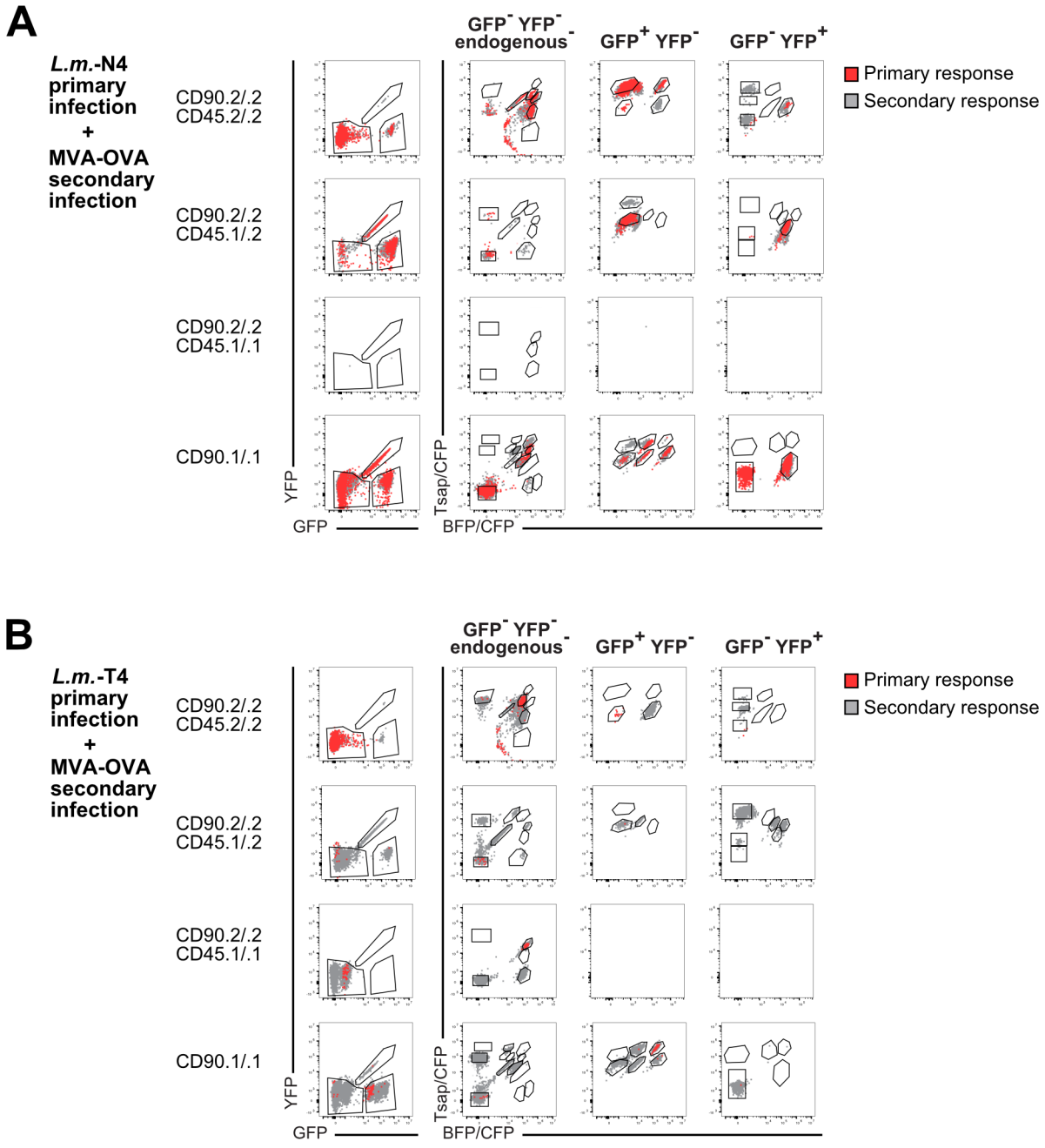

Figure 6: Identification of T cell families by combination of congenic and retrogenic color-barcoding

Exemplary gating for the detection of transferred single OT1 T cell-derived responses. The primary response (red) was overlaid over the secondary response (grey) for a representative mouse of the *L.m.*-N4 (A) and *L.m.*-T4 group (B). T cell clones were distinguished by their combinatorial color-congenic barcode: first by gating on their congenic marker combination and then and then their unique color-barcode (GFP and YFP (left) followed by BFP/CFP and T-Sap/CFP (right)). Note: the 90.1/.1 population displayed in this figure contained only unique color- barcodes and was therefore not further segregated into CD45.1/.1 and CD45.1/.2 subpopulations. The plots show data from one representative mouse of each experimental group of the experiment described in Fig. 7.

Results

After infection with *L.m.*-N4 or *L.m.*-T4 we sampled these T cell responses on day 8 p.i. by hemisplenectomy. In this surgical method, we remove approximately 1/4 of the spleen to sample and phenotypically characterize single-cell-derived T cell families. At this timepoint T cell families are equally distributed throughout the spleen (Tubo et al., 2016). One month after primary infection we performed heterologous secondary infection with MVA-OVA and analyzed the responses on day 8 p.i. (Figure 7A).

On day 8 after primary infection, we could detect 204 out of 809 transferred clones after *L.m.*-N4 infection (Figure 7B top panel) but only 83 out of 1259 transferred clones in *L.m.*-T4 infected mice (Figure 7C top panels). As shown before, single-cell derived responses to *L.m.*-N4 were significantly larger than those to *L.m.*-T4 (Figure 7D, left panel). Furthermore, the recovery rate of T cell families was significantly higher after *L.m.*-N4 than *L.m.*-T4 infection, indicating more efficient T cell recruitment (Figure 7D, left panel).

After secondary infection with high-avidity antigen, we could detect T cell families with a similar recovery rate regardless of the avidity of the priming stimulus (Figure 7D, right panel). Exemplary dot plots show the recall responses of previously recruited as well as the entry of new clones after secondary infection (Figure 7B and C top vs lower panels). In these plots red gates show transferred but undetected clones on day 8 p.i.. In addition to recovery, the median response size was also equal in between the experimental groups (Figure 7D).

In summary, previously unrecruited T cells entered the MVA-OVA response in substantial numbers (Figure 7B,C lower panel), especially in low-avidity primed animals. This showed that unrecruited T cells remain functional and persist in a state of clonal ignorance. Furthermore, in the high-avidity primary – high-avidity secondary infection group, the presence of high-avidity memory T cells did not preclude previously unrecruited high-avidity T cells from entering the secondary response. This finding is in line with population derived data showing that naive high-avidity T cells are capable of expansion in a heterosubtypic re-infection, whereas expansion of low-avidity T cells is drastically suppressed by competitive effects (Oberle et al., 2016).

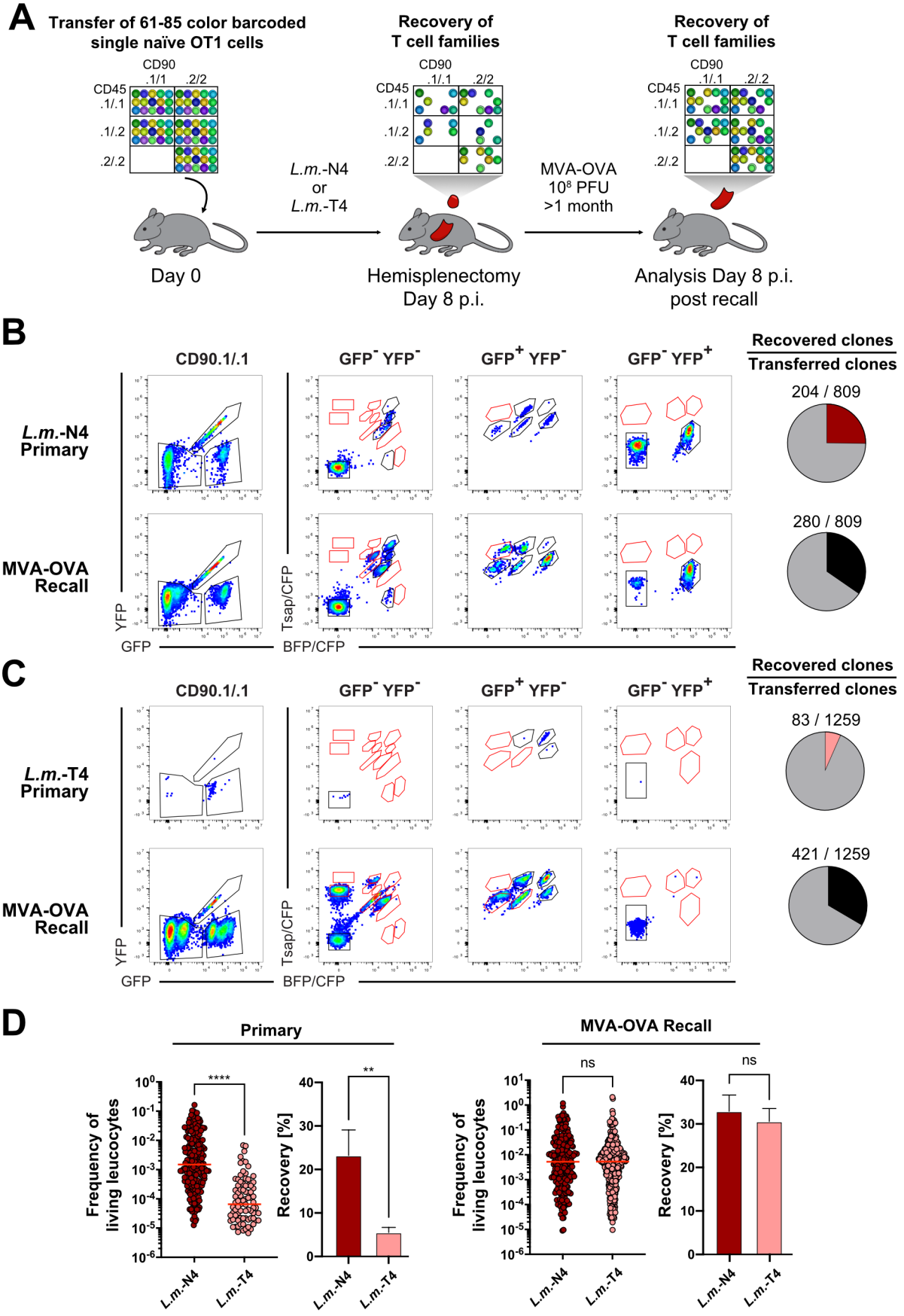

Figure 7: T cell clones left unrecruited during the primary response can enter the response to heterologous high-avidity secondary infection

(A) 61-85 uniquely barcoded single naive OT1 T cells were transferred into CD11c-DTR-GFP recipients followed by infection with 5000 CFU *L.m.*-N4 or *L.m.*-T4. Recovery and size of individual T cell clones were initially assessed by hemi-splenectomy on day 8 p.i. Secondary responses within the same recipients were then assessed on day 8 after a heterologous challenge with 10^8 PFU MVA-OVA. (B) Quantification and representative pseudo color plots showing detection of T cell clones on day 8 after primary infection with *L.m.*-N4 (upper row) and post MVA-OVA challenge (lower row). (C) Same as is (B), but for primary infection with *L.m.*- T4. (B-C) T cell clones were distinguished by their combinatorial color-congenic barcode: first by gating on their congenic marker combination and then and then their unique color-barcode (GFP and YFP (left) followed by BFP/CFP and T-Sap/CFP (right)). Note: the 90.1/.1 population displayed in this figure contained only unique color-barcodes and was therefore not further segregated into CD45.1/.1 and CD45.1/.2 subpopulations (a gating strategy containing all congenic-color combinations is included in Fig. 6). Red gates represent barcodes of transferred single cells, where no progeny was recovered in the shown recipient on day 8 p.i. Pie charts show the ratio of recovered to transferred single T cells. (D) Scatter plots depicting the response size and bar graphs depicting the percentage of recovered single T cell clones after primary infection (left panel) and after secondary infection (right panel). Data are compiled from 5 independent experiments with n=3 mice in the *L.m.*-N4 and n=4 mice in the *L.m.*-T4 group. Lines in the scatter plot indicate the median, bar graphs indicate the mean and SEM. Significances in (D) are calculated using t-Test (Mann-Whitney). $*P < 0.05$, $**P < 0.01$, $***P < 0.001$, $****P < 0.0001$.

We analyzed the clonal recovery on day 8 after secondary infection to allow for maximum expansion and efficient detection of newly recruited T cells. As responses to secondary infection peak earlier than primary responses, expansion differences between *L.m.*-N4 and *L.m.*-T4 primed T cell populations could be masked at day 8 after secondary infection. Therefore, we additionally examined the responses of T cell families on day 4 after secondary infection (Figure 8A). At this timepoint, expansion differences generated by differential-avidity priming were maintained (Figure 8B). Of note, we still observed differences in recovery at this timepoint in contrast to day 8 after secondary infection. Comparing the relative response size changes from day 4 to day 8 after secondary infection in between the experimental groups we could show that high-avidity primed – high-avidity secondary responses did not increase in size significantly between these timepoints. In contrast, low-avidity primed – high-avidity secondary responses showed an increase in relative response size of roughly 8-fold between day 4 and day 8 after secondary infection (Figure 8C). Therefore, the response kinetic after secondary infection was dependent on the avidity of the priming stimulus.

Together these findings implicate that the delayed response kinetic in the low-avidity primed – high-avidity secondary infection group arises because the response is initiated from fewer memory T cells (amount and number of clones) and newly recruited cells only significantly contribute to response size at later timepoints.

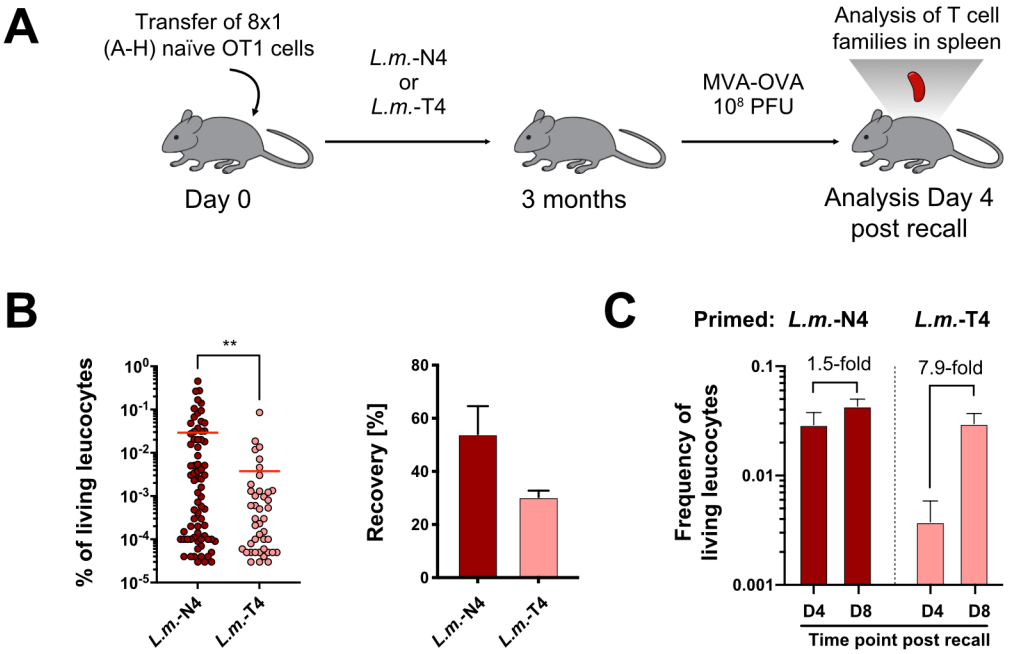

Figure 8: Distinct dynamics of responses to secondary infection following high- or low-avidity T cell priming

(A) 8x1 naive OT1 T cells were transferred into C57BL/6 recipients followed by infection with either *L.m.*-N4 or *L.m.*-T4. Three months after primary infection the recipients infected with MVA-OVA and the response assessed on day 4 after secondary infection. (B) Response size and recovery of single T cell-derived responses after secondary infection. (C) Change in response size between day 4 and day 8 after secondary infection in *L.m.*-N4 and *L.m.*-T4 primed responses. Day 4 post MVA-OVA infection data are derived from 2 independent experiments with n=6 mice per group, day 8 post MVA-OVA infection data are taken from the hemisplenectomy experiment shown in Fig. 7. Lines in the scatter plot indicate the mean, bar graphs show the mean with error bars indicating the SEM.

Previously it had been shown for population derived immune responses, that response sizes to *L.m.*-N4 and *L.m.*-T4 were highly distinct after primary infection but were virtually identical after heterologous secondary infection with high-avidity antigen (Zehn et al., 2009), which we could confirm for the average expansion of T cell families. However, we found that TCR avidity-dependent recruitment leads to a previously unrecognized heterogeneity of secondary responses on a clonal level. In high-avidity primed – high-avidity secondary responses, 36 % of contributing clones were newly recruited, in contrast to low-avidity primed – high-avidity secondary responses where 82 % of responding clones were newly recruited (Figure 9A). The response size of recalled T cell families was significantly larger than the response of clones newly recruited during secondary infection. Importantly, the response size of newly recruited clones was not significantly different between the experimental conditions and corresponded to the median response size of single-cell derived primary responses to MVA-OVA (Figure 9B). While most of the secondary response size is derived from memory T cell responses, the clonality of the response is substantially diversified by the entry of new T cell clones (Figure 9C). Phenotypically, recalled clones show a more effector differentiated profile as had been

described by Plumlee and colleagues, while newly recruited clones possess higher frequencies of memory precursor and effector memory cells (Figure 9D) (Plumlee et al., 2013).

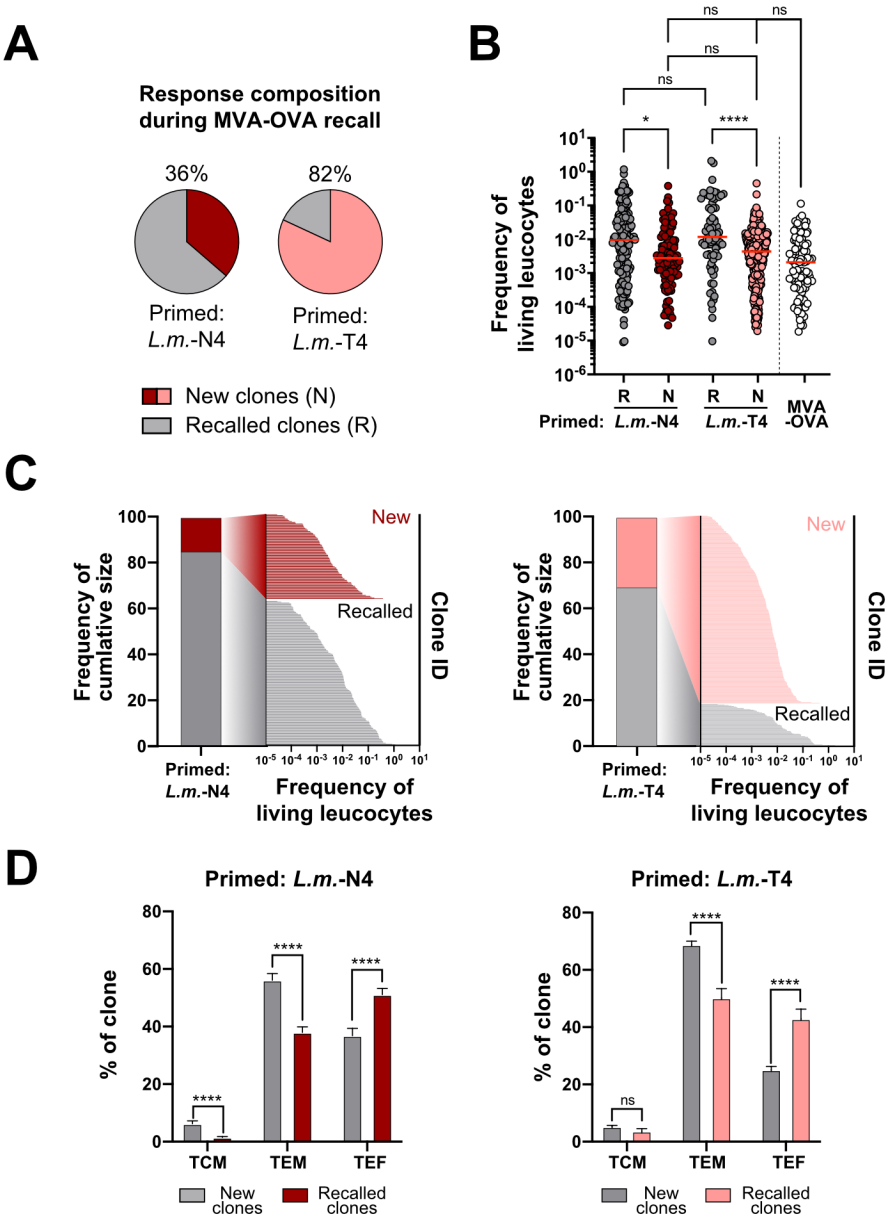

Figure 9: Low-avidity primed – high-avidity secondary T cell responses are mainly comprised of newly recruited T cell clones

The experimental data corresponds the experiments described in Fig. 7. (A) Pie charts show the percentage of recalled (R) and newly recruited (N) clones after MVA-OVA secondary infection. (B) Response size of recalled and newly recruited T cell clones in comparison to single cell-derived primary responses to MVA-OVA infection. (C) Contribution of newly recruited and recalled clones to cumulative response size and clonal composition after *L.m.*-N4 (left) or *L.m.*-T4 priming (right). The bar graphs show the contribution of recalled and newly recruited clones to the cumulative response size of all recovered T cell clones (left y-axis). The line graphs show the response size of each detected clonal response (x-axis), as well as the number of detected responses (right y-axis). Clones are colored according to their status as new clones or recalled clones. (D) Average phenotypic composition of recalled and newly recruited T cell clones in *L.m.*-N4 (left) and *L.m.*-T4 (right) primed mice. Data are compiled from 5 independent experiments with n=3 mice in the *L.m.*-N4 and n=4 mice in the *L.m.*-T4

group and 2 independent experiments with n=8 mice (MVA-OVA primary). Lines indicate in the scatter plot indicate the median, bar graphs show the mean and error bars the SEM. Significances in (B) are calculated using one-way ANOVA (Kruskal-Wallis) and Dunn's multiple comparison test. Significances in (D) are calculated using multiple unpaired t-Test (Welch t-Test). *P < 0.05, **P < 0.01, ***P < 0.001, ****P < 0.0001

4.2 Influence of TCR avidity on CD4$^+$ T cell fate

4.2.1 Viral persistence and infectious dose shape CD4$^+$ T cell differentiation and expansion

Upon viral infection, helper T cells mainly undergo Th1 and Tfh differentiation shaped by multiple environmental factors (Vella et al., 2017). In the LCMV infection model, viral persistence and antigen load can be modified by choice of strain and infectious dose (Parish et al., 2014; Zhou et al., 2012). While the LCMV Armstrong strain causes an acutely resolving infection, LCMV CL13 infection leads to a chronic infection characterized by high antigen loads and T cell exhaustion (Crawford et al., 2014; Matloubian et al., 1993). CD4$^+$ T cells specific for the IA(b) GP66-77 epitope undergo substantial expansion after LCMV Armstrong infection peaking around day 8 p.i. followed by strong contraction into the memory phase after viral clearance (Figure 10A). In comparison, expansion is reduced after LCMV CL13 infection, and antigen-specific T cells persist at roughly the same frequency into the chronic infection phase (Figure 10A).

To establish a phenotypic staining panel to characterize CD4$^+$ T cell responses to LCMV we analyzed CD4$^+$ specific for the IA(b) GP66-77 epitope by tetramer staining for expression of the markers CXCR3, CXCR5, CXCR6, PD1, TIM3 and CCR7. To validate CXCR6 as a surrogate marker for IFN-γ expression we infected SMART-GREAT-VertX (SGX) mice, which express reporters for IL-17A, IFN-γ and IL-10 with LCMV Armstrong. Th1 differentiation is characterized by the expression of IFN-y, which correlates strongly with CXCR6 expression (Figure 10C). Unsupervised clustering using the FlowSOM algorithm (van Gassen et al., 2015) revealed three phenotypic clusters upon LCMV infection (Figure 10B). All clusters shared CXCR3 expression, which was disregarded for further analysis. TCMp cells were characterized by CCR7 expression and low to intermediate expression of CXCR5. Tfh cells could be identified as CCR7$^-$ CXCR5$^+$ CXCR6$^-$ and Th1 cells as CCR7$^-$ CXCR5$^-$ CXCR6$^+$.

In contrast to acute infections, Th1 cells show upregulation of the inhibitory receptor TIM3 at early time points during chronic infection (Figure 10B). Tfh differentiation, was relatively increased after infection with LCMV CL13. The proportion of Tfh cells further increased with time after LCMV CL13 infection at the expense of Th1 cells (Figure 10B). TCMp cells, were largely absent after infection with LCMV CL13. However, they made up a large part of the

antigen-specific T cell pool in the memory phase of LCMV Armstrong infection and could additionally be identified at the peak of infection (Figure 10B).

In contrast to the establishment of chronic infection after infection with intermediate or high doses of LCMV CL13 infection, low dose infection leads to an acutely resolving response similar to LCMV Armstrong infection (Parish et al., 2014; Stamm et al., 2012). The effects of antigen persistence on T cell differentiation could also be observed using this acute model of LCMV CL13 infection. Lower infectious doses allowed more robust expansion of antigen-specific $CD4^+$ T cells in comparison to high dose LCMV CL13 infection (Figure 10D). Additionally, responses of acute LCMV CL13 infection resemble responses to LCMV Armstrong phenotypically, with higher frequencies of Th1 and TCMp cells in comparison to intermediate and high dose LCMV CL13 infection (Figure 10E). Additionally, cells lacking expression of the three main phenotypic markers (CCR7, CXCR6 and CXCR5) are present at higher frequencies in chronic infection (Figure 10E). These cells will be referred to as Th0 as they cannot be assigned to a specific helper type. Most likely they represent Th1 cells that have stopped IFN-γ expression (known to be associated with CXCR6 downregulation).

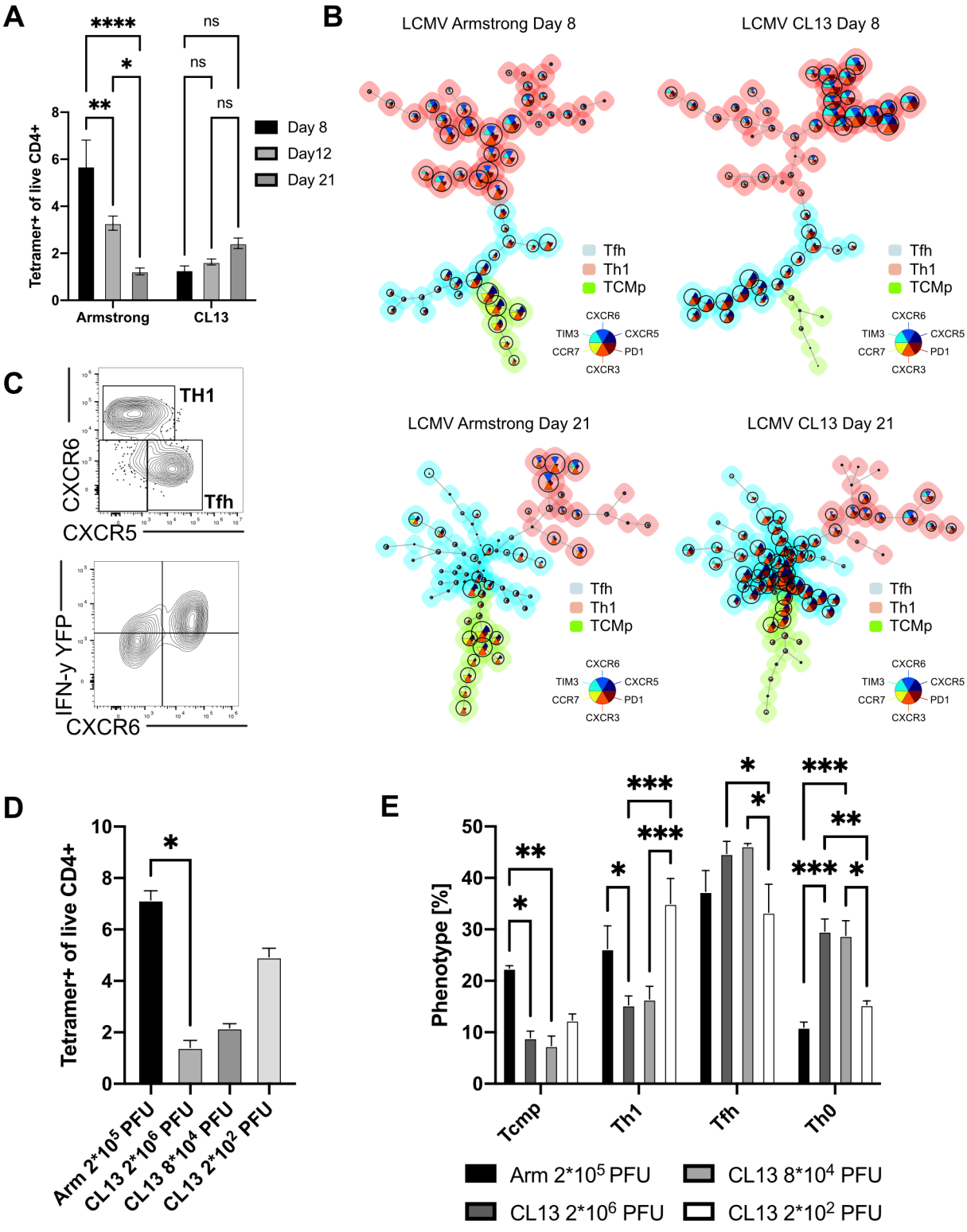

Figure 10: Viral persistence and infectious dose shape CD4⁺ T cell differentiation and expansion

C57BL/6 or SGX mice were infected with LCMV Armstrong (Arm) or LCMV CL13 (CL13) with the indicated doses. The IA(b) GP66-77 specific T cell response was characterized at the indicated time by tetramer staining. (A) Frequency of tetramer⁺ cells among live CD4⁺ T cells at the indicated time points post-infection. (B) Responding CD4⁺ T cells from LCMV Armstrong and LCMV CL13 mice (n=3 per group) were concatenated and clustered by their expression of the phenotypic markers CXCR5, CXCR6, CCR7, CXCR3, TIM3, and PD1 with the FlowSOM

algorithm (van Gassen et al., 2015). The resulting clustering of the self-organizing map (SOM) is visualized as a minimal spanning tree. Pies indicate the expression of a given marker in the corresponding node, while the color indicates the annotation of a node to a given cluster. (C) Contour plots show the discrimination of $CXCR5^+$ Tfh and $CXCR6^+$ Th1 cells and the correlation between IFN-γ and CXCR6 expression in an LCMV Armstrong infected SGX mouse. (D, E) Bar graphs show the frequency and phenotype of $tetramer^+$ cell on day 8 p.i. with LCMV Armstrong or different doses of LCMV CL13. Bar graphs show the mean, error bars indicate SEM. Significances are calculated using one-way ANOVA (Kruskal-Wallis) and Dunn's multiple comparison test(D) or two-way ANOVA (A, E). Data shown are from n=3-6 mice per group. *P < 0.05, **P < 0.01, ***P < 0.001, ****P < 0.0001.

4.2.2 Isolation of TCRs from the naive repertoire towards IA(b) GP66-77

As highlighted in the introduction, the binding strength of a TCR to its cognate pMHC ligand has been shown to influence differentiation into T helper cell subsets. Factors such as TCR affinity, avidity, antigen load and persistence influence the cumulative signal strength T cells receive through their TCR. To study the influence of TCR avidity on $CD4^+$ T cell differentiation in acute and chronic infection, we set out to identify TCRs of varying functional avidity to the LCMV GP66-77 epitope. Such TCRs would allow us to vary the stimulation strength that antigen-specific T cells receive without altering factors such as antigen load and persistence. We could then separate the effects of signal quality and quantity on $CD4^+$ T cell differentiation and revisit the question to what extent a given TCR has a deterministic influence on $CD4^+$ T cell fate decisions.

Previously, TCRs specific to the LCMV GP66-77 epitope have been isolated from a fixed alpha chain mouse model in response to LCMV Armstrong infection (C. Kim et al., 2013). In contrast, we opted to isolate TCRs from the naive repertoire to sample a repertoire of unreduced structural diversity that had not been subjected to selective pressure. By this, we hoped to isolate TCRs from an unreduced spectrum of functional avidities including also TCRs of very low binding strength to the target pMHC.

From naive C57BL/6 mice we sorted single live $CD4^+$ $CD44^{low}$ IA(b) GP66-77^+ T cells into 384-well plates for single clone expansion, after pre-enrichment from total splenocytes by speed enrichment on tetramer binding cells (Figure 11A). Importantly, we stained splenocytes with equimolar concentrations of IA(b) GP66-77 multimerized on Streptavidin-PE or Streptavidin-BV421. By this we hoped to exclude false positive binding cells from the sort as true positive staining shows a linear dependency for both dyes. Sorting gates were established with a spike in control of SMARTA T cells, expressing a TCR specific for the IA(b) GP66-77 epitope (Figure 11B).

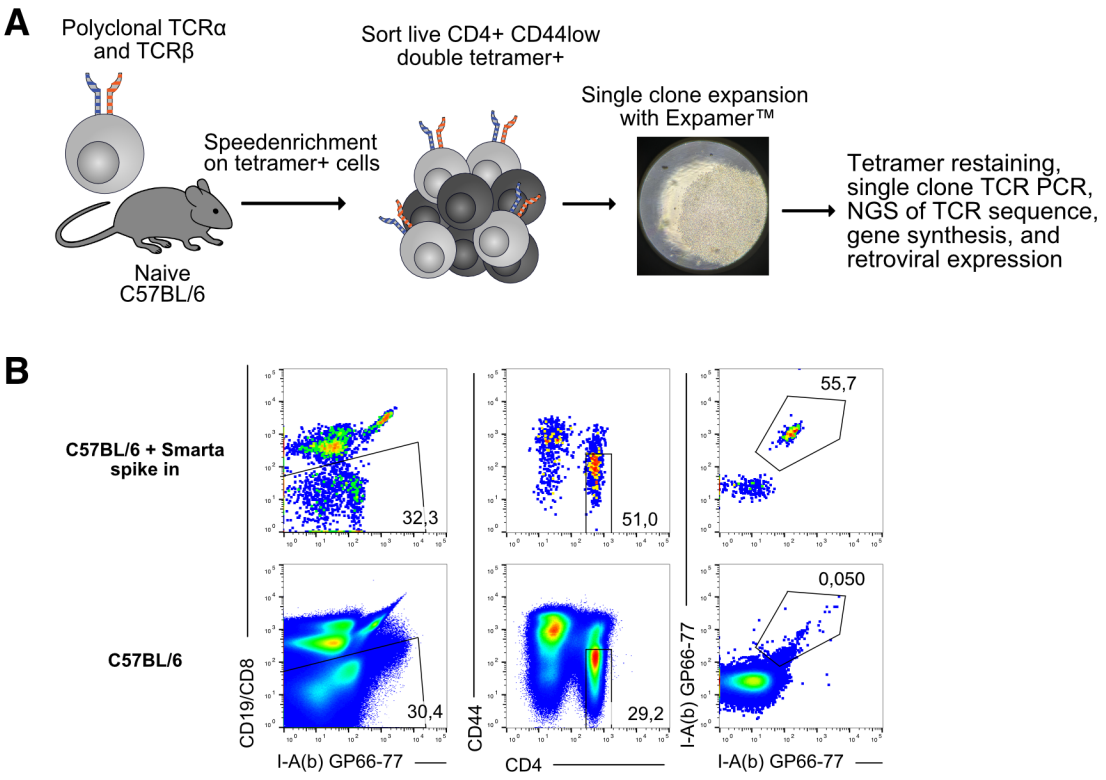

Figure 11: Isolation of TCRs from the naive repertoire towards IA(b) GP66-77

The scheme depicts the isolation strategy for antigen specific TCRs from the naive repertoire. Briefly, Total splenocytes of 3 naive C57BL/6 mice were double tetramer stained (IA(b) GP66-77) and speed enriched for tetramer binding as described in the methods. Live single $CD4^+$ $CD44^{low}$ double $tetramer^+$ cells were sorted into a 384-well plate and expanded using anti-CD3 anti-CD28 stimulation with Expamer. Expanded clones were restrained with IA(b) GP66-77 tetramer, the TCR sequence was amplified by TCR-SCAN RACE PCR and sequenced by NGS. Complete TCR sequences were assembled *in silico*, generated by gene synthesis, and cloned into a retroviral expression vector (A). (B) Sorting strategy for isolating single-naive T cells from the naive repertoire. The top panels show gating setup with Smarta T cell spike-in control; bottom panels show sort data.

Single T cells were expanded using Expamers (Poltorak et al., 2020) and IL-2. Expamers constitute monovalent low-affinity Twin-Step-tagged anti-CD3 and anti-CD28 Fab fragments bound to a polymerized Strep-Tactin backbone. By addition of D-biotin the Fab fragments can be displaced from the backbone, followed by dissociation from the CD3 and CD28 proteins, thereby stopping T cell stimulation. Cells were removed from anti-CD3 anti-CD28 stimulus 12 hours before IA(b) GP66-77 tetramer restraining by addition of D-biotin, to allow for more efficient tetramer re-staining. Tetramer re-staining was performed on expanded clones and compared to tetramer staining of expanded SMARTA and $tetramer^-$ $CD4^+$ T cells to confirm antigen specificity (Figure 12A). After TCR-SCAN RACE PCR (Dössinger et al., 2013), TCR sequences were sequenced by NGS. We chose six TCRs with varying degrees of tetramer re-staining for further characterization and retroviral expression (Figure 12B). Expression

constructs for these TCRs were assembled *in silico*, generated by gene synthesis, and cloned into retroviral expression vectors.

A

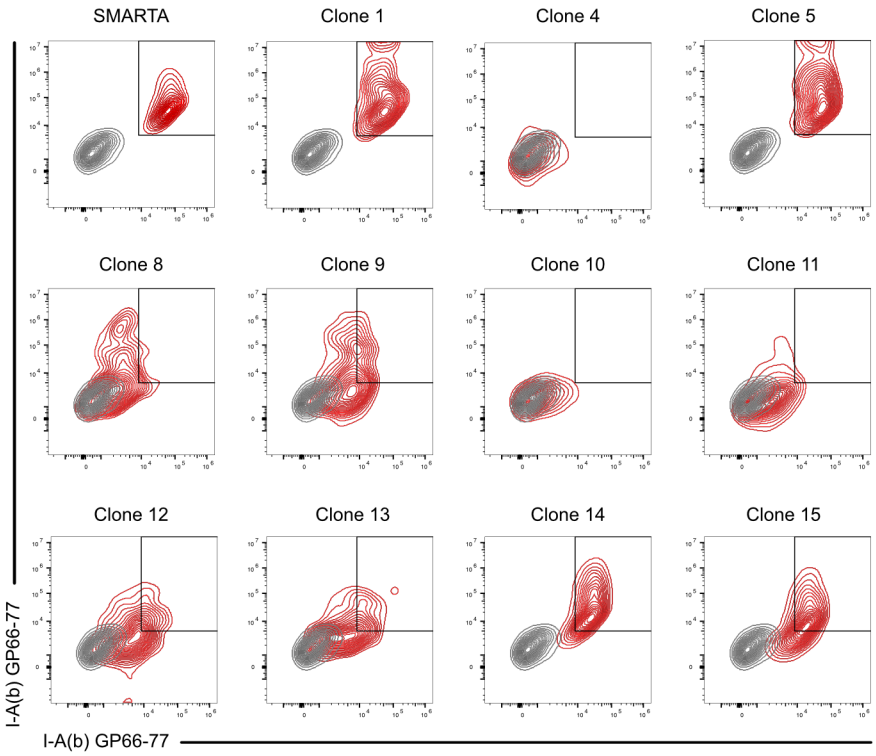

B

Clone/TCR ID	CDR3α	CDR3β	Restaining Intensity
TCR 5	CALSSGTYQRF	CASGDAGGADQDTQYF	high
TCR 1	CAAANNYAQGLTF	CASSDRGPNERLFF	
TCR 14	CAASFGNNNAPRF	CASSGENERLFF	
TCR 15	CAASGNNNAPRF	CASSDHQDTQYF	
TCR 9	CAASSGGYKVVF	CASSLAGGASETLYF	
TCR 11	CALSTGTYQRF	CASGDLGGVNQDTQYF	low

Figure 12: Expanded T cell clones show varying degree of tetramer restaining

(A) Expanded clones were restrained with IA(b) GP66-77 tetramer to confirm antigen specificity. The TCR sequence was amplified by TCR-SCAN RACE PCR and sequenced by NGS. Contour plots show tetramer restaining data of stained and expanded clones (red) over sorted and expanded tetramer$^-$ CD4$^+$ T cells (grey). (B) The table shows the CDR3α and CDR3β amino acid sequences as well as the relative restaining intensity of TCRs chosen for re-expression.

4.2.3 TCRs isolated from the naive repertoire show a broad range of functional avidities

To characterize the functional avidity of the isolated TCRs, we made use of a Jurkat cell line which possesses three reporters for TCR signaling. In this cell line, response elements for NFAT, NFκB, and AP1 drive the expression of eGFP, CFP, and mCherry, respectively (Rosskopf et al., 2018). We transduced this cell line with the isolated TCRs and murine CD4 to assess the effect of coreceptor help on functional avidity. Thus, we generated a Jurkat cell line expressing only the TCR of interest with and without expression of murine CD4. These cell lines were stimulated on splenocytes with varying doses of GP61-80 peptide for 24 hours, followed by measurement of the reporter expression by flow cytometry (Figure 13A).

After peptide stimulation, the NFAT and NFκB reporters were faithfully induced in a dose-dependent manner (Figure 13B). Of note, we observed digital activation of the NFκB reporter and analog activation of the NFAT reporter. This notion corresponded well to the described activation characteristics of these signaling pathways (Christo et al., 2015; Kingeter et al., 2010; Rosette et al., 2001). After normalization and curve fitting (Figure 13C), we determined the EC50 values of reporter activation. Herby, we could show that the isolated TCRs showed a broad range of functional avidities (Figure 13D). Co-expression of murine CD4 increased the peptide sensitivity of the Jurkat cell lines overall, but more strongly so for TCRs of lower functional avidity (Figure 13E). When correlated with *in vivo* expansion of TCR retrogenic populations, we found the EC50 values, determined in Jurkat cells without murine CD4 using the NFAT reporter, to be a strong predictor of T cell expansion (Figure 13E). We, therefore, chose to use these values and *in vivo* expansion to characterize a given TCRs functional avidity

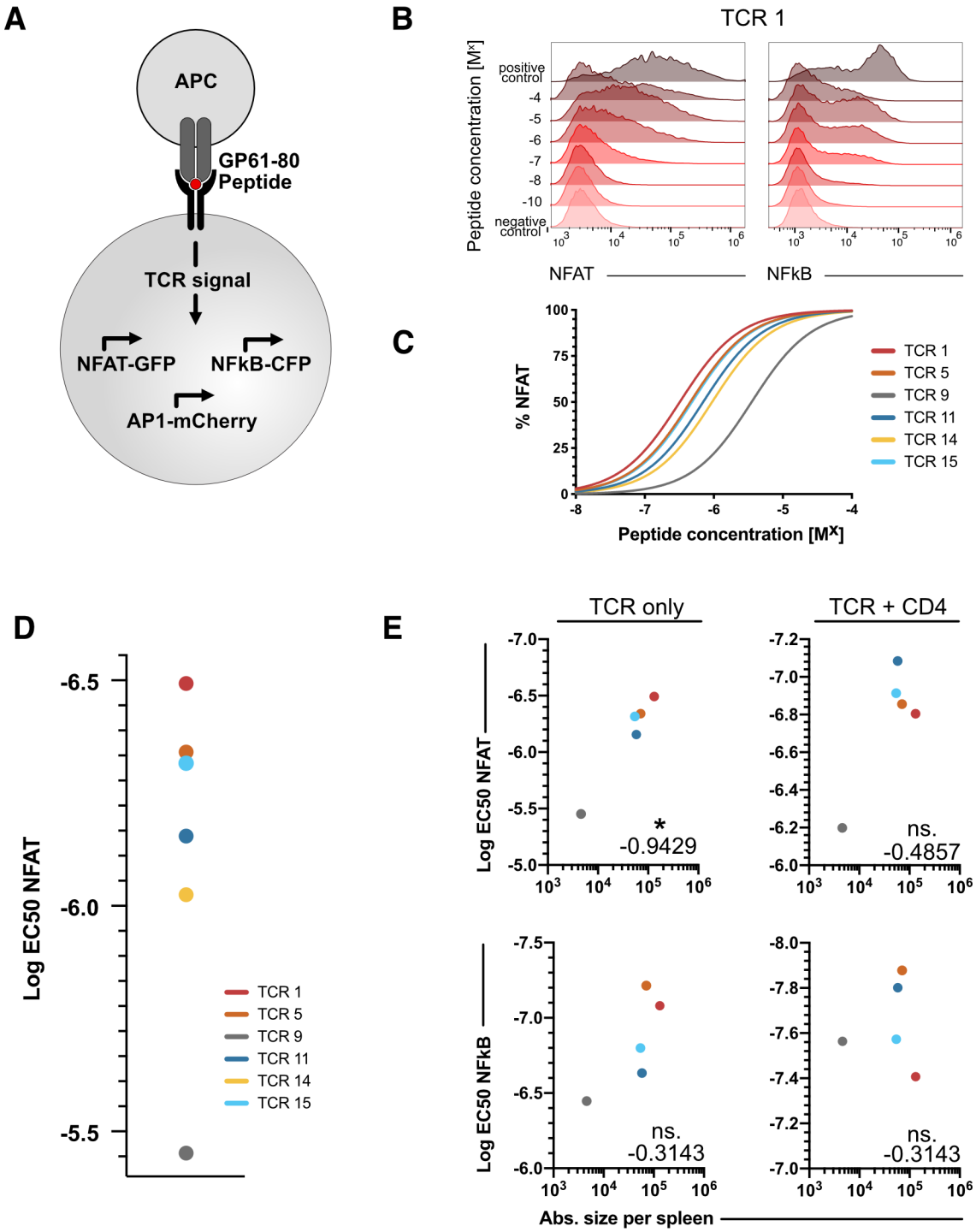

Figure 13: TCRs isolated from the naive repertoire show a broad range of functional avidity

(A) Jurkat triple reporter cells (with and without murine CD4) were transduced with TCRs and sorted for identical levels of TCR expression. The generated Jurkat reporter cell lines were activated on splenocytes with varying concentrations of GP61-80 peptide for 18 hours after which reporter activity was read out by flow cytometry. Histograms depict reporter expression of the NFAT and NFκB reporters at indicated peptide concentrations (B). Reporter expression values were normalized to the positive control and fitted by a nonlinear dose-response curve to determine EC50 values. Graphs depict curve fit of NFAT reporter expression (C) and determined EC50 values (D). Graphs show a correlation between determined EC50 values and absolute response size per spleen of 100 T cells harboring the given TCRs (E). Correlation

computed by nonparametric Spearman correlation. Data in C, D, and E are pooled from three independent experiments with technical triplicates, absolute response size in E is derived from n=6 per TCR. *P < 0.05, **P < 0.01, ***P < 0.001, ****P < 0.0001.

4.2.4 Retrogenic TCR expression and color-barcoding allows observation of characterized polyclonal responses within the same recipient

To generate traceable T cells expressing the isolated TCRs *in vivo*, we made use of TCR retrogenic mice (Holst et al., 2006) and retrogenic color-barcoding (Grassmann et al., 2019). To generate TCR retrogenic mice, we isolated and expanded HSCs from Rag1-/- mice bearing a diverse set of congenic markers to identify transferred cells. We transduced the stem cells with retrovirus encoding a given TCR. For experiments in which we needed to co-transfer multiple populations or single T cells, we additionally co-transduced the stem cells with six fluorescent proteins of the GFP family (GFP, YFP, CFP, BFP, Ametrine or T-sapphire). Fluorescent color codes are generated by combinatorial transduction with different fluorescent proteins. The expression of this color code is stable and allows the tracking of transferred immune cells in recipient mice. Roughly four weeks after the transplantation of the transduced HSCs into irradiated recipient mice, naive barcoded T cells could be sorted from the blood or splenocytes of the retrogenic mice and transferred to naive recipients for subsequent experiments (Figure 14A).

To show the versatility of this approach, we co-transferred 100 cells expressing TCR 1 (GFP), TCR 15 (YFP), TCR 5 (CFP), TCR 11 (CD45.1^{+}), and TCR 9 (BFP), respectively, into naive recipient mice and analyzed the response to LCMV Armstrong infection. To our knowledge, this is the first time the influence of TCR avidity on CD4 T cell differentiation could be studied for such a large number of characterized TCRs within the same recipient mouse. The T cell populations could be detected faithfully by their barcode expression (Figure 14C). T cell expansion was observed in the hierarchy predicted by the Jurkat reporter assay (EC50 NFAT) (Figure 14B). In addition, we could establish the combination of retrogenic color code detection with the phenotypic characterization of the transferred populations based on the surface markers CCR7, CXCR6, and CXCR5 (Figure 14D).

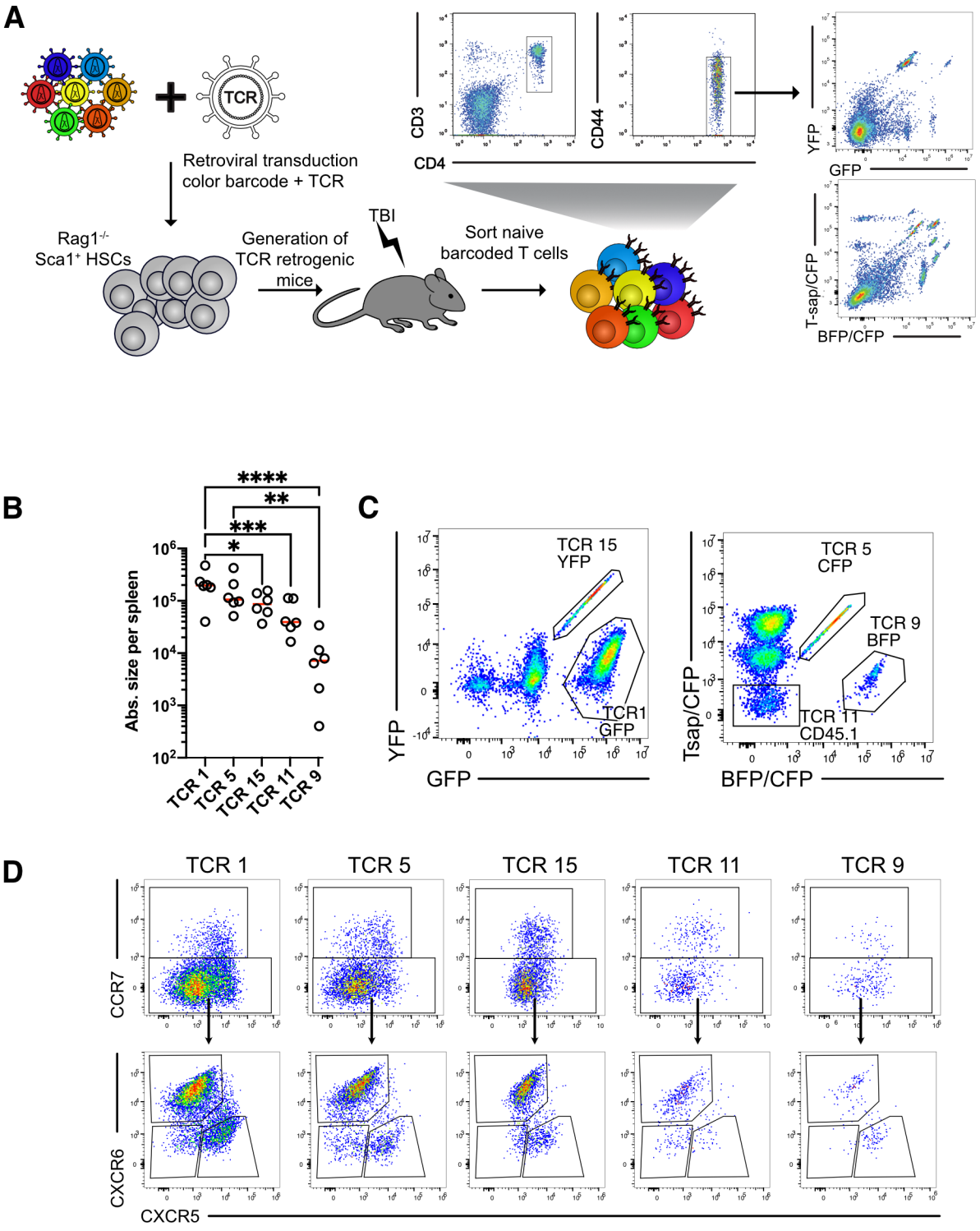

Figure 14: Retrogenic TCR expression and color-barcoding allows observation of characterized polyclonal responses within the same recipient

(A) Shows the generation of color-barcoded TCR retrogenic T cells. Sca1^{+} hematopoietic stem cells were sorted from the bone marrow of Rag1$^{-/-}$ mice and combinatorically transduced with retrovirus encoding for the expression of a TCR and virus encoding for the expression of five distinct fluorescent proteins. After transduction and transplantation of stem cells into irradiated recipients, naive color-barcoded T cells can be sorted from the blood after about four weeks. After co-transfer of 100 naive T cells expressing a given TCR and color or congenic barcode, mice were infected with LCMV Armstrong, and the polyclonal responses were analyzed on day 8 post-infection in the spleen (B-D). (C) Pseudocolor plots show the identification of a given

TCR retrogenic population by expressing a given fluorescent protein or congenic marker (pregated on live $CD4^+$ $CD45.1^+$ $CD19^-$ $CD8^-$ cells). The retrogenic T cell populations show unique response sizes (B). (D) The phenotype of T cell populations identified in C. Data shown is from one experiment with n=6 mice. The line indicates the mean. Significances are calculated using one-way ANOVA (Kruskal-Wallis) and Dunn's multiple comparison test. *P < 0.05, **P < 0.01, ***P < 0.001, ****P < 0.0001.

4.2.5 scRNA sequencing reveals heterogenous $CD4^+$ T cell responses to acute and chronic LCMV infection

To gain deeper insights into the interplay between TCR avidity and helper cell differentiation on a transcriptional level we performed scRNA sequencing in acute and chronic LCMV infection. In the LCMV Armstrong cohort, we co-transferred 500 naive-color-barcoded T cells expressing TCR 1, 5, 15, 11, 14, and 9 per recipient mouse. In addition to these populations, we sorted endogenous IA(b) GP66-77 $tetramer^+$ cells at day 8 and day 28 p.i. Unfortunately, we could not recover enough cells of TCR 9 at day 28 p.i. for sequencing. Furthermore, we found that tetramer staining at 37 °C stimulated the endogenous T cells, which led to upregulation of transcripts associated with TCR signaling in comparison to the other T cells (data not shown). For this reason, we excluded endogenous epitope specific T cells from the analysis of these samples. Due to technical hurdles that made it difficult to harvest enough cells for sequencing in response to LCMV Armstrong we opted to modify the experiment for the LCMV CL13 cohort, as chronic infection led to smaller T cell responses. Here, we transferred 5000 T cells expressing TCR 1, 11 and 9 into separate recipients followed by infection with LCMV CL13. We sorted transferred cells at day 8 and 28 p.i., additionally we sorted endogenous IA(b) GP66-77 $tetramer^+$ T cells from these samples after tetramer staining at 4 °C. Sequencing results were preprocessed, batch corrected and concatenated for analysis as described in the methods section.

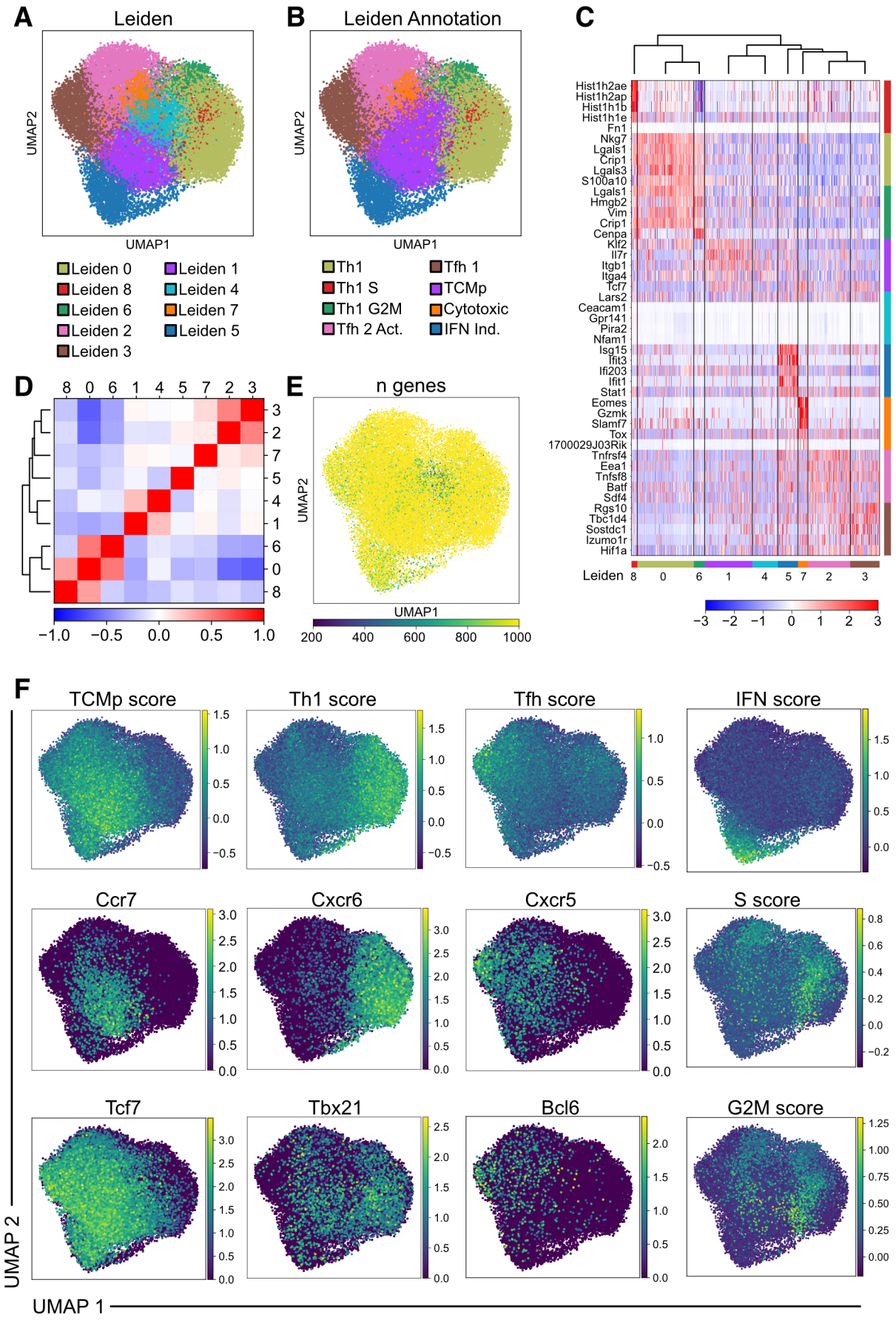
A
Leiden
UMAP2
UMAP1
Leiden 0
Leiden 1
Leiden 8
Leiden 4
Leiden 6
Leiden 7
Leiden 2
Leiden 5
Leiden 3
B
Leiden Annotation
UMAP2
UMAP1
Th1
Tfh 1
Th1 S
TCMp
Th1 G2M
Cytotoxic
Tfh 2 Act.
IFN Ind.
C
Hist1h2ae
Hist1h2ap
Hist1h1b
Hist1h1e
Fn1
Nkg7
Lgals1
Crip1
Lgals3
S100a10
Lgals1
Hmgb2
Vim
Crip1
Cenpa
Klf2
Il7r
Itgb1
Itga4
Tcf7
Lars2
Ceacam1
Gpr141
Pira2
Nfam1
Isg15
Ifit3
Ifi203
Ifit1
Stat1
Eomes
Gzmk
Slamf7
Tox
1700029J03Rik
Tnfrsf4
Eea1
Tnfsf8
Batf
Sdf4
Rgs10
Tbc1d4
Sostdc1
Izumo1r
Hif1a
Leiden 8 0 6 1 4 5 7 2 3
−3 −2 −1 0 1 2 3
D
8 0 6 1 4 5 7 2 3
3 2 7 5 4 1 6 0 8
−1.0 −0.5 0.0 0.5 1.0
E
n genes
UMAP2
UMAP1
200 400 600 800 1000
F
TCMp score
Th1 score
Tfh score
IFN score
Ccr7
Cxcr6
Cxcr5
S score
Tcf7
Tbx21
Bcl6
G2M score
UMAP 2
UMAP 1

Figure 15: scRNA sequencing reveals heterogenous CD4$^+$ T cell responses to acute and chronic LCMV infection

Color or congenic barcoded T cells expressing TCRs of varying avidity were transferred to recipient mice which were subsequently infected with LCMV Armstrong or LCMV CL13. On day 8 and day 28 p.i. transferred cells were enriched by speed enrichment, labeled with hashtag antibodies, and sorted for transcriptome analysis by scRNA sequencing. Full preprocessing and experimental setup are outlined in the methods section. Dimensionality reduction using uniform manifold approximation and projection (UMAP) shows Leiden clusters (A) and their annotation (B) based on marker gene expression and scoring of marker gene sets. (C) Heatmap showing expression of the top 5 highest ranked marker genes for each Leiden cluster. (D) Dendrogram matrix plot showing similarity between Leiden clusters by Pearson correlation. (E) UMAP projection of the number of expressed genes in all cells. (F) UMAP projection of exemplary calculated scores or marker genes used to annotate the Leiden clusters. TCMp, Th1 and Tfh associated scores/genes are shown in the first, second and third column, respectively. The Fourth column depicts scores used to determine subsets that were activated or in the cell cycle.

Leiden clustering revealed nine transcriptionally distinct clusters. The top 5 marker genes of each Leiden cluster are visualized as a heatmap in Figure 15C. The Leiden clusters were annotated by their expression of marker genes and scores calculated for published gene sets (Figure 15F). Clustering mainly revealed the differentiation into TCMp, Th1 and Tfh cells. Leiden clusters 0, 8 and 6 were annotated as Th1 cells due to their high Th1 score encompassing the Th1 associated genes *Cxcr6*, *Tbx21*, *Nkg7*, *Ifng*, *Tnf*, *Ly6c2*, and *Gzmb*. Clusters 8 and 6 showed high expression of cell-cycle associated genes and were annotated to be in the G2M and S phase, respectively. Similarly, two Tfh clusters (Leiden 2 and 3) could be identified by their high Tfh score calculated from the expression of *Cxcr5*, *Bcl6*, *Pdcd1*, *Icos*, *Il6*, *Il21* and *Ascl2*. Cluster 2 showed higher expression of genes associated with TCR stimulation such as *NFκBia*, *Tnfrsf4* and *Tnfrsf9* and were thus annotated as activated Tfh cells. Leiden cluster 1 showed high expression of memory-associated markers such as *Ccr7*, *Tcf7*, *Id3*, *Il7r*, *Slamf6*, *Bcl2*, and *Klf2* determined as TCMp score. Leiden cluster 4 expressed fewer genes than other Leiden clusters possibly corresponding to a resting cell state (Figure 15E). Leiden cluster 4 was transcriptionally most similar to Leiden cluster 1 as shown by Pearson correlation (Figure 15D). Therefore, these two clusters were grouped together and annotated as TCMp cells. Leiden Cluster 5 showed upregulated expression of type I Interferon-induced genes such as *Ifit3*, *Isg15* and *Ifit1*. To verify this finding, the cells were scored for the expression of a gene set upregulated 16 hours after IFNβ stimulation of human memory T cells (Cano-Gamez et al., 2020).

The three identified Th1 and two identified Tfh clusters showed a high degree of transcriptional similarity, as shown by the Pearson correlation between the annotated clusters (Figure 15B). Th1 cells were transcriptionally distinct from Tfh and memory cells, (Figure 15B). Tfh and TCMp cells showed more similar transcriptional profiles in this regard.

Furthermore, Leiden clustering revealed a subset with marker genes associated with effector CD8$^+$ T cells suggesting cytotoxic function (*Eomes*, *Gzmk, Ctla2a*) (Figure 16). Additionally, this cluster expressed *Xcl1* and *Crtam*, possibly indicative of interactions with cross-presenting XCR-1+ Necl2-expressing DCs. Furthermore, the cells in this cluster highly expressed markers associated with inhibitory functions such as *Slamf7*, *Tgfbr3* and *Il10ra*. Such cytotoxic CD4$^+$ T cells have been described in a wide variety of model systems, yet their exact function and how they differentiate remains to be determined (Appay, 2004; Juno et al., 2017; Mucida et al., 2013; Weiskopf et al., 2015).

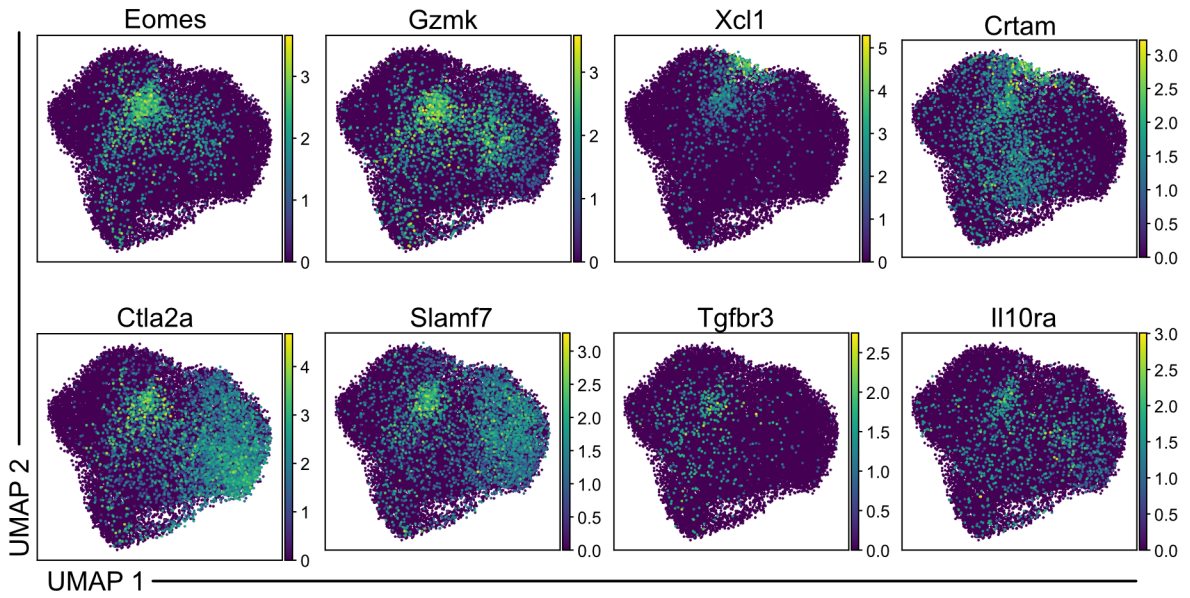

Figure 16: Markers of cytotoxic subset

Plots show cytotoxic marker gene expression in UMAP embedding of all sequenced cells from LCMV Armstrong and LCMV CL13 infection

Leiden clusters were differentially distributed after LCMV Armstrong and LCMV CL13 infection (Figure 17A). The response to LCMV Armstrong was dominated by Th1 cells and showed only low frequencies of Tfh cells 8 days p.i., as determined before by flow cytometry. In contrast, Tfh frequency was markedly increased eight days after LCMV CL13 infection at the expense of Th1 and memory cells. In the memory phase after LCMV Armstrong infection, memory cells (TCMp clusters) made up more than 60 % of the isolated T cell population. The next largest population consisted of TH1 cells, while Tfh cells were largely absent at this timepoint. Similarly, an increase in memory cells could be seen 28 days after LCMV Cl13 infection, however much less pronounced than after LCMV Armstrong infection. While Tfh cells were still present at high frequencies, Th1 cells were almost completely lost at this timepoint. Cells that were type I interferon activated were present at similar frequencies eight days after LCMV Armstrong or LCMV CL13 infection. While absent in the memory phase after LCMV Armstrong infection, these cells increased in frequency from day 8 to day 28 after LCMV CL13 infection.

Additionally cytotoxic CD4$^+$ T cells could mainly be detected during the chronic phase of LCMV CL13 infection (Figure 17B).

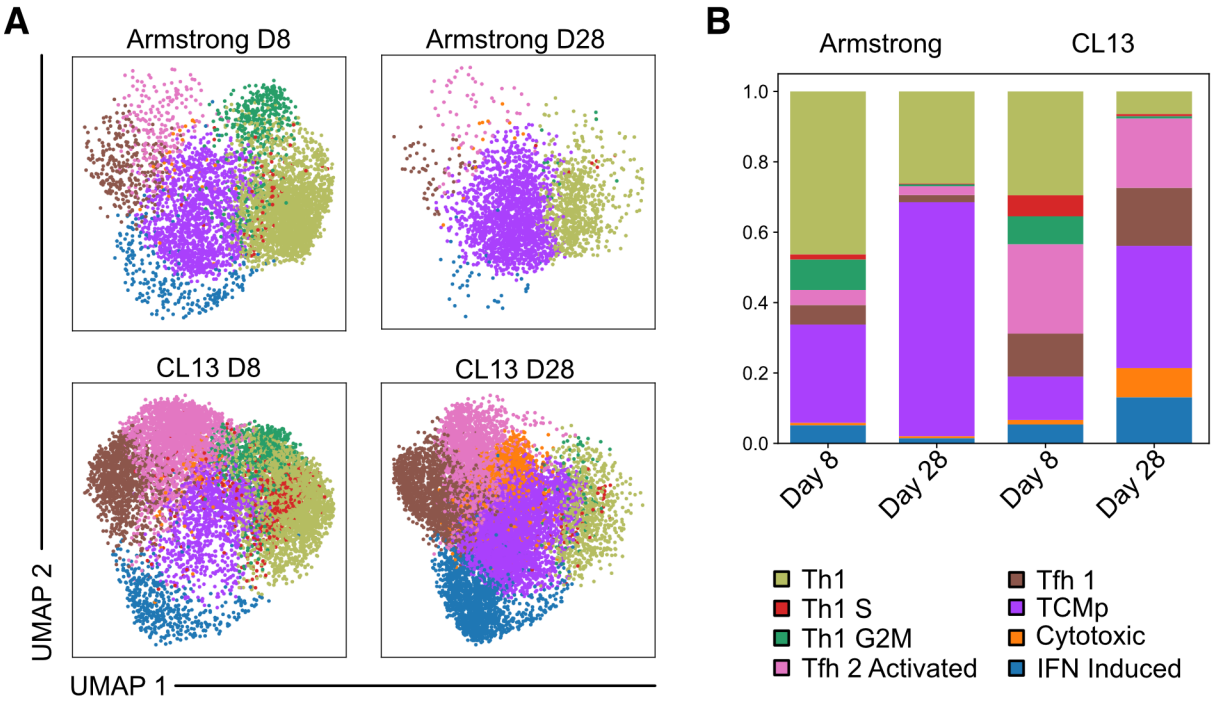

Figure 17: Temporal subset composition and marker gene expression

UMAP based projection of Leiden clusters shows their differential distribution at the indicated timepoints and viral infections (A). The bar graph depicts the Leiden cluster frequencies at day 8 and day 28 after LCMV Armstrong or LCMV CL13 infection (B).

4.2.6 TCR avidity influences expansion and Th1 differentiation after LCMV Armstrong infection

Next, we wanted to study the influence of TCR avidity on these differentiation processes. For example, we wondered if higher TCR avidity could lead to similar signal strength accumulation as in chronic infection and favor the generation of Tfh cells. To address these questions, we transferred 500 naive T cells expressing TCR 1 (high avidity), TCR 11 (intermediate avidity) or TCR 9 (low avidity) into C57BL/6 mice, followed by infection with LCMV Armstrong. We analyzed the frequencies of TCMp (CCR7$^+$), Th1 (CCR7$^-$ CXCR6$^+$), Tfh (CCR7$^-$ CXCR6$^-$ CXCR5$^+$), GC Tfh (CCR7$^-$ CXCR6$^-$ CXCR5^{high} PD1^{high}) and Th0 cells (CCR7$^-$ CXCR6$^-$ CXCR5$^-$) of the transferred populations as shown in Figure 18A. We found that the expression of CCR7 correlated with the expression of Ly108 a surrogate marker for TCF7 expression (Z. Chen et al., 2019), which has been described to be important for memory development of CD8$^+$ and CD4$^+$ T cells (Gullicksrud et al., 2017; Pais Ferreira et al., 2020). Additionally, CCR7 and

CXCR6 expression were mutually exclusive and CXCR6$^+$ cells showed reduced levels of Ly108. Together these show the terminal effector characteristics of CXCR6$^+$ Th1 cells.

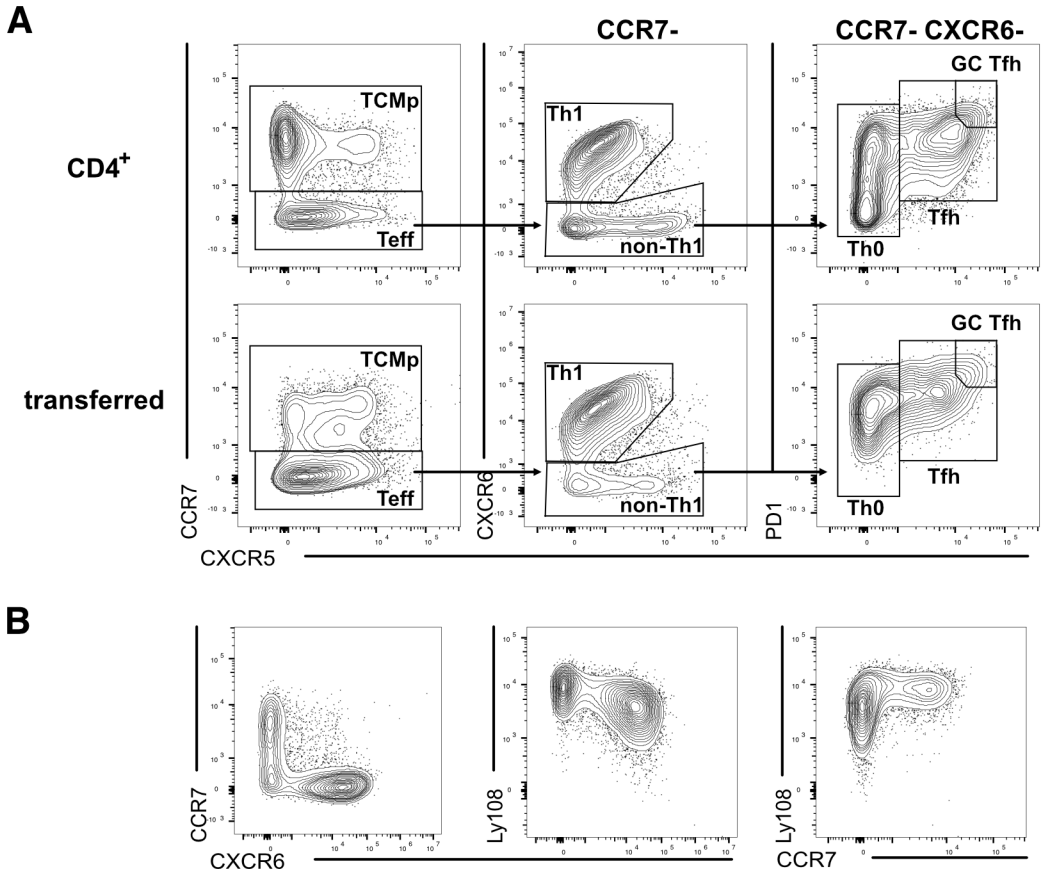

Figure 18: Gating strategy for phenotyping CD4$^+$ T cell responses to LCMV

(A) The contour plots show the gating strategy for phenotyping of CD4$^+$ T cell responses to LCMV. Live CD4$^+$ T cells were segregated into TCMp and effector cells (Teff) by expression of CCR7 or lack thereof. Effector cells were further separated into Th1 (CCR7$^-$ CXCR6$^+$), Th0 (CCR7$^-$ CXCR6$^-$ CXCR5$^-$), Tfh (CCR7$^-$ CXCR6$^-$ CXCR5$^+$) or GC Tfh cells (CCR7$^-$ CXCR6$^-$ CXCR5^{high} PD1^{high}). Gates were set up on endogenous CD4$^+$ T cells and then applied to transferred cells. (B) contour plots show the expression of CXCR6 against the memory markers CCR7 (left panel) and Ly108 (TCF7 surrogate marker) (middle panel). (B right panel) Contour plots how co-expression of Ly108 and CCR7. The plots show an exemplary gating of one mouse transferred with 500 TCR1 expressing cells and infected with LCMV Armstrong.

We could show that TCR avidity strongly influenced T cell expansion, with 3-fold expansion differences between TCR 1 and TCR 11 and 25-fold expansion differences between TCR 1 and TCR 9 on day 8 p.i. (Figure 19A, left panel). In the memory phase, responses in the TCR 1 group showed similar size to those from the TCR 11 group, due to more pronounced contraction of the higher avidity population. TCR 9 derived responses were roughly 20-fold smaller than TCR 1 derived populations at this timepoint (Figure 19A, right panel).

Phenotypically, we found a slight but significant increase in Th1 cells associated to higher TCR avidity at the peak of infection as detected by flow cytometry (Figure 19B, left panel).

Transcriptionally however, these populations were remarkably similar as shown by Leiden cluster frequency distribution from scRNA seq analysis (Figure 19B, right panel). Of note, the frequency of detected Tfh cells by transcriptional analysis is slightly underrepresented in favor of TCMp cells in comparison to analysis by flow cytometry. This could be due to a stricter definition of Tfh cells on a transcriptional level (score for *Cxcr5*, *Bcl6*, *Pdcd1*, *Icos*, *Il6*, *Il21* and *Ascl2*) in comparison to surface marker staining ($CCR7^-$ $CXCR6^-$ $CXCR5^+$). At the memory time point we could not detect significant differences in differentiation by flow cytometry or scRNA sequencing (Figure 19C). At this timepoint Tfh cells were again underrepresented in transcriptional analysis in comparison to analysis by flow cytometry.

In summary changes in TCR avidity strongly influenced T cell expansion. However, influences on T cell differentiation were relatively small. An increase in TCR avidity led to an increase in Th1 cells at the peak of infection. Additionally, these experiments showed that TCR avidity influences T cell differentiation in a different manner than antigen persistence as the responses of T cells with high-avidity TCRs in comparison to T cells with low-avidity TCRs did not resemble the average $CD4^+$ T cell phenotype after chronic infection (increased Tfh, decreased Th1 and TCMp differentiation).

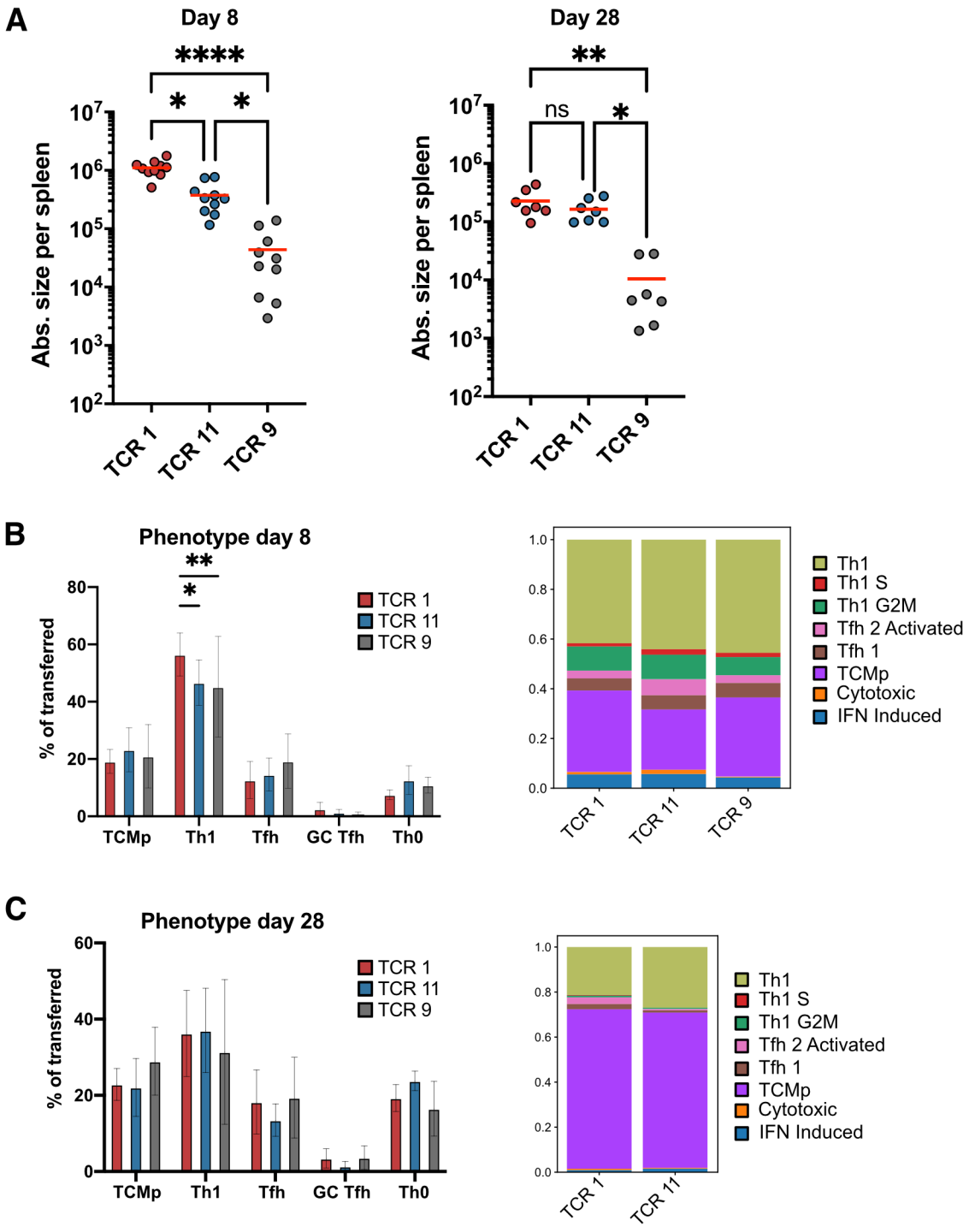

Figure 19: Influence of TCR avidity on expansion and phenotype after LCMV Armstrong infection

500 naive T cells expressing either TCR 1, 11, or 9 were transferred into naive recipients which were subsequently infected with LCMV Armstrong. (A) Absolute response size of transferred populations on day 8 (left panel) and day 28 (right panel) p.i. with LCMV Armstrong. The phenotypic composition of the response was assessed by flow cytometry (left panel) and scRNA sequencing (right panel) on day 8 (B) and day 28 (C) p.i. Bar graphs show the mean, error bars indicate SD. Significances are calculated using one-way ANOVA (Kruskal-Wallis) and Dunn's multiple comparison test(A) or two-way ANOVA (B,C). Flow cytometric data is

pooled from at least two independent experiments with n = 4-6 mice per group. *P < 0.05, **P < 0.01, ***P < 0.001, ****P < 0.0001.

4.2.7 Chronic infection favors Tfh differentiation and loss of Th1 cells

In addition to the acute infection model, we also repeated these experiments in the chronic LCMV CL13 infection model. As persistent antigen load could amplify the avidity-dependent signal intensity T cells receive, this could lead to an increased effect on T cell differentiation. As shown for LCMV Armstrong infection, we observed avidity-dependent expansion differences. However, the average total response size of T cell populations expressing the investigated TCRs (TCR 1, 11 and 9) was reduced roughly 10-fold in comparison to LCMV Armstrong infection. T cells harboring TCR 1 expanded on average 4-fold more than TCR 11 and 16-fold more than TCR 9 (Figure 20A, left panel). In the chronic infection phase, significant expansion differences were only found for TCRs 1 and 11 in relation to TCR 9. Interestingly, during the chronic phase T cell populations expressing TCRs of higher functional avidity (TCRs 1 and 11) showed more variation in expansion size than those a TCR of low functional avidity (TCR 9). In fact, 40 % of TCR-1-driven responses showed pronounced contraction between the acute and chronic time point (Figure 20A, right panel).

Transcriptome analysis showed that increases in TCR avidity correlated with the frequency of Th1 cells at the expense of Tfh and memory differentiation (Figure 20B, right panel). Increased Th1 differentiation could be confirmed by flow cytometry at day 8 p.i. (Figure 20B left panel). While transcriptome analysis identified similar frequencies of Th1 and Tfh cells, more TCMp cells could be detected in comparison to analysis by flow cytometry. However, both methods showed that higher TCR avidity leads to increased Th1 effector differentiation (Figure 20 B). In the chronic phase of infection, the response composition was not significantly altered by TCR avidity (Figure 20C, left panel). While Th1 differentiated cells were largely absent at this time point in all experimental groups, TCR 9 showed a slight increase in memory cell differentiation at the expense of Tfh cell differentiation on a transcriptional level (Figure 20C, right panel). Unlike in the phenotypic analysis by flow cytometry a high frequency of memory cells could be identified by scRNA sequencing. Possibly cells identified as Th0 by flow cytometry are annotated as memory cells by Leiden clustering (Figure 20C). Furthermore, scRNA sequencing reveals the presence of cytotoxic $CD4^+$ T cells in the chronic phase of infection, which slightly increase with TCR avidity.

In summary, increasing TCR avidity favors the generation of Th1 cells after LCMV CL13 infection. The loss of these cells in the transition to the chronic infection phase could explain the more pronounced contraction of higher avidity TCR populations. Persistent antigen presence also increases the frequency of Tfh cells but did so independent of TCR avidity. The

increase in Tfh cells seems to be at the expense of TCMp differentiation, as the frequency of TCMp cells is markedly reduced in comparison to LCMV Armstrong infection at day 8 post infection while the Th1 frequencies are largely similar.

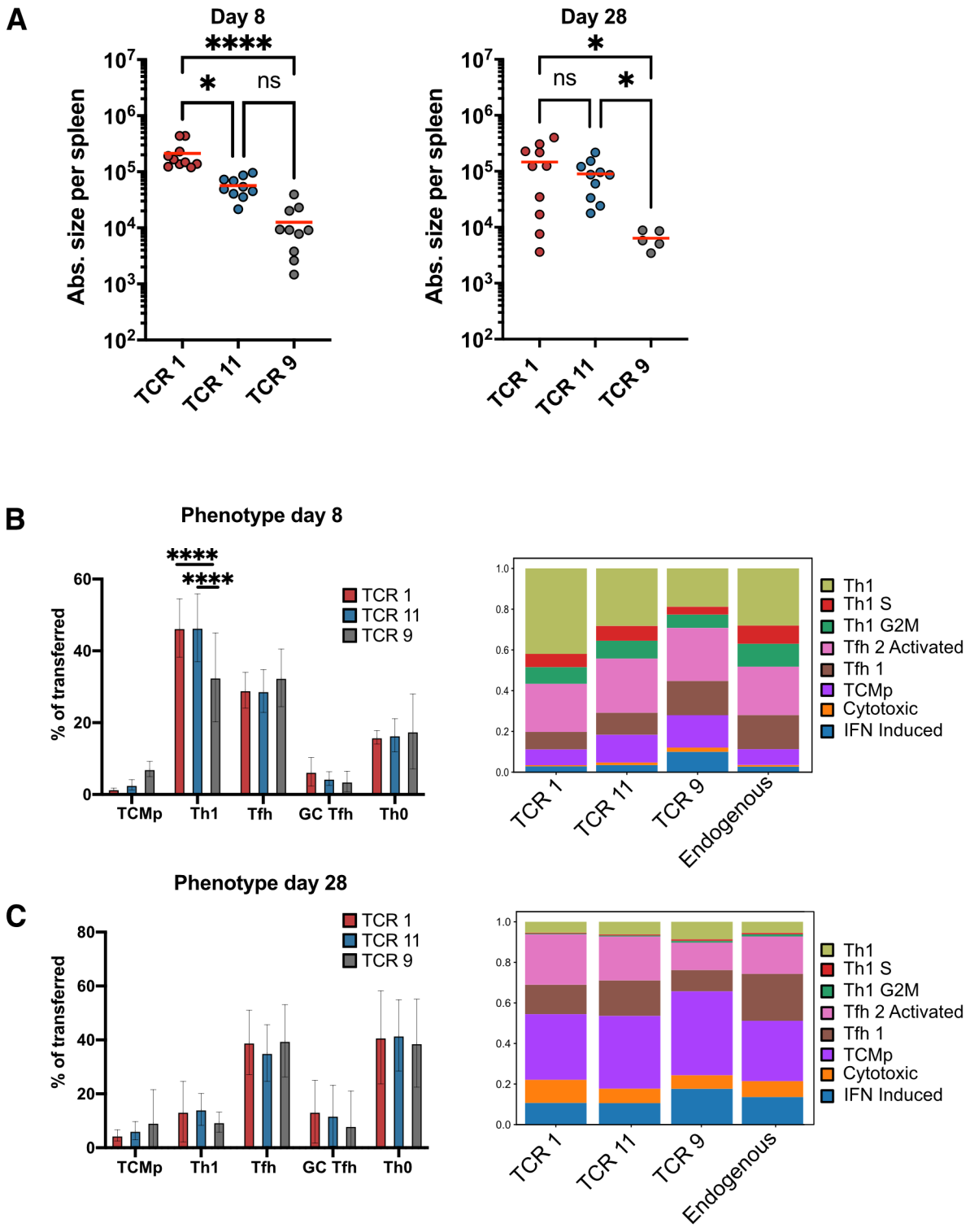

Figure 20: Influence of TCR avidity on expansion and phenotype after LCMV CL13 infection

500 naive T cells expressing either TCR 1, 11, or 9 were transferred into naive recipients, which were subsequently infected with LCMV CL13. (A) Absolute response size of transferred populations on day 8 (left panel) and day 28 (right panel) p.i. with LCMV CL13. The phenotypic composition of the response was assessed by flow cytometry (left panel) and scRNA sequencing (right panel) at day 8 (B) and day 28 (C) p.i. Bar graphs show mean, error bars indicate SD. Significances are calculated using one-way ANOVA (Kruskal-Wallis) and Dunn's multiple comparison test (A) or two-way ANOVA (B,C). Flow cytometric data is pooled from at least two independent experiments n = 4-6 mice per group. Data for D28 TCR 9 is derived from 5 mice. *P < 0.05, **P < 0.01, ***P < 0.001, ****P < 0.0001.

4.2.8 TCR avidity is not deterministic for single CD4$^+$ T cell fate

Next, we wanted to determine how these differences on the population level were generated on a clonal level. To this end single-cell derived responses could either show similar responses with general shifts in the differentiation profile. Alternatively, population responses could be derived from biased clonal Th1 and Tfh responses with TCR avidity altering the balance between these responses.

To distinguish between these scenarios, we transferred single color-barcoded T cells expressing either TCR 1 or TCR 11 into naive recipients followed by infection with LCMV Armstrong and assessment of response magnitude and phenotypic composition at day 8 p.i. in the spleen. We did not transfer T cells expressing TCR 9, as this TCR led to 16–25-fold smaller population-derived responses in comparison to TCR 1, which made efficient detection of single-cell-derived progeny seem unlikely.

Single-cell derived responses showed drastic variability in their response size, that could not be attributed to TCR avidity. On this clonal level, we could not detect significant expansion differences between progeny derived from single cells expressing TCR 1 or TCR 11 (Figure 21A). However, in analogy to the avidity-dependent recruitment of CD8$^+$ T cells described in earlier chapters, we found differences in the efficiency with which we recovered single-cell derived response of TCR1 and TCR 11 expressing cells (Figure 21A). As outlined before, T cell recruitment amplifies the differences in response size seen on the population level and can help to explain the response size discrepancy between population- and single-cell derived responses. In addition to highly variable expansion, single T cell derived responses also showed a highly variable phenotypic composition, but again phenotypic differentiation induced by TCR 1 vs. TCR 11 differed only very little. We found that the response patterns of T cell families could be grouped into families that showed dominant Th1, Tfh or mixed differentiation patterns (Figure 21B). These three groups overall possessed a similar average differentiation pattern largely independent of TCR avidity. We found however that the frequency with which these three patterns were generated was dependent on TCR avidity. Both TCRs generated Tfh biased T cell families with similar frequencies (TCR 1: 33.5 %, TCR 11: 32%). Th1 biased T cell families were generated more frequently with higher TCR avidity (TCR 1: 37,5 %, TCR

11: 30,5 %). In comparison, lower TCR avidity favored the generation of unbiased clonal families (TCR 1: 29 %, TCR 11: 37,5 %) (Figure 21C). On average, T cell families showing the strongest Th1 bias were significantly larger than Tfh or unbiased T cell families (Figure 21D).

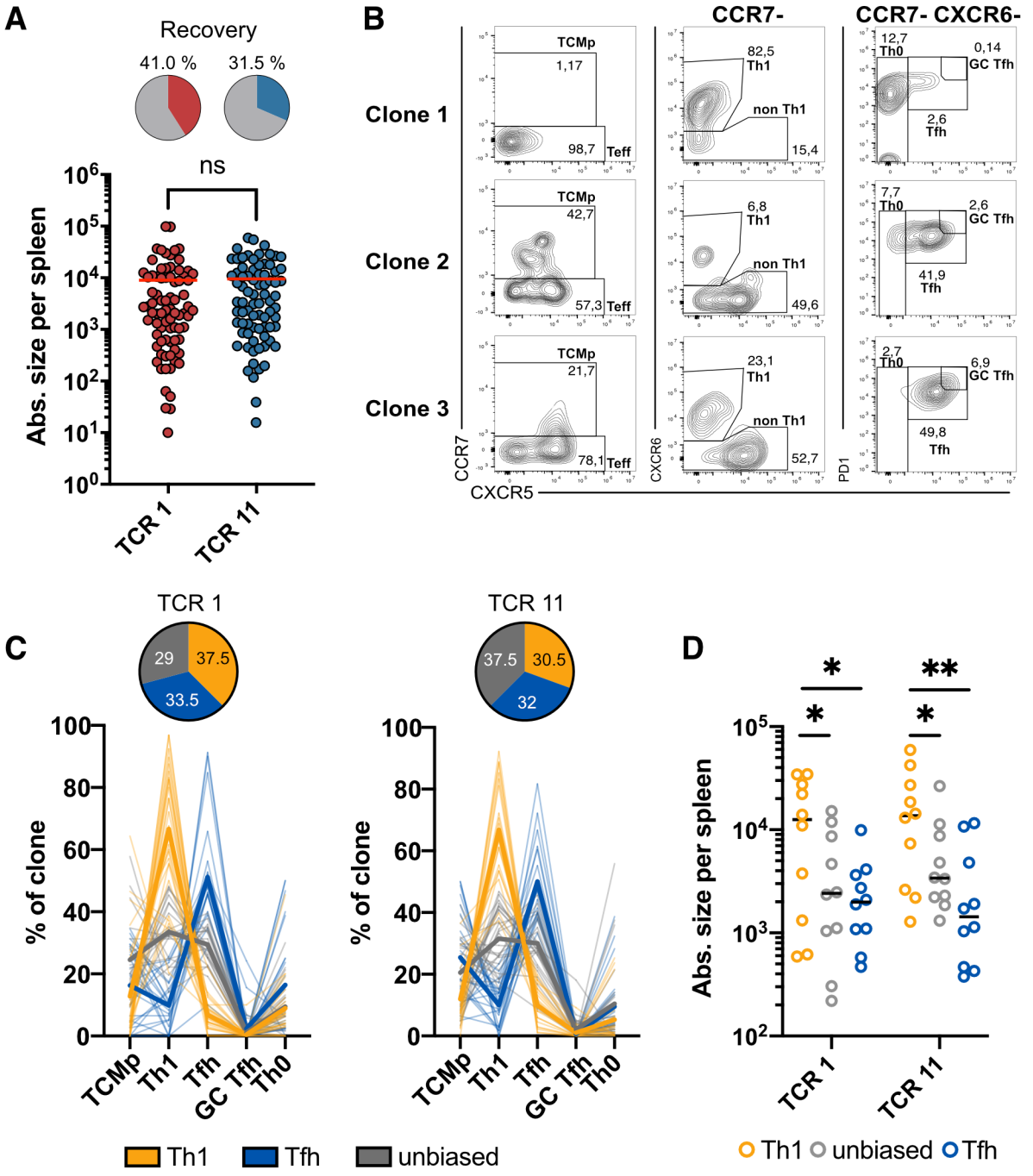

Figure 21: Population-derived responses are made up of clonally unique single-cell responses

Single naive color-barcoded T cells expressing TCR 1 or 11 were adoptively transferred into C57BL/6 recipients which were subsequently infected with LCMV Armstrong. 8 days p.i. size and phenotype of the T cell families in the spleen were measured by flow cytometry. (A) Absolute sizes of detected single-cell derived responses and their recovery frequency. (B) Contour plots showing the differentiation of three exemplary TCR 1 expressing T cell families. The numbers indicate the frequency [%] of the labeled population within the T cell family (C)

Phenotypic response pattern of T cell families with absolute size per spleen > 200 to ensure robust phenotyping. T cell families with a Th1 bias are shown in orange, Tfh biased families in blue and unbiased families in gray. Thick lines represent average response pattern of each group. The pie charts show the frequency [%] (numbers in the pie chart) of the three phenotypic groups among the clonal responses of each TCR. Families were assigned to a biased group if the frequency of Th1 was twice as high as Tfh and vice versa. (D) Absolute size per spleen of the top 10 families in regard to their Th1 or Tfh cell frequency and the top 10 families that showed the least degree of differentiation bias. Lines in the scatter plots indicate the mean (A and D). Significances in are calculated using t-Test (Mann-Whitney) (A) and a two-way ANOVA (D). Flow cytometric data is pooled from three experiments for TCR 1 and two experiments for TCR 11, with a total of n=23 mice for TCR 1 and n=28 mice for TCR 11. *P < 0.05, **P < 0.01, ***P < 0.001, ****P < 0.0001.

It has been shown that the Th1 and Tfh differentiation pathways diverge early (Y. S. Choi et al., 2013; Ditoro et al., 2018). We found a strong negative correlation between the frequency of Th1 and Tfh cells, in line with this early fate bifurcation. Furthermore, we found that the frequency of TCMp cells correlated negatively with Th1 and positively with Tfh frequency. While the frequency of $CXCR6^+$ T cells correlated positively with the absolute size of a T cell family, the frequency of $CXCR5^+$ showed an inverse correlation with response size (Figure 22A). There was no correlation between size and frequency of TCMp cells. Generally, the frequency of Th1 cells was a positive predictor of T cell family size. Interestingly, this effect seemed to peak at a Th1 frequency of 80 % after which response size was again reduced (Figure 22B).

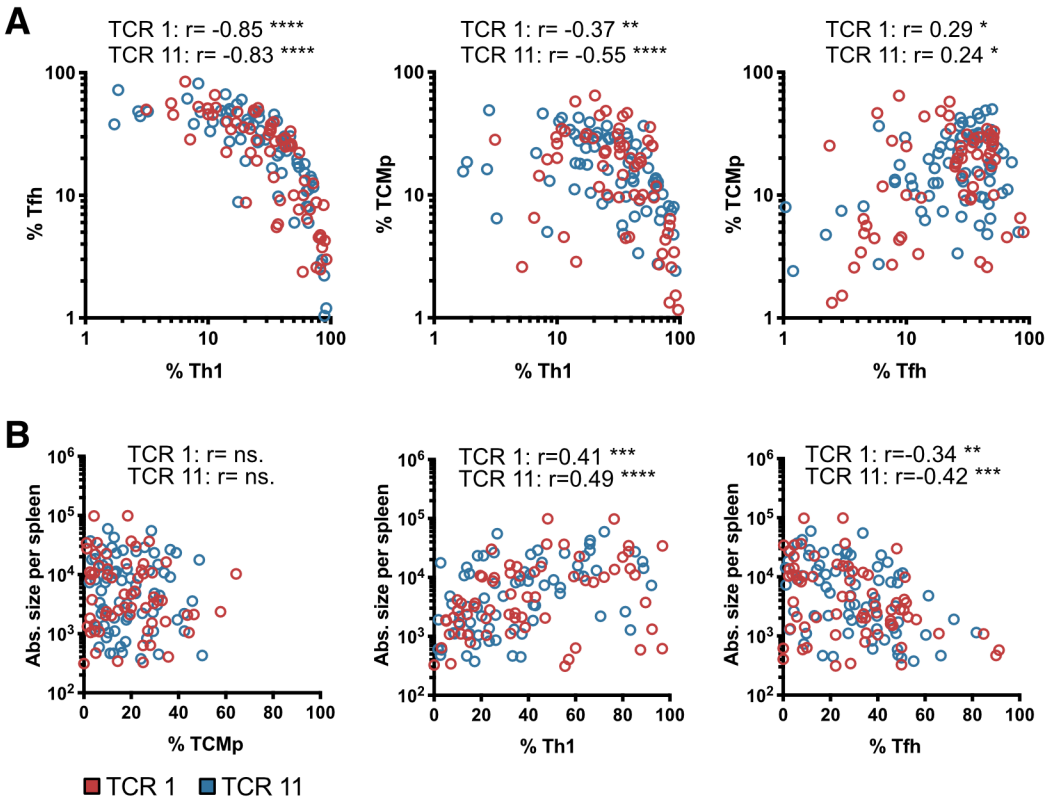

Figure 22: Th1 and Tfh fate diverge early and are differentially associated with response size

(A) Correlation of the frequencies of certain Th cell subsets within T cell families for TCR1 in red and TCR 11 in blue. (B) Correlations between the absolute size of a T cell family and the frequency of TCMp, Th1 and Tfh cells within that family for TCR 1 in red and TCR 11 in blue. Data is derived from the experiment described in Fig. 21. Correlations computed by nonparametric Spearman correlation. *P < 0.05, **P < 0.01, ***P < 0.001, ****P < 0.0001

TCR avidity influenced the probability of T cell families to generate a Th1, Tfh or unbiased response pattern. Higher vs. lower TCR avidity preferentially led to the generation of more T cell families with a Th1 bias and to a stronger Th1 bias within these families – at the expense of Tfh and TCMp cells (Figure 23A). Thus higher TCR avidity increases the probability of generating a clonally biased T cell family as well as the degree of this bias (Figure 23B).

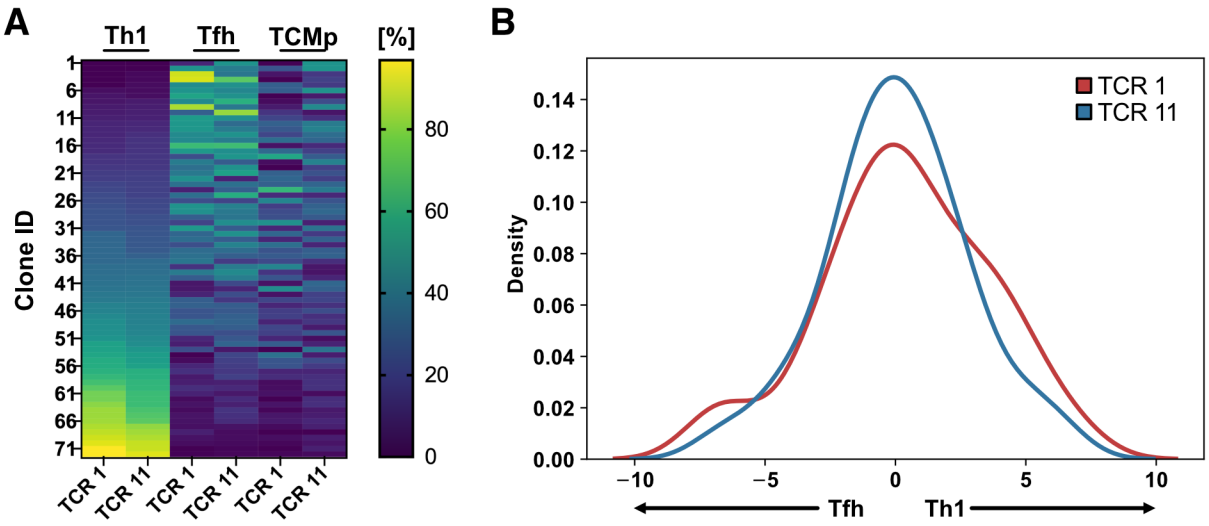

Figure 23: Clonal bias increases with TCR avidity

(A) Comparative heatmap between TCR 1 and TCR 11 showing T cell families with absolute size per spleen > 200 to ensure robust phenotyping, sorted by ascending Th1 (CXCR6$^+$) frequency. (B) Kernel density estimate of the log2 transformed ratio of Th1/Tfh frequencies within a T cell family. Hereby negative values correspond to stronger Tfh, positive values to stronger Th1 bias. Data is derived from the experiment described in Fig. 21.

4.2.9 Highly Th1-differentiated clones show poor recall capacity

We found single-cell derived CD4$^+$ T cell responses to LCMV Armstrong to be highly variable with distinct phenotypic profiles. We wanted to use this fact to our advantage to determine the phenotypic properties of T cell families that positively and negatively correlate with recall capacity to renewed infection. To assess the recall capacity based on the phenotypic composition and independent of TCR avidity we chose to use SMARTA transgenic cells for this experiment. We used HSCs from SMARTA transgenic mice (Oxenius et al., 1998), which express a TCR specific for the LCMV GP66-77 epitope, to generate congenic and color-barcoded T cells by retrogenic expression. The use of TCR transgenic HSCs for the generation of retrogenic mice has the additional benefit that higher barcoding efficiency is achieved, because all barcoded stem cells produce T cells of the desired TCR specificity. From these retrogenic donors we transferred single-naive color-barcoded CD45.1$^+$ SMARTA transgenic T and subsequently infected the recipient mice with LCMV Armstrong. As the acute phase of LCMV Armstrong infection was not compatible with the hemisplenectomy procedure we opted for a retransfer approach. At the peak of infection, we retransferred CD45.1$^+$ cells from 4/5 of total splenocytes after speed enrichment into secondary recipients by i.v. injection. The remaining 1/5 was used to determine the phenotype of the contained single-cell derived responses. One month after primary infection, we infected the secondary recipients with LCMV Armstrong and characterized the recall responses of the transferred cells after eight days.

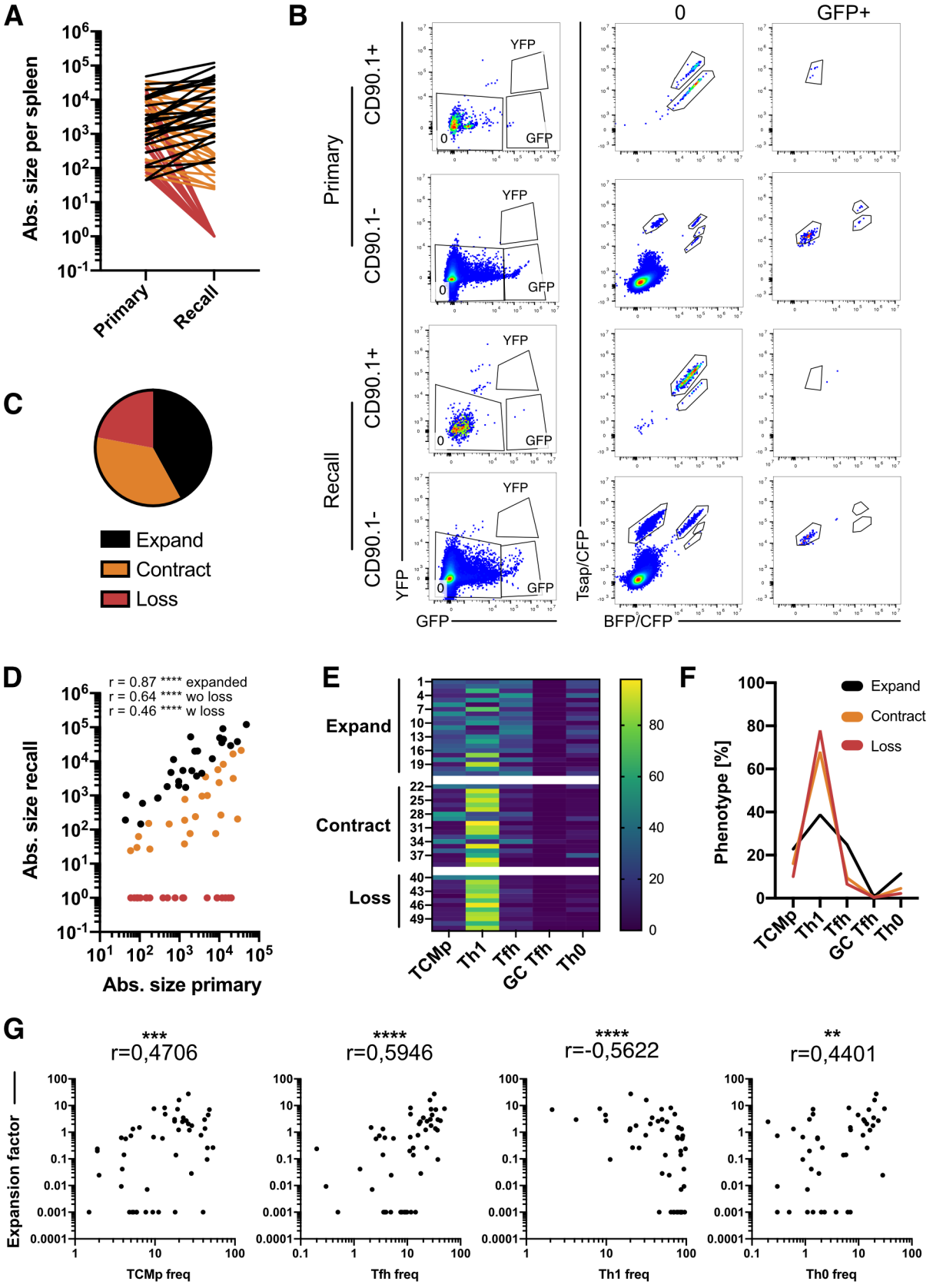

Figure 24: Single-cell fate mapping reveals positive and negative predictors of a T cell families recall capacity

Single naive color-barcoded CD45.1^{+} Smarta Rag1$^{-/-}$ cells were adoptively transferred into CD11c-DTR-GFP recipients followed by infection with LCMV Armstrong. On day 8 p.i., 4/5 of total splenocytes were enriched on CD45.1 by speed enrichment and retransferred i.v. to secondary recipients. The remaining splenocytes were used to characterize T cell family size

and phenotype. On month after retransfer, secondary recipients were infected with LCMV Armstrong, and the secondary response of transferred cells measured eight days p.i. (A) Primary and recall response size of detected T cell families connected by lines. Hereby, black color indicates recall response size > primary response size, orange color indicates recall response size < primary response size, red color indicates loss of family detected at the peak of primary response. (B) Dot plots show T cell families' detection after primary infection and recall. (C) The pie chart shows T cell families' frequency classified as expanded, contracted, or lost after recall. (D) Correlation between primary and recall response size and spearman r for all points, (w loss), all data points besides lost families (wo loss) and expanded families only (expanded). (E) Heatmap depicting the phenotype of T cell families classified as expanded, contracted, or lost after recall. (F) Average response patterns of the groups depicted in E. (G) Correlations between the expansion factor (abs. size recall/ abs. size primary) and phenotypic marker frequency within a T cell family after primary response. Data derived from n=9 mice. Correlation computed by nonparametric Spearman correlation. *P < 0.05, **P < 0.01, ***P < 0.001, ****P < 0.0001.

We could detect T cell families based on their congenic and color-barcode (Figure 24B) and found drastic size variability of primary responses as previously described on day 8 p.i., showing a coefficient of variation of 150 %. Connecting the recall responses of a given T cell family to its primary response, we found three possible outcomes after retransfer. While 42 % of recovered clones expanded after recall, 36 % had contracted (showed smaller response size) in comparison to their primary response. Additionally, 22 % of T cell families detected at day 8 p.i. did not mount recall responses (Figure 24A, C) and were lost. Overall, primary response size was positively correlated with recall response size, presumably due to the generation of a larger memory cell pool (Figure 24D).

Additionally, we found that the phenotypic response pattern of a T cell family at the peak of the primary response was predictive of its recall capability. Families expanded after recall on average showed a differentiation profile containing high numbers of $CCR7^+$ memory and $CXCR5^+$ Tfh cells, while the frequency of $CXCR6^+$ Th1 cells was relatively low. In contrast, contracted and lost families showed high frequencies of Th1 differentiation. Lost T cell families showed further increased frequencies of Th1 cells and lower frequencies of Tfh and TCMp cells in comparison to contracted T cell families (Figure 24E and F). When correlating the expansion factor (abs. size recall/abs size primary) to the frequency of TCMp, Tfh, Th1 and Th0 cells within a T cell family at the peak of the primary response, we found that the content of Tfh cells was the strongest positive predictor of recall capacity followed by the frequency of TCMp cells. Furthermore, the frequency of Th0 cells corelated positively with recall expansion. In contrast, the frequency of Th1 cells was a strong negative predictor of a T cell families recall capacity.

In summary, we found that a strongly Th1-biased differentiation pattern at the peak of primary expansion, predicted a reduction or loss of recall capacity in the respective families. In contrast, T cell families showing a less Th1 differentiated and more Tfh and TCMp differentiated pattern were readily capable of mounting recall responses.

5 Discussion

5.1 Influence of TCR avidity on the recruitment of CD8$^+$ T cells

5.1.1 CD8$^+$ T cell response magnitude is influenced by multiple factors

Upon infection, antigen specific T cells are clonally selected from the naive T cell pool to expand, differentiate, and ultimately build a pool of memory T cells that provides improved protection upon reinfection. The overall response magnitude and thus the size of the memory pool has been described to be dependent on the precursor frequency of antigen specific cells as well as the extent of T cell proliferation (Busch & Pamer, 1999; Jenkins & Moon, 2012; Zehn et al., 2009). The extent of T cell proliferation is influenced by TCR signal strength (avidity and antigen dose) as well as other stimulatory signals such as IL-2 (Marchingo et al., 2014). The size of the naive T cell pool has been shown to be predictive of response size in some cases (Obar et al., 2008) but not others (la Gruta et al., 2010). This disparity could be explained by differential recruitment efficiency of T cells from the naive T cell pool into the immune response.

To this end van Heijst and colleagues showed that recruitment of a monoclonal high avidity T cells was remarkably efficient and largely independent of antigen dose or vector (van Heijst et al., 2009). However, an influence of low TCR avidity on T cell recruitment was not addressed. Each T cell that is recruited into the immune response crosses an activation threshold sufficient to initiate proliferation. It has been shown that this threshold functions in a digital manner (Au-Yeung et al., 2014).This digital nature implies, that high avidity T cells easily cross this threshold leading to a high probability of recruitment. With decreasing avidity however, the probability to cross this threshold should decrease. Therefore, the recruitment probability of T cells should be influenced by their TCR avidity. Along these lines it has been shown that the rate at which T cells cross this activation threshold is dependent on TCR affinity for the pMHC, but the functionality (cytolytic capacity) of activated T cells is independent on priming affinity *in vitro* (Richard et al., 2018).

We examined the influence of TCR avidity on T cell response size using OT1 transgenic T cells and a *L.m.* APL model infection system. We found substantially larger expansion differences between population- than single-cell derived responses depending on TCR avidity. Because the recovery rate of single-cell derived responses was avidity-dependent we hypothesized that the discrepancies observed in expansion between the population and single-cell level could

be caused by avidity dependent recruitment. Indeed, we could show that the recruitment probability of a T cell is dependent on its TCR avidity using a refined flow cytometric assay to detect unrecruited T cells. Importantly we could confirm these findings with TCRs with distinct avidity toward the same antigen, controlling for potential differences in antigen presentation due to the use of APLs.

Taken together we could show that TCR avidity regulates the recruitment of T cells into the primary response. TCR avidity furthermore positively correlates with the degree of clonal expansion. Therefore, avidity-dependent proliferation differences are amplified by differences in recruitment as the number of cells from which the response is initiated increases with higher TCR avidity.

5.1.2 Unrecruited cells persist in a state of clonal ignorance and can be recruited into secondary responses

Since we had shown that a substantial number of T cells remained unrecruited after infection in an avidity-dependent manner, we wondered whether these unrecruited cells remain functional. A possible fate for these unrecruited T cells could be anergy. As an important mechanism of peripheral tolerance, anergy is induced in T cells after TCR stimulation in the absence of costimulatory- or the presence of strong coinhibitory signals (Chappert & Schwartz, 2010; Schwartz, 2003). Anergy is characterized by inhibition of proliferation and effector functions (Schwartz, 2003). Additionally, it has been shown for $CD4^+$ T cells that anergy can be induced by low-affinity ligands as well as low ligand doses (Korb et al., 1999; Mirshahidi et al., 2004). Alternatively, unrecruited T cells could remain in a state of clonal ignorance, a term that has been used to describe T cells that do not seem to be influenced in any way by the presence of the relevant antigen in the context of autoimmunity and tumor diseases (Ochsenbein, 2005; Salaman & Gould, 2020). In this state, unrecruited T cells could be recruited to secondary responses as long as they are not excluded by the increased competition from memory T cells (Kedl et al., 2003; Oberle et al., 2016).

To discern between these T cell fates, we utilized a highly multiplexed barcoding approach to analyze the clonal composition of responses after primary- and secondary infection within the same recipient. We sampled the clonal composition at the acute timepoint by hemisplenectomy to detect the entry of previously unrecruited clones upon secondary infection. Of note, by combining congenic and retrogenic color-barcoding we were able to transfer up to 85 traceable single T cells into one recipient mouse. This technological advancement allowed us to track the clonal evolution of T cell responses within the range of the endogenous precursor frequencies, which has been described to lie between 70 and 170 SIINFEKL specific T cells per mouse in most studies (Jenkins & Moon, 2012).

Discussion

After high-avidity priming, we found that about one third of the total clones participating in responses to a heterologous high-avidity secondary infections were newly recruited. This frequency further increased after heterologous high-avidity secondary infection of low-avidity primed mice. In this constellation, over 80% of T cells participating in this secondary response were newly recruited. These findings show that high-avidity T cells can enter a secondary response even in competition to other high-avidity memory T cells. Additionally, it shows that T cells that were not recruited in suboptimal priming conditions were not functionally impaired to initiate proliferation. Furthermore, these T cells can efficiently enter responses when they are better-suited to respond i.e. show a higher avidity to a heterologous secondary infection. It would be interesting to see if unrecruited T cells could enter a secondary response to a heterologous low-avidity antigen, or if they would be excluded from the response in this scenario. In this regard, it has been shown on the population level that epitope overlap between a primary and secondary infection diminishes the expansion of naive low-avidity T cells upon secondary infection, even if the epitope which the T cells recognize was not present in the primary infection (Oberle et al., 2016). This highlights that competition between T cells is not limited to the same epitope but also exists between different epitopes (Kedl et al., 2003; Oberle et al., 2016). Together this suggests that the recruitment of naive T cells to secondary responses is dependent on the TCR avidity and the degree of competition with memory T cells. By this low-avidity T cells could be excluded from secondary infection with a similar pathogen but possibly enter responses to a heterologous secondary infection.

Phenotypically the recalled clones showed a differentiation bias toward TEF cells as has been described by Plumlee and colleagues (Plumlee et al., 2013). In contrast, newly recruited clones were mainly TEMp differentiated at day 8 post secondary infection and were therefore phenotypically distinct from the responses of recalled T cell families. Furthermore, newly recruited clones showed the same response size regardless of the avidity of the priming stimulus, which was not significantly different from the primary response size to MVA-OVA.

In addition to T cell recruitment, we found that the response kinetic of the secondary response differed depending on the avidity of the priming stimulus. While the secondary response continued to grow between day 4 and day 8 p.i. in the low-avidity primed group, response size did not change substantially in the high-avidity primed group. These altered kinetics are most likely due to two factors. Secondary responses after high-avidity priming start out from greater numbers of memory cells and should therefore peak earlier. Furthermore, a greater part of the total response size in the low-avidity primed – high avidity secondary infection group can be attributed to newly recruited clones, which should show the response kinetic of a primary response and therefore shift the overall response peak towards a later timepoint.

The low-avidity primed – high-avidity secondary infection group simulates an infection with a mutated pathogen, changing the T cell’s avidity towards the new epitope. Evolutionarily, it

makes sense that T cells which did not optimally recognize the original pathogenic strain but are better suited to respond to the mutated pathogen are not excluded from participation in this response. In this sense, the recruitment of new T cell clones upon secondary infection could be beneficial as it diversifies the T cell response and provides an opportunity for the selection of new optimal responders and adaptation towards an altered pathogen.

In the context of tumor immunity, clonal ignorance has been proposed as a mechanism to explain the failure of T cells to respond to tumor neoantigens (Nüssing et al., 2020). Therefore, strategies to overcome this failure of T cell recruitment constitute a promising immunotherapeutic approach in addition to, for example, checkpoint therapy. Ignorance could be overcome by the isolation of high-avidity TCRs for neoantigens and their use for adoptive cell therapy. Furthermore, it has been shown that ignorance can be overcome by increasing tumor antigen expression (Spiotto et al., 2002). Along these lines tumor-targeted CD40 agonists could act by increasing the recruitment of tumor specific T cells, as they have been shown to target tumor antigens to cross presenting DCs, thereby increasing their activation and thus costimulatory capacity (Sum et al., 2022).

5.2 Influence of TCR avidity on CD4$^+$ T cell fate

5.2.1 Technical advancements to study T cell responses

TCR signal strength can be modulated altering antigen dose, antigen avidity (in form of APLs) or by the use of TCRs with unique binding characteristics. We chose to utilize unique TCRs because this offers some advantages over the use of APLs or pathogens expressing APLs. For example, the mutations introduced in altered peptide ligands can alter the binding to MHC molecules thus affecting the efficiency of antigen presentation (Wieczorek et al., 2017). Furthermore, introduction of these mutation into their respective pathogen can change infectivity. Künzli et al. generated several LCMV Armstrong and LCMV CL13 strains expressing mutations in the IA(b) GP66-77 epitope. These strains showed some differences in viral loads and tissue distribution that need to be kept in mind when working with such models (Künzli et al., 2021).

Previously TCRs specific for the IA(b) GP66-77 epitope have been isolated from T cells transferred into secondary recipients from a SMARTA-alpha transgenic mouse followed by LCMV Armstrong infection. These T cells all share the same TCR alpha chain derived from the SMARTA TCR which is specific for the LCMV GP66-77 epitope, thus reducing the possible repertoire diversity. Furthermore, these TCR were selected from an ongoing infection, which

leads to the preferential selection of TCRs that lead to stronger expansion, which has been correlated with higher avidity (Busch & Pamer, 1999; Savage et al., 1999).

We therefore chose to isolate TCRs from the naive repertoire, in order to sample from a unreduced structural repertoire that had not been subjected to selective pressure by infection. To obtain T cells expressing the isolated TCRs we opted to utilize TCR retrogenic mice. Retrogenic TCR expression has the advantage, that mature naive T cells expressing the TCR of interest can be obtained in about 6 weeks. This is much faster than the generation of a transgenic line. However, the transgene cannot be passed on to offspring because only somatic cells are modified. By combining retrogenic TCR expression with congenic- and color-barcoding we were able to transfer and analyze TCRs of known functional avidity which could be identified by their congenic- or color-barcode. By this approach we could follow up to 6 populations with unique TCR avidities within the same recipient mouse. Furthermore, this barcoding approach allowed the fate mapping of single T cells of defined avidity, modified by the expression of unique TCRs in contrast to the measurement of the response of one TCR to APLs.

5.2.2 Increased TCR avidity leads to stronger expansion and Th1 differentiation of T cell populations

TCR avidity has been shown to influence $CD4^+$ T cell expansion and differentiation into helper subsets. For example, the transgenic TCRs 5CC7 and 2B4, specific for pigeon cytochrome c, lead to 2-4 fold expansion differences (Fazilleau et al., 2009). The fixed alpha chain TCR specific for the LCMV GP66-77 epitope isolated by Kim et al. showed up to 10-fold expansion differences at the peak of LCMV Armstrong infection (C. Kim et al., 2013). In comparison, the TCRs we isolated form the naive repertoire led up to 25-fold expansion differences after LCMV Armstrong infection, suggesting that they encompass a broader avidity range than TCRs that had previously been studied. Modification of TCR signal strength using APLs has however been able to generate larger expansion differences of a fixed transgenic TCR (Künzli et al., 2021). However, the use of APLs potentially comes with certain drawbacks as discussed in the previous section (5.2.1).

In line with published data, we could show that higher TCR avidity favored the generation of Th1 differentiated cells. Responses to LCMV APL strains that led to a 20-fold difference in SMARTA T cell expansion showed a 10 % difference in the frequency of Th1 cells (Künzli et al., 2021). In comparison, we also found a difference of 10 % in the generation of Th1 cells, for TCRs that led to 25-fold expansion differences. In contrast, we found a positive association of TCR avidity with Th1 differentiation at day 8 p.i. with LCMV CL13 infection in contrast to Künzli and colleagues. This discrepancy could be due to the use different markers to identify

Th1 cells. While CXCR6 was used to identify Th1 cells in this study, Künzli and colleagues used a combination of Ly6c and PSGL1. It has been shown that CXCR6$^+$ Th1 cells can be subdivided into Ly6c high and low subsets transcriptionally after LCMV infection (Khatun et al., 2021), potentially explaining these different findings.

The persistent presence of antigen such as in LCMV CL13 infection increases the frequency of Tfh cells (Baumjohann et al., 2013; Fahey et al., 2011). Regardless of TCR avidity we could show an increase of Tfh cell frequency after chronic infection of about 3-fold. We saw a slight tendency of increased GC Tfh differentiation with higher TCR avidity in chronic LCMV CL13 infection, but this trend was not statistically significant. Therefore, we could not recapitulate a positive influence of TCR avidity on Tfh differentiation, but instead found a greater importance for sustained antigenic signals (Fazilleau et al., 2009).

At later stages of LCMV CL13 infection the response was further skewed away from Th1 towards Tfh differentiation, most likely due to exhaustion and contraction of Th1 cells. We could show that high-avidity T cell populations showed more pronounced contraction into the memory phase than their lower avidity counterpart. This effect was even more pronounced in infection with LCMV CL13 during the transition into the chronic infection phase. The stronger contraction of high-avidity T cells could be explained by the increased Th1 differentiation of high-avidity T cell populations. Consistent with this observation Snook and colleagues showed that stronger TCR signals increased the frequency of CD25$^+$ Th1 effector cells accompanied by stronger contraction after LCMV Armstrong infection (Snook et al., 2018).

We wondered how this pronounced contraction could be explained in accordance with only small differences in differentiation seen on the population level. We therefore hypothesized that the clonal composition of these responses differed.

5.2.3 TCR avidity influences the frequency and extent of clonally biased differentiation

To this end we sought to analyze the influence of TCR avidity on single CD4$^+$ T cell fate. We studied whether TCR avidity changed differentiation patterns across all T cell families, or if avidity altered the probability of a T cell to adopt a certain fate. It had been shown that responses derived from single CD4$^+$ T cells can adopt clonally biased fates with substantial inter-clonal variability, suggesting an influence of the TCR on this process (Tubo et al., 2013). However, responses of single T cells bearing an identical TCR could produce similar degrees of inter-clonal variability, highlighting the probabilistic nature of this process and influence of additional differentiation cues (Cho et al., 2017).

Discussion

We found that responses derived from single T cells varied drastically in their absolute response size. Expansion differences seen on the population level between T cells expressing TCR 1 (high avidity) and TCR 11 (intermediate avidity) were lost on the single-cell level. In addition to variable expansion, T cell families showed highly variable fates. Ranging from strongly Th1- over unbiased to strongly Tfh biased, regardless of their TCR avidity. These findings highlight that the robust expansion and differentiation patterns seen in population derived responses are achieved by averaging the highly variable response pattern of T cell families. Moreover, we found that avidity-independent factors exerted effects on single T cell differentiation that far exceeded the rather subtle deterministic influence TCR avidity on single T cell behavior. These observations, were based on directly comparing two TCRs of distinct avidity on the single-cell level. They, thereby, add further support to previous findings concentrating on a single TCR (Cho et al., 2017).

It has been described that bifurcation of Th1 and Tfh fate is determined early during the immune response (Y. S. Choi et al., 2013; Ditoro et al., 2018). In accordance with these findings, we found a strong negative correlation between the frequency of Th1 and Tfh cells within a T cell family. Furthermore, the frequency of Th1 cells was negatively associated with the frequency of TCMp cells which highlights the terminal effector characteristics of Th1 differentiation. This has also been highlighted by Snook and colleagues that showed pronounce contraction and decreased memory differentiation of CD25 high (Th1 effector) cells (Snook et al., 2018). In contrast the frequency of Tfh and TCMp cells showed a positive association, in accordance with the findings that the development of these subsets share a transcriptional profile and possibly a precursor state (Ciucci et al., 2019; Pepper et al., 2011).

We found that the phenotype of T cell families could be grouped into strongly Th1- or Tfh biased as well as unbiased patterns. The average patterns of these groups were only slightly influenced by TCR avidity. In contrast, we found an influence of TCR avidity on the probability of T cell families to adopt one of these differentiation patterns. Higher TCR avidity increased the probability of adopting a Th1 or Tfh biased fate over an unbiased differentiation pattern. Mechanistically this could be explained by an influence of TCR avidity on the timing of the early Th1 or Tfh fate decision. While some studies have shown very early bifurcation of Th1 and Tfh fate within the first 72 hours of infection (Y. S. Choi et al., 2013; Ditoro et al., 2018) others have proposed this decision to occur between day 2 and 4 post infection (Lönnberg et al., 2017). These findings have been derived from different experimental systems, which could coincide with different strength of T cell stimulation at early timepoints; early bifurcation was found after LCMV or *L.m.* infection whereas late bifurcation was found after *Plasmodium* infection. It is therefore an intriguing idea to speculate, that higher TCR avidity leads to an earlier fate commitment due more robust accumulation of fate determining signals.

During T cell priming antigen specific T cells form long stable contacts with DCs for around one day before they begin to proliferate (Obst, 2015). It has been shown that higher TCR avidity leads to longer interaction times of T cells with DCs (Gottschalk et al., 2012). Mechanistically, higher TCR avidity could thereby lead to more robust fate commitment by longer interaction times in a polarizing environment or by faster accumulation of fate determining signals. By this, fate commitment could occur before extensive division leading to homogenous (biased) differentiation of the daughter cells. In contrast, lower TCR avidity could lead to the accumulation of fate determining signals only after the first rounds of cell division leading to divergent (more unbiased) differentiation outcomes within the same T cell family. In support of this hypothesis, T cell families with a high-avidity TCR showed a slightly larger degree of differentiation bias within the same family and a higher probability of adopting a biased over unbiased fate.

5.2.4 Clonally highly biased Th1 cell differentiation is associated with pronounced contraction

As we observed a high degree of phenotypic diversity of single $CD4^+$ T cell responses we wanted to address whether a certain differentiation pattern could be associated with enhanced memory formation and recall capacity. To address this question independent of TCR avidity we retransferred T cell families derived from single SMARTA T cells after infection with LCMV Armstrong and recalled these families after resting in secondary recipients. This allowed us to associate the primary response profile with recall capability.

We found that, while some T cell families showed expansion in comparison to their primary response magnitude, others showed contraction (smaller response size) or were not recovered at all. The loss of very large as well as small T cell families speaks against loss of these families simply due to retransfer. Generally, we found that recall response size was associated with the magnitude of the primary response. This speaks to the importance of the number of memory cells generated during the primary response for recall response size. Furthermore, we found that contraction and clonal loss were correlated with the degree of Th1 bias of the primary response. While a high degree of Th1 differentiation bias was associated with contraction, T cell families that were lost showed additional increase in Th1 bias at the expense of Tfh and TCMp cells.

Taken together these findings could explain the phenotype of increased contraction of high-avidity T cell populations found in transition to the memory or chronic infection phase. The response size of Th1-biased T cell families was significantly larger than the size of unbiased or Tfh biased families. Moreover, higher TCR avidity was associated with an increased probability to generate such Th1 biased T cell families. Together, this implies that expansion

differences seen between T cell populations of varying avidity are mainly caused by few T cell families with a high degree of Th1 differentiation. For higher TCR avidities this bias is stronger and more frequent. The pronounced contraction of high-avidity T cell population could thereby be explained by the contraction or possibly clonal loss of highly Th1-biased T cell families. To reconcile these findings, it would be interesting to see if high-avidity $CD4^+$ T cell populations show a loss of clonal diversity in comparison to intermediate- or low-avidity populations after recall.

6 Summary

In this thesis, we studied the influence of TCR avidity on the fate decisions of single $CD8^+$ and $CD4^+$ T cells. It has been shown that the recruitment of high-avidity T cells into the immune response is near complete and largely independent of antigen dose or vector upon systemic infection (van Heijst et al., 2009). However, it has remained unclear whether this is also the case for low-avidity T cells. Using OT1 transgenic T cells and *L.m.*-APL strains, we show here that the probability of $CD8^+$ T cell recruitment into the immune response is dependent on TCR avidity. Using an improved flow cytometric assay to detect unrecruited T cells, we show that infection with *L.m.* expressing low-avidity APLs left substantial fractions of OT1 T cells unrecruited. We corroborated these findings using two TCRs (OT1 and OT3) of distinct avidity for the same antigen. Additionally, we showed that T cells left unrecruited during a primary infection could participate in heterologous secondary infections with high-avidity antigen.

Taken together, these findings show that after systemic infection, large parts of antigen-specific but low-avidity T cells are left in a clonally ignorant state, meaning that they were left unaffected by this infection. The probability of T cells showing clonal ignorance to infection was negatively correlated with TCR-avidity. Importantly, these T cells could readily participate in secondary infection to high-avidity antigens. These findings shed new light on the clonal composition and clonal dynamics of secondary immune responses.

To analyze the influence of TCR avidity on $CD4^+$ T cell fate, we isolated TCRs from the naive repertoire of mice specific for the LCMV IA(b) GP66-77 epitope. The isolated TCRs showed a broad range of functional avidity encompassing a larger spectrum than previously utilized TCRs. By combining retrogenic TCR expression with congenic and retroviral color barcoding, we could track the fate of T cells expressing TCRs of defined characteristics in a highly multiplexed fashion. Studying the response of these T cells to acute and chronic LCMV infection, we found that high-avidity T cells expanded more vigorously but also showed stronger contraction, especially in chronic LCMV infection. Furthermore, we could confirm that TCR avidity and antigen persistence have distinct influences on $CD4^+$ T cell differentiation. Using T cell population transfers, our findings underlined that high TCR avidity favors the generation of Th1 cells, while Tfh generation is more dependent on prolonged antigenic signals as had been suggested before (Fahey et al., 2011; Keck et al., 2014; Tubo & Jenkins, 2014).

By studying single-cell derived responses of T cells harboring distinct TCRs, we could gather insights into the clonal composition of such responses and how deterministic vs. probabilistic factors shape them. To this end, we could show that T cell fate is not fully determined by TCR avidity but underlies a substantial degree of stochasticity. T cells were, in principle, capable of differentiation into Th1 or Tfh cells regardless of their TCR avidity. We found that the frequency

of Th1 cells was positively correlated with TCR avidity on the population level. This effect was not achieved by an overall increase of Th1 differentiation in all responding T cell clones. Instead, it was driven by an increase in the overall number of Th1-dominated clones and by a more extreme Th1 vs. Tfh bias in these clones. This could indicate that higher TCR avidity more frequently induces an early fate commitment to Th1 or Tfh development before substantial clonal expansion has occurred, while lower avidity interactions lead to delayed fate commitment enabling more balanced Th1 and Tfh differentiation emerging after several rounds of proliferation.

Additionally, we found that the phenotype of pronounced contraction of high avidity T cell populations could be explained by the more frequent generation of highly Th1 differentiated T cell families on the clonal level. These families contributed more to population response size than unbiased or Tfh biased T cell families. Moreover, the degree of Th1 differentiation was negatively associated with a T cell family's capability to expand upon recall, and a very high degree of Th1 differentiation bias was predictive of contraction or loss of T cell families. By this, high avidity T cell populations were more prone to pronounced contraction, especially in chronic LCMV infection that favors loss of Th1 cells.

In summary, we could confirm that TCR avidity shapes the response of single T cells in a probabilistic manner, by using TCRs of unique avidity for the same antigen. Predictable, TCR avidity dependent, response patterns are achieved by averaging mechanisms on the population level. While high TCR avidity leads to vigorous expansion, it frequently induces highly clonally biased Th1 differentiation, associated with pronounced contraction. In contrast, low TCR avidity favors a balanced differentiation profile but only leads to weak expansion. In the context of adoptive cancer immunotherapy, it might be advantageous to utilize intermediate avidity TCRs that lead to robust expansion and a more balanced differentiation profile less prone to contraction, thereby possibly providing more durable responses.

7 Bibliography

Appay, V. (2004). The physiological role of cytotoxic CD4+ T-cells: the holy grail? *Clinical and Experimental Immunology*, *138*(1), 10. https://doi.org/10.1111/J.1365-2249.2004.02605.X

Au-Yeung, B. B., Zikherman, J., Mueller, J. L., Ashouri, J. F., Matloubian, M., Cheng, D. A., Chen, Y., Shokat, K. M., & Weiss, A. (2014). A sharp T-cell antigen receptor signaling threshold for T-cell proliferation. *Proceedings of the National Academy of Sciences of the United States of America*, *111*(35). https://doi.org/10.1073/PNAS.1413726111

Badovinac, V. P., Porter, B. B., & Harty, J. T. (2002). Programmed contraction of CD8(+) T cells after infection. *Nature Immunology*, *3*(7), 619–626. https://doi.org/10.1038/NI804

Battegay, M., Cooper, S., Althage, A., Bänziger, J., Hengartner, H., & Zinkernagel, R. M. (1991). Quantification of lymphocytic choriomeningitis virus with an immunological focus assay in 24- or 96-well plates. *Journal of Virological Methods*, *33*(1–2), 191–198. https://doi.org/10.1016/0166-0934(91)90018-U

Baumjohann, D., Preite, S., Reboldi, A., Ronchi, F., Ansel, K. M., Lanzavecchia, A., & Sallusto, F. (2013). Persistent Antigen and Germinal Center B Cells Sustain T Follicular Helper Cell Responses and Phenotype. *Immunity*, *38*(3), 596–605. https://doi.org/10.1016/J.IMMUNI.2012.11.020/ATTACHMENT/58B7ACFC-502E-4986-9549-D847B1FFC27B/MMC1.PDF

Bernstein, N. J., Fong, N. L., Lam, I., Roy, M. A., Hendrickson, D. G., & Kelley, D. R. (2020). Solo: Doublet Identification in Single-Cell RNA-Seq via Semi-Supervised Deep Learning. *Cell Systems*, *11*(1), 95-101.e5. https://doi.org/10.1016/J.CELS.2020.05.010/ATTACHMENT/7C5ADF89-E777-4D52-A2FD-FC847A072E10/MMC2.PDF

Bhattacharyya, N. D., & Feng, C. G. (2020). Regulation of T Helper Cell Fate by TCR Signal Strength. *Frontiers in Immunology*, *11*, 624. https://doi.org/10.3389/FIMMU.2020.00624/BIBTEX

Bilate, A. M., & Lafaille, J. J. (2012). Induced CD4+Foxp3+ Regulatory T Cells in Immune Tolerance. *Https://Doi.Org/10.1146/Annurev-Immunol-020711-075043*, *30*, 733–758. https://doi.org/10.1146/ANNUREV-IMMUNOL-020711-075043

Blander, J. M., Sant'Angelo, D. B., Bottomly, K., & Janeway, C. A. (2000). Alteration at a Single Amino Acid Residue in the T Cell Receptor α Chain Complementarity Determining Region 2 Changes the Differentiation of Naive Cd4 T Cells in Response to Antigen from T Helper Cell Type 1 (Th1) to Th2. *Journal of Experimental Medicine*, *191*(12), 2065–2074. https://doi.org/10.1084/JEM.191.12.2065

Breitfeld, D., Ohl, L., Kremmer, E., Ellwart, J., Sallusto, F., Lipp, M., & Förster, R. (2000). Follicular B helper T cells express CXC chemokine receptor 5, localize to B cell follicles, and support immunoglobulin production. *The Journal of Experimental Medicine*, *192*(11), 1545–1551. https://doi.org/10.1084/JEM.192.11.1545

Brochet, X., Lefranc, M. P., & Giudicelli, V. (2008). IMGT/V-QUEST: the highly customized and integrated system for IG and TR standardized V-J and V-D-J sequence analysis. *Nucleic Acids Research*, *36*(Web Server issue). https://doi.org/10.1093/NAR/GKN316

Brogdon, J. L., Leitenberg, D., & Bottomly, K. (2002). The Potency of TCR Signaling Differentially Regulates NFATc/p Activity and Early IL-4 Transcription in Naive CD4+ T Cells. *The Journal of Immunology*, *168*(8), 3825–3832. https://doi.org/10.4049/JIMMUNOL.168.8.3825

Brownlie, R. J., & Zamoyska, R. (2013). T cell receptor signalling networks: branched, diversified and bounded. *Nature Reviews Immunology 2013 13:4*, *13*(4), 257–269. https://doi.org/10.1038/nri3403

Buchholz, V. R., & Flossdorf, M. (2018). Single-Cell Resolution of T Cell Immune Responses. *Advances in Immunology*, *137*, 1–41. https://doi.org/10.1016/BS.AI.2017.12.001

Buchholz, V. R., Flossdorf, M., Hensel, I., Kretschmer, L., Weissbrich, B., Gräf, P., Verschoor, A., Schiemann, M., Höfer, T., & Busch, D. H. (2013). Disparate individual

fates compose robust CD8+ T cell immunity. *Science*, *340*(6132), 630–635. https://doi.org/10.1126/SCIENCE.1235454/SUPPL_FILE/BUCHOLZ.SM.PDF

Buchholz, V. R., Schumacher, T. N. M., & Busch, D. H. (2016). T Cell Fate at the Single-Cell Level. *Http://Dx.Doi.Org.Eaccess.Ub.Tum.de/10.1146/Annurev-Immunol-032414-112014*, *34*, 65–92. https://doi.org/10.1146/ANNUREV-IMMUNOL-032414-112014

Busch, D. H., & Pamer, E. G. (1999). T cell affinity maturation by selective expansion during infection. *J. Exp. Med.*, *189*(4), 701–709. https://doi.org/10.1084/jem.189.4.701

Campillo-Davo, D., Flumens, D., & Lion, E. (2020). The Quest for the Best: How TCR Affinity, Avidity, and Functional Avidity Affect TCR-Engineered T-Cell Antitumor Responses. *Cells*, *9*(7). https://doi.org/10.3390/CELLS9071720

Cano-Gamez, E., Soskic, B., Roumeliotis, T. I., So, E., Smyth, D. J., Baldrighi, M., Willé, D., Nakic, N., Esparza-Gordillo, J., Larminie, C. G. C., Bronson, P. G., Tough, D. F., Rowan, W. C., Choudhary, J. S., & Trynka, G. (2020). Single-cell transcriptomics identifies an effectorness gradient shaping the response of CD4+ T cells to cytokines. *Nature Communications 2020 11:1*, *11*(1), 1–15. https://doi.org/10.1038/s41467-020-15543-y

Chappert, P., & Schwartz, R. H. (2010). Induction of T cell anergy: integration of environmental cues and infectious tolerance. *Current Opinion in Immunology*. https://doi.org/10.1016/j.coi.2010.08.005

Chen, J.-L., Morgan, A. J., Stewart-Jones, G., Shepherd, D., Bossi, G., Wooldridge, L., Hutchinson, S. L., Sewell, A. K., Griffiths, G. M., Merwe, P. A. van der, Jones, E. Y., Galione, A., & Cerundolo, V. (2010). Ca2+ Release from the Endoplasmic Reticulum of NY-ESO-1–Specific T Cells Is Modulated by the Affinity of TCR and by the Use of the CD8 Coreceptor. *The Journal of Immunology*, *184*(4), 1829–1839. https://doi.org/10.4049/JIMMUNOL.0902103

Chen, Z., Ji, Z., Ngiow, S. F., Manne, S., Cai, Z., Huang, A. C., Johnson, J., Staupe, R. P., Bengsch, B., Xu, C., Yu, S., Kurachi, M., Herati, R. S., Vella, L. A., Baxter, A. E., Wu, J. E., Khan, O., Beltra, J. C., Giles, J. R., … Wherry, E. J. (2019). TCF-1-Centered Transcriptional Network Drives an Effector versus Exhausted CD8 T Cell-Fate Decision. *Immunity*, *51*(5), 840-855.e5. https://doi.org/10.1016/J.IMMUNI.2019.09.013

Cho, Y. L., Flossdorf, M., Kretschmer, L., Höfer, T., Busch, D. H., & Buchholz, V. R. (2017). TCR Signal Quality Modulates Fate Decisions of Single CD4+ T Cells in a Probabilistic Manner. *Cell Reports*, *20*(4), 806–818. https://doi.org/10.1016/J.CELREP.2017.07.005/ATTACHMENT/CEFDA9BE-141D-458F-9EC1-D5D0710EBC06/MMC1.PDF

Choi, J., & Crotty, S. (2021). Bcl6-Mediated Transcriptional Regulation of Follicular Helper T cells (TFH). *Trends in Immunology*, *42*(4), 336–349. https://doi.org/10.1016/J.IT.2021.02.002

Choi, Y. S., Yang, J. A., Yusuf, I., Johnston, R. J., Greenbaum, J., Peters, B., & Crotty, S. (2013). Bcl6 Expressing Follicular Helper CD4 T Cells Are Fate Committed Early and Have the Capacity To Form Memory. *The Journal of Immunology*, *190*(8), 4014–4026. https://doi.org/10.4049/JIMMUNOL.1202963

Christo, S. N., Diener, K. R., Nordon, R. E., Brown, M. P., Griesser, H. J., Vasilev, K., Christo, F. C., & Hayball, J. D. (2015). Scrutinizing calcium flux oscillations in T lymphocytes to deduce the strength of stimulus. *Scientific Reports 2015 5:1*, *5*(1), 1–8. https://doi.org/10.1038/srep07760

Ciucci, T., Vacchio, M. S., Gao, Y., Tomassoni Ardori, F., Candia, J., Mehta, M., Zhao, Y., Tran, B., Pepper, M., Tessarollo, L., McGavern, D. B., & Bosselut, R. (2019). The Emergence and Functional Fitness of Memory CD4 + T Cells Require the Transcription Factor Thpok. *Immunity*, *50*(1), 91-105.e4. https://doi.org/10.1016/J.IMMUNI.2018.12.019/ATTACHMENT/7FCD02DE-DFAB-4AC0-892E-2CE28674A582/MMC1.PDF

Condotta, S. A., Richer, M. J., Badovinac, V. P., & Harty, J. T. (2012). Probing CD8 T cell responses with Listeria monocytogenes infection. *Advances in Immunology*, *113*, 51–80. https://doi.org/10.1016/B978-0-12-394590-7.00005-1

Bibliography

Conley, J. M., Gallagher, M. P., & Berg, L. J. (2016). T cells and gene regulation: The switching on and turning up of genes after T cell receptor stimulation in CD8 T cells. *Frontiers in Immunology*, *7*(FEB). https://doi.org/10.3389/FIMMU.2016.00076

Conley, J. M., Gallagher, M. P., Rao, A., & Berg, L. J. (2020). Activation of the Tec kinase ITK controls graded IRF4 expression in response to variations in TCR signal strength. *Journal of Immunology (Baltimore, Md. : 1950)*, *205*(2), 335. https://doi.org/10.4049/JIMMUNOL.1900853

Constant, S., Pfeiffer, C., Woodard, A., Pasqualini, T., & Bottomly, K. (1995). Extent of T cell receptor ligation can determine the functional differentiation of naive CD4+ T cells. *The Journal of Experimental Medicine*, *182*(5), 1591–1596. https://doi.org/10.1084/JEM.182.5.1591

Crawford, A., Angelosanto, J. M., Kao, C., Doering, T. A., Odorizzi, P. M., Barnett, B. E., & Wherry, E. J. (2014). Molecular and Transcriptional Basis of CD4+ T Cell Dysfunction during Chronic Infection. *Immunity*, *40*(2), 289–302. https://doi.org/10.1016/J.IMMUNI.2014.01.005

Crotty, S. (2019). T Follicular Helper Cell Biology: A Decade of Discovery and Diseases. *Immunity*, *50*(5), 1132–1148. https://doi.org/10.1016/J.IMMUNI.2019.04.011/ATTACHMENT/F65FBD1E-AAF9-4BF5-B165-50FD23230D6D/MMC1.MP4

Daniels, M. A., Teixeiro, E., Gill, J., Hausmann, B., Roubaty, D., Holmberg, K., Werlen, G., Holländer, G. A., Gascoigne, N. R. J., & Palmer, E. (2006). Thymic selection threshold defined by compartmentalization of Ras/MAPK signalling. *Nature 2006 444:7120*, *444*(7120), 724–729. https://doi.org/10.1038/nature05269

Das, J., Ho, M., Zikherman, J., Govern, C., Yang, M., Weiss, A., Chakraborty, A. K., & Roose, J. P. (2009). Digital signaling and hysteresis characterize ras activation in lymphoid cells. *Cell*, *136*(2), 337–351. https://doi.org/10.1016/J.CELL.2008.11.051

Ditoro, D., Winstead, C., Pham, D., Witte, S., Andargachew, R., Singer, J. R., Wilson, C. G., Zindl, C. L., Luther, R. J., Silberger, D. J., Weaver, B., Kolawole, M., Martinez, R. J., Turner, H., Hatton, R. D., Moon, J., Way, S. S., Evavold, B. D., & Weaver, C. T. (2018). Differential IL-2 expression defines developmental fates of follicular versus nonfollicular helper T cells. *Science*, *361*(6407). https://doi.org/10.1126/SCIENCE.AAO2933

Dössinger, G., Bunse, M., Bet, J., Albrecht, J., Paszkiewicz, P. J., Weißbrich, B., Schiedewitz, I., Henkel, L., Schiemann, M., Neuenhahn, M., Uckert, W., & Busch, D. H. (2013). MHC multimer-guided and cell culture-independent isolation of functional T cell receptors from single cells facilitates TCR identification for immunotherapy. *PloS One*, *8*(4). https://doi.org/10.1371/JOURNAL.PONE.0061384

Dushek, O., Aleksic, M., Wheeler, R. J., Zhang, H., Cordoba, S. P., Peng, Y. C., Chen, J. L., Cerundolo, V., Dong, T., Coombs, D., & van der Merwe, P. A. (2011). Antigen potency and maximal efficacy reveal a mechanism of efficient T cell activation. *Science Signaling*, *4*(176). https://doi.org/10.1126/SCISIGNAL.2001430

Embgenbroich, M., & Burgdorf, S. (2018). Current concepts of antigen cross-presentation. *Frontiers in Immunology*, *9*(JUL), 1643. https://doi.org/10.3389/FIMMU.2018.01643/BIBTEX

Enouz, S., Carrié, L., Merkler, D., Bevan, M. J., & Zehn, D. (2012). Autoreactive T cells bypass negative selection and respond to self-antigen stimulation during infection. *The Journal of Experimental Medicine*, *209*(10), 1769. https://doi.org/10.1084/JEM.20120905

Fahey, L. M., Wilson, E. B., Elsaesser, H., Fistonich, C. D., McGavern, D. B., & Brooks, D. G. (2011). Viral persistence redirects CD4 T cell differentiation toward T follicular helper cells. *The Journal of Experimental Medicine*, *208*(5), 987. https://doi.org/10.1084/JEM.20101773

Fazilleau, N., McHeyzer-Williams, L. J., Rosen, H., & McHeyzer-Williams, M. G. (2009). The function of follicular helper T cells is regulated by the strength of T cell antigen receptor binding. *Nature Immunology*, *10*(4), 375–384. https://doi.org/10.1038/NI.1704

Flommersfeld, S., Böttcher, J. P., Ersching, J., Flossdorf, M., Meiser, P., Pachmayr, L. O., Leube, J., Hensel, I., Jarosch, S., Zhang, Q., Chaudhry, M. Z., Andrae, I., Schiemann,

M., Busch, D. H., Cicin-Sain, L., Sun, J. C., Gasteiger, G., Victora, G. D., Höfer, T., … Grassmann, S. (2021). Fate mapping of single NK cells identifies a type 1 innate lymphoid-like lineage that bridges innate and adaptive recognition of viral infection. *Immunity*, *54*(10), 2288-2304.e7. https://doi.org/10.1016/J.IMMUNI.2021.08.002/ATTACHMENT/D580B8D8-82CD-48F7-9143-74069275E608/MMC3.XLS

Fu, S., Zhang, N., Yopp, A. C., Chen, D., Mao, M., Chen, D., Zhang, H., Ding, Y., & Bromberg, J. S. (2004). TGF-beta induces Foxp3 + T-regulatory cells from CD4 + CD25 - precursors. *American Journal of Transplantation : Official Journal of the American Society of Transplantation and the American Society of Transplant Surgeons*, *4*(10), 1614–1627. https://doi.org/10.1111/J.1600-6143.2004.00566.X

Gerlach, C., Rohr, J. C., Perié, L., van Rooij, N., van Heijst, J. W. J., Velds, A., Urbanus, J., Naik, S. H., Jacobs, H., Beltman, J. B., de Boer, R. J., & Schumacher, T. N. M. (2013). Heterogeneous differentiation patterns of individual CD8+ T cells. *Science (New York, N.Y.)*, *340*(6132), 635–639. https://doi.org/10.1126/SCIENCE.1235487

Gottschalk, R. A., Hathorn, M. M., Beuneu, H., Corse, E., Dustin, M. L., Altan-Bonnet, G., & Allison, J. P. (2012). Distinct influences of peptide-MHC quality and quantity on in vivo T-cell responses. *Proceedings of the National Academy of Sciences of the United States of America*, *109*(3), 881–886. https://doi.org/10.1073/PNAS.1119763109

Graef, P., Buchholz, V. R., Stemberger, C., Flossdorf, M., Henkel, L., Schiemann, M., Drexler, I., Höfer, T., Riddell, S. R., & Busch, D. H. (2014). Serial Transfer of Single-Cell-Derived Immunocompetence Reveals Stemness of CD8+ Central Memory T Cells. *Immunity*, *41*(1), 116–126. https://doi.org/10.1016/J.IMMUNI.2014.05.018/ATTACHMENT/8396BEF2-4B52-435A-8870-CEC6330F8DD6/MMC1.PDF

Grassmann, S., Mihatsch, L., Mir, J., Kazeroonian, A., Rahimi, R., Flommersfeld, S., Schober, K., Hensel, I., Leube, J., Pachmayr, L. O., Kretschmer, L., Zhang, Q., Jolly, A., Chaudhry, M. Z., Schiemann, M., Cicin-Sain, L., Höfer, T., Busch, D. H., Flossdorf, M., & Buchholz, V. R. (2020). Early emergence of T central memory precursors programs clonal dominance during chronic viral infection. *Nature Immunology*, *21*(12), 1563–1573. https://doi.org/10.1038/s41590-020-00807-y

Grassmann, S., Pachmayr, L. O., Leube, J., Schiemann, M., Flossdorf, M., & Buchholz Correspondence, V. R. (2019). Distinct Surface Expression of Activating Receptor Ly49H Drives Differential Expansion of NK Cell Clones upon Murine Cytomegalovirus Infection. *Immunity*, *50*, 1391–1400. https://doi.org/10.1016/j.immuni.2019.04.015

Grassmann, S., Sun, J. C., & Buchholz, V. R. (2022). *Retrogenic Color-Barcoding for Fate Mapping of Single Innate Lymphocytes*. 117–127. https://doi.org/10.1007/978-1-0716-2160-8_9

Gullicksrud, J. A., Li, F., Xing, S., Zeng, Z., Peng, W., Badovinac, V. P., Harty, J. T., & Xue, H.-H. (2017). Differential requirements for Tcf1 long isoforms in CD8+ and CD4+ T cell responses to acute viral infection. *Journal of Immunology (Baltimore, Md. : 1950)*, *199*(3), 911. https://doi.org/10.4049/JIMMUNOL.1700595

Harrington, L. E., Hatton, R. D., Mangan, P. R., Turner, H., Murphy, T. L., Murphy, K. M., & Weaver, C. T. (2005). Interleukin 17–producing CD4+ effector T cells develop via a lineage distinct from the T helper type 1 and 2 lineages. *Nature Immunology 2005 6:11*, *6*(11), 1123–1132. https://doi.org/10.1038/ni1254

Hogquist, K. A., Jameson, S. C., Heath, W. R., Howard, J. L., Bevan, M. J., & Carbone, F. R. (1994). T cell receptor antagonist peptides induce positive selection. *Cell*, *76*(1), 17–27. https://doi.org/10.1016/0092-8674(94)90169-4

Holst, J., Szymczak-Workman, A. L., Vignali, K. M., Burton, A. R., Workman, C. J., & Vignali, D. A. A. (2006). Generation of T-cell receptor retrogenic mice. *Nature Protocols*, *1*(1), 406–417. https://doi.org/10.1038/NPROT.2006.61

Hori, S., Nomura, T., & Sakaguchi, S. (2003). Control of regulatory T cell development by the transcription factor Foxp3. *Science (New York, N.Y.)*, *299*(5609), 981–985. https://doi.org/10.1126/SCIENCE.1079490

Bibliography

Hosken, N. A., Shibuya, K., Heath, A. W., Murphy, K. M., & O'Garra, A. (1995). The effect of antigen dose on CD4+ T helper cell phenotype development in a T cell receptor-alpha beta-transgenic model. *Journal of Experimental Medicine*, *182*(5), 1579–1584. https://doi.org/10.1084/JEM.182.5.1579

Ivanov, I. I., McKenzie, B. S., Zhou, L., Tadokoro, C. E., Lepelley, A., Lafaille, J. J., Cua, D. J., & Littman, D. R. (2006). The orphan nuclear receptor RORgammat directs the differentiation program of proinflammatory IL-17+ T helper cells. *Cell*, *126*(6), 1121–1133. https://doi.org/10.1016/J.CELL.2006.07.035

Jelley-Gibbs, D. M., Lepak, N. M., Yen, M., & Swain, S. L. (2000). Two Distinct Stages in the Transition from Naive CD4 T Cells to Effectors, Early Antigen-Dependent and Late Cytokine-Driven Expansion and Differentiation. *The Journal of Immunology*, *165*(9), 5017–5026. https://doi.org/10.4049/JIMMUNOL.165.9.5017

Jenkins, M. K., & Moon, J. J. (2012). The Role of Naive T Cell Precursor Frequency and Recruitment in Dictating Immune Response Magnitude. *The Journal of Immunology*, *188*(9), 4135–4140. https://doi.org/10.4049/JIMMUNOL.1102661

Johnston, R. J., Poholek, A. C., DiToro, D., Yusuf, I., Eto, D., Barnett, B., Dent, A. L., Craft, J., & Crotty, S. (2009). Bcl6 and Blimp-1 are reciprocal and antagonistic regulators of T follicular helper cell differentiation. *Science*, *325*(5943), 1006–1010. https://doi.org/10.1126/SCIENCE.1175870/SUPPL_FILE/JOHNSTON.SOM.PDF

Jorritsma, P. J., Brogdon, J. L., & Bottomly, K. (2003). Role of TCR-Induced Extracellular Signal-Regulated Kinase Activation in the Regulation of Early IL-4 Expression in Naive CD4+ T Cells. *The Journal of Immunology*, *170*(5), 2427–2434. https://doi.org/10.4049/JIMMUNOL.170.5.2427

Juno, J. A., Bockel, D. van, Kent, S. J., Kelleher, A. D., Zaunders, J. J., & Munier, C. M. L. (2017). Cytotoxic CD4 T cells-friend or foe during viral infection? *Frontiers in Immunology*, *8*(JAN), 19. https://doi.org/10.3389/FIMMU.2017.00019/BIBTEX

Keck, S., Schmaler, M., Ganter, S., Wyss, L., Oberle, S., Huseby, E. S., Zehn, D., & King, C. G. (2014). Antigen affinity and antigen dose exert distinct influences on CD4 T-cell differentiation. *Proceedings of the National Academy of Sciences of the United States of America*, *111*(41), 14852–14857. https://doi.org/10.1073/PNAS.1403271111/SUPPL_FILE/PNAS.201403271SI.PDF

Kedl, R. M., Kappler, J. W., & Marrack, P. (2003). Epitope dominance, competition and T cell affinity maturation. *Current Opinion in Immunology*, *15*(1), 120–127. https://doi.org/10.1016/s0952-7915(02)00009-2

Khatun, A., Kasmani, M. Y., Zander, R., Schauder, D. M., Snook, J. P., Shen, J., Wu, X., Burns, R., Chen, Y. G., Lin, C. W., Williams, M. A., & Cui, W. (2021). Single-cell lineage mapping of a diverse virus-specific naive CD4 T cell repertoire. *The Journal of Experimental Medicine*, *218*(3). https://doi.org/10.1084/JEM.20200650/211542

Kim, C. H., Rott, L. S., Clark-Lewis, I., Campbell, D. J., Wu, L., & Butcher, E. C. (2001). Subspecialization of CXCR5+ T cells: B helper activity is focused in a germinal center-localized subset of CXCR5+ T cells. *The Journal of Experimental Medicine*, *193*(12), 1373–1381. https://doi.org/10.1084/JEM.193.12.1373

Kim, C., Wilson, T., Fischer, K. F., & Williams, M. A. (2013). Sustained Interactions between T Cell Receptors and Antigens Promote the Differentiation of CD4+ Memory T Cells. *Immunity*, *39*(3), 508–520. https://doi.org/10.1016/J.IMMUNI.2013.08.033

Kingeter, L. M., Paul, S., Maynard, S. K., Cartwright, N. G., & Schaefer, B. C. (2010). Cutting Edge: TCR Ligation Triggers Digital Activation of NF-κB. *The Journal of Immunology*, *185*(8), 4520–4524. https://doi.org/10.4049/JIMMUNOL.1001051

Klein, L., Kyewski, B., Allen, P. M., & Hogquist, K. A. (2014). Positive and negative selection of the T cell repertoire: what thymocytes see (and don't see). *Nature Reviews. Immunology*, *14*(6), 377–391. https://doi.org/10.1038/NRI3667

Korb, L. C., Mirshahidi, S., Ramyar, K., Sadighi Akha, A. A., & Sadegh-Nasseri, S. (1999). Induction of T Cell Anergy by Low Numbers of Agonist Ligands. *The Journal of Immunology*, *162*(11).

Kotov, D. I., Mitchell, J. S., Pengo, T., Ruedl, C., Way, S. S., Langlois, R. A., Fife, B. T., & Jenkins, M. K. (2019). TCR Affinity Biases Th Cell Differentiation by Regulating CD25,

Eef1e1, and Gbp2. *The Journal of Immunology*, *202*(9), 2535–2545. https://doi.org/10.4049/JIMMUNOL.1801609/-/DCSUPPLEMENTAL

Kretschmer, L., Flossdorf, M., Mir, J., Cho, Y. L., Plambeck, M., Treise, I., Toska, A., Heinzel, S., Schiemann, M., Busch, D. H., & Buchholz, V. R. (2020). Differential expansion of T central memory precursor and effector subsets is regulated by division speed. *Nature Communications 2020 11:1*, *11*(1), 1–12. https://doi.org/10.1038/s41467-019-13788-w

Kumar, V., Bhardwaj, V., Soares, L., Alexander, J., Sette, A., & Sercaz, E. (1995). Major histocompatibility complex binding affinity of an antigenic determinant is crucial for the differential secretion of interleukin 4/5 or interferon γ by T cells. *Proceedings of the National Academy of Sciences of the United States of America*, *92*(21), 9510–9514. https://doi.org/10.1073/PNAS.92.21.9510

Künzli, M., Reuther, P., Pinschewer, D. D., & King, C. G. (2021). Opposing effects of T cell receptor signal strength on CD4 T cells responding to acute versus chronic viral infection. *ELife*, *10*. https://doi.org/10.7554/ELIFE.61869

la Gruta, N. L., Rothwell, W. T., Cukalac, T., Swan, N. G., Valkenburg, S. A., Kedzierska, K., Thomas, P. G., Doherty, P. C., & Turner, S. J. (2010). Primary CTL response magnitude in mice is determined by the extent of naive T cell recruitment and subsequent clonal expansion. *The Journal of Clinical Investigation*, *120*(6), 1885–1894. https://doi.org/10.1172/JCI41538

Laydon, D. J., Bangham, C. R. M., & Asquith, B. (2015). Estimating T-cell repertoire diversity: limitations of classical estimators and a new approach. *Philosophical Transactions of the Royal Society B: Biological Sciences*, *370*(1675). https://doi.org/10.1098/RSTB.2014.0291

Leube, J. (2017). *The Influence of TCR Affinity on the Development of CD8+ Memory T cells* [Master Thesis, unpublished]. Technical University of Munich.

Lever, M., Maini, P. K., Anton van der Merwe, P., & Dushek, O. (2014). Phenotypic models of T cell activation. *Nature Publishing Group*. https://doi.org/10.1038/nri3728

Lewis, M., Tarlton, J. F., & Cose, S. (2008). Memory versus naive T-cell migration. *Immunology and Cell Biology*, *86*(3), 226–231. https://doi.org/10.1038/SJ.ICB.7100132

Lindqvist, M., van Lunzen, J., Soghoian, D. Z., Kuhl, B. D., Ranasinghe, S., Kranias, G., Flanders, M. D., Cutler, S., Yudanin, N., Muller, M. I., Davis, I., Farber, D., Hartjen, P., Haag, F., Alter, G., zur Wiesch, J. S., & Streeck, H. (2012). Expansion of HIV-specific T follicular helper cells in chronic HIV infection. *The Journal of Clinical Investigation*, *122*(9), 3271–3280. https://doi.org/10.1172/JCI64314

Lönnberg, T., Svensson, V., James, K. R., Fernandez-Ruiz, D., Sebina, I., Montandon, R., Soon, M. S. F., Fogg, L. G., Nair, A. S., Liligeto, U. N., Stubbington, M. J. T., Ly, L. H., Bagger, F. O., Zwiessele, M., Lawrence, N. D., Souza-Fonseca-Guimaraes, F., Bunn, P. T., Engwerda, C. R., Heath, W. R., … Teichmann, S. A. (2017). Single-cell RNA-seq and computational analysis using temporal mixture modelling resolves Th1/Tfh fate bifurcation in malaria. *Science Immunology*, *2*(9). https://doi.org/10.1126/SCIIMMUNOL.AAL2192

Malherbe, L., Hausl, C., Teyton, L., & McHeyzer-Williams, M. G. (2004). Clonal selection of helper T cells is determined by an affinity threshold with no further skewing of TCR binding properties. *Immunity*, *21*(5), 669–679. https://doi.org/10.1016/J.IMMUNI.2004.09.008/ATTACHMENT/F3B6CC54-5D40-45DC-8ADF-A2D056A1C605/MMC1.JPG

Marchingo, J. M., Kan, A., Sutherland, R. M., Duffy, K. R., Wellard, C. J., Belz, G. T., Lew, A. M., Dowling, M. R., Heinzel, S., & Hodgkin, P. D. (2014). Antigen affinity, costimulation, and cytokine inputs sum linearly to amplify T cell expansion. *Science*, *346*(6213), 1123–1127. https://doi.org/10.1126/SCIENCE.1260044

Matloubian, M., Kolhekar, S. R., Somasundaram, T., & Ahmed, R. (1993). Molecular determinants of macrophage tropism and viral persistence: importance of single amino acid changes in the polymerase and glycoprotein of lymphocytic choriomeningitis virus. *Journal of Virology*, *67*(12), 7340–7349. https://doi.org/10.1128/JVI.67.12.7340-7349.1993

Bibliography

Mirshahidi, S., Ferris, L. C. K., & Sadegh-Nasseri, S. (2004). The magnitude of TCR engagement is a critical predictor of T cell anergy or activation. *Journal of Immunology (Baltimore, Md. : 1950)*, *172*(9), 5346–5355. https://doi.org/10.4049/JIMMUNOL.172.9.5346

Moon, J. J., Chu, H. H., Pepper, M., McSorley, S. J., Jameson, S. C., Kedl, R. M. M., & Jenkins, M. K. (2007). Naive CD4(+) T cell frequency varies for different epitopes and predicts repertoire diversity and response magnitude. *Immunity*, *27*(2), 203–213. https://doi.org/10.1016/J.IMMUNI.2007.07.007

Mosmann, T. R., Cherwinski, H., Bond, M. W., Giedlin, M. A., & Coffman, R. L. (1986). Two types of murine helper T cell clone. I. Definition according to profiles of lymphokine activities and secreted proteins. *The Journal of Immunology*, *136*(7).

Mucida, D., Husain, M. M., Muroi, S., van Wijk, F., Shinnakasu, R., Naoe, Y., Reis, B. S., Huang, Y., Lambolez, F., Docherty, M., Attinger, A., Shui, J. W., Kim, G., Lena, C. J., Sakaguchi, S., Miyamoto, C., Wang, P., Atarashi, K., Park, Y., … Cheroutre, H. (2013). Transcriptional reprogramming of mature CD4+ helper T cells generates distinct MHC class II–restricted cytotoxic T lymphocytes. *Nature Immunology 2013 14:3*, *14*(3), 281–289. https://doi.org/10.1038/ni.2523

Nikolich-Žugich, J., Slifka, M. K., & Messaoudi, I. (2004). The many important facets of T-cell repertoire diversity. *Nature Reviews Immunology 2004 4:2*, *4*(2), 123–132. https://doi.org/10.1038/nri1292

Nüssing, S., Trapani, J. A., & Parish, I. A. (2020). Revisiting T Cell Tolerance as a Checkpoint Target for Cancer Immunotherapy. *Frontiers in Immunology*, *11*, 2461. https://doi.org/10.3389/FIMMU.2020.589641/BIBTEX

Obar, J. J., Khanna, K. M., & Lefrançois, L. (2008). Endogenous naive CD8+ T cell precursor frequency regulates primary and memory responses to infection. *Immunity*, *28*(6), 859–869. https://doi.org/10.1016/J.IMMUNI.2008.04.010

Oberle, S. G., Hanna-El-Daher, L., Chennupati, V., Enouz, S., Scherer, S., Prlic, M., & Zehn, D. (2016). A Minimum Epitope Overlap between Infections Strongly Narrows the Emerging T Cell Repertoire. *Cell Reports*, *17*(3), 627–635. https://doi.org/10.1016/J.CELREP.2016.09.072/ATTACHMENT/27810D79-10C6-471A-9261-FB87341A4382/MMC1.PDF

Obst, R. (2015). The timing of T cell priming and cycling. *Frontiers in Immunology*, *6*(NOV), 563. https://doi.org/10.3389/FIMMU.2015.00563/BIBTEX

Ochsenbein, A. F. (2005). Immunological ignorance of solid tumors. *Springer Seminars in Immunopathology*, *27*(1), 19–35. https://doi.org/10.1007/S00281-004-0192-0

Ouyang, W., Löhning, M., Gao, Z., Assenmacher, M., Ranganath, S., Radbruch, A., & Murphy, K. M. (2000). Stat6-independent GATA-3 autoactivation directs IL-4-independent Th2 development and commitment. *Immunity*, *12*(1), 27–37. https://doi.org/10.1016/S1074-7613(00)80156-9

Oxenius, A., Bachmann, M. F., Ashton-Rickardt, P. G., Tonegawa, S., Zinkernagel, R. M., & Hengartner, H. (1995). Presentation of endogenous viral proteins in association with major histocompatibility complex class II: On the role of intracellular compartmentalization, invariant chain and the TAP transporter system. *European Journal of Immunology*, *25*(12), 3402–3411. https://doi.org/10.1002/EJI.1830251230

Oxenius, A., Bachmann, M. F., Zinkernagel, R. M., & Hengartner, H. (1998). Virus-specific MHC class II-restricted TCR-transgenic mice: effects on humoral and cellular immune responses after viral infection. *European Journal of Immunology*, *Jan*(1), 390–400.

Oxenius, A., Fidler, S., Brady, M., Dawson, S. J., Ruth, K., Easterbrook, P. J., Weber, J. N., Phillips, R. E., & Price, D. A. (2001). Variable fate of virus-specific CD4 + T cells during primary HIV-1 infection. *Eur J Immunol.*, *12*, 3782–3788. https://doi.org/10.1002/1521-4141

Pais Ferreira, D., Silva, J. G., Wyss, T., Fuertes Marraco, S. A., Scarpellino, L., Charmoy, M., Maas, R., Siddiqui, I., Tang, L., Joyce, J. A., Delorenzi, M., Luther, S. A., Speiser, D. E., & Held, W. (2020). Central memory CD8 + T cells derive from stem-like Tcf7 hi effector cells in the absence of cytotoxic differentiation. *Immunity*, *53*(5), 985-1000.e11. https://doi.org/10.1016/J.IMMUNI.2020.09.005

Bibliography

Parish, I. A., Marshall, H. D., Staron, M. M., Lang, P. A., Brüstle, A., Chen, J. H., Cui, W., Tsui, Y. C., Perry, C., Laidlaw, B. J., Ohashi, P. S., Weaver, C. T., & Kaech, S. M. (2014). Chronic viral infection promotes sustained Th1-derived immunoregulatory IL-10 via BLIMP-1. *Journal of Clinical Investigation*, *124*(8), 3455–3468. https://doi.org/10.1172/JCI66108

Park, H., Li, Z., Yang, X. O., Chang, S. H., Nurieva, R., Wang, Y. H., Wang, Y., Hood, L., Zhu, Z., Tian, Q., & Dong, C. (2005). A distinct lineage of CD4 T cells regulates tissue inflammation by producing interleukin 17. *Nature Immunology*, *6*(11), 1133–1141. https://doi.org/10.1038/NI1261

Pei, W., Feyerabend, T. B., Rössler, J., Wang, X., Postrach, D., Busch, K., Rode, I., Klapproth, K., Dietlein, N., Quedenau, C., Chen, W., Sauer, S., Wolf, S., Höfer, T., & Rodewald, H. R. (2017). Polylox barcoding reveals haematopoietic stem cell fates realized in vivo. *Nature*, *548*(7668), 456–460. https://doi.org/10.1038/NATURE23653

Pepper, M., Pagán, A. J., Igyártó, B. Z., Taylor, J. J., & Jenkins, M. K. (2011). Opposing Signals from the Bcl6 Transcription Factor and the Interleukin-2 Receptor Generate T Helper 1 Central and Effector Memory Cells. *Immunity*, *35*(4), 583–595. https://doi.org/10.1016/J.IMMUNI.2011.09.009/ATTACHMENT/54C03EF3-9B6C-4D1B-AF19-CD5BFDA31675/MMC1.PDF

Plumlee, C. R., Sheridan, B. S., Cicek, B. B., & Lefrançois, L. (2013). Environmental Cues Dictate the Fate of Individual CD8+ T Cells Responding to Infection. *Immunity*, *39*(2), 347–356. https://doi.org/10.1016/J.IMMUNI.2013.07.014

Poltorak, M. P., Graef, P., Tschulik, C., Wagner, M., Cletiu, V., Dreher, S., Borjan, B., Fraessle, S. P., Effenberger, M., Turk, M., Busch, D. H., Plitzko, J., Kugler, D. G., Ragan, S., Schmidt, T., Stemberger, C., & Germeroth, L. (2020). Expamers: a new technology to control T cell activation. *Scientific Reports 2020 10:1*, *10*(1), 1–15. https://doi.org/10.1038/s41598-020-74595-8

Raziorrouh, B., Sacher, K., Tawar, R. G., Emmerich, F., Neumann-Haefelin, C., Baumert, T. F., Thimme, R., & Boettler, T. (2016). Virus-Specific CD4+ T Cells Have Functional and Phenotypic Characteristics of Follicular T-Helper Cells in Patients With Acute and Chronic HCV Infections. *Gastroenterology*, *150*(3), 696-706.e3. https://doi.org/10.1053/J.GASTRO.2015.11.005

Richard, A. C., Lun, A. T. L., Lau, W. W. Y., Göttgens, B., Marioni, J. C., & Griffiths, G. M. (2018). T cell cytolytic capacity is independent of initial stimulation strength. *Nature Immunology*, *19*(8), 849–858. https://doi.org/10.1038/S41590-018-0160-9

Rogner, U. C., & Avner, P. (2003). Congenic mice: cutting tools for complex immune disorders. *Nature Reviews Immunology 2003 3:3*, *3*(3), 243–252. https://doi.org/10.1038/nri1031

Rosette, C., Werlen, G., Daniels, M. A., Holman, P. O., Alam, S. M., Travers, P. J., Gascoigne, N. R. J., Palmer, E., & Jameson, S. C. (2001). The Impact of Duration versus Extent of TCR Occupancy on T Cell Activation: A Revision of the Kinetic Proofreading Model. *Immunity*, *15*(1), 59–70. https://doi.org/10.1016/S1074-7613(01)00173-X

Rosskopf, S., Leitner, J., Paster, W., Morton, L. T., Hagedoorn, R. S., Steinberger, P., & Heemskerk, M. H. M. (2018). A Jurkat 76 based triple parameter reporter system to evaluate TCR functions and adoptive T cell strategies. *Oncotarget*, *9*(25), 17608–17619. https://doi.org/10.18632/ONCOTARGET.24807

Ruterbusch, M., Pruner, K. B., Shehata, L., & Pepper, M. (2020). *In Vivo CD4 + T Cell Differentiation and Function: Revisiting the Th1/Th2 Paradigm*. https://doi.org/10.1146/annurev-immunol-103019

Sakaguchi, S., Sakaguchi, N., Asano, M., Itoh, M., & Toda, M. (1995). Immunologic self-tolerance maintained by activated T cells expressing IL-2 receptor alpha-chains (CD25). Breakdown of a single mechanism of self-tolerance causes various autoimmune diseases. *The Journal of Immunology*, *155*(3).

Salaman, M. R., & Gould, K. G. (2020). Breakdown of T-cell ignorance: The tolerance failure responsible for mainstream autoimmune diseases? *Journal of Translational Autoimmunity*, *3*, 100070. https://doi.org/10.1016/J.JTAUTO.2020.100070

Bibliography

Saravia, J., Chapman, N. M., & Chi, H. (2019). Helper T cell differentiation. *Cellular & Molecular Immunology 2019 16:7*, *16*(7), 634–643. https://doi.org/10.1038/s41423-019-0220-6

Savage, P. A., Boniface, J. J., & Davis, M. M. (1999). A kinetic basis for T cell receptor repertoire selection during an immune response. *Immunity*, *10*(4), 485–492. https://doi.org/10.1016/s1074-7613(00)80048-5

Schaerli, P., Willimann, K., Lang, A. B., Lipp, M., Loetscher, P., & Moser, B. (2000). Cxc Chemokine Receptor 5 Expression Defines Follicular Homing T Cells with B Cell Helper Function. *The Journal of Experimental Medicine*, *192*(11), 1553. https://doi.org/10.1084/JEM.192.11.1553

Schepers, K., Swart, E., van Heijst, J. W. J., Gerlach, C., Castrucci, M., Sie, D., Heimerikx, M., Velds, A., Kerkhoven, R. M., Arens, R., & Schumacher, T. N. M. (2008). Dissecting T cell lineage relationships by cellular barcoding. *Journal of Experimental Medicine*, *205*(10), 2309–2318. https://doi.org/10.1084/JEM.20072462

Schmitt, E. G., & Williams, C. B. (2013). Generation and function of induced regulatory T cells. *Frontiers in Immunology*, *4*(JUN), 152. https://doi.org/10.3389/FIMMU.2013.00152/BIBTEX

Schulze zur Wiesch, J., Ciuffreda, D., Lewis-Ximenez, L., Kasprowicz, V., Nolan, B. E., Streeck, H., Aneja, J., Reyor, L. L., Allen, T. M., Lohse, A. W., McGovern, B., Chung, R. T., Kwok, W. W., Kim, A. Y., & Lauer, G. M. (2012). Broadly directed virus-specific CD4+ T cell responses are primed during acute hepatitis C infection, but rapidly disappear from human blood with viral persistence. *The Journal of Experimental Medicine*, *209*(1), 61–75. https://doi.org/10.1084/JEM.20100388

Schwartz, R. H. (2003). T cell anergy. *Annual Review of Immunology*, *21*, 305–334. https://doi.org/10.1146/ANNUREV.IMMUNOL.21.120601.141110

Sheikh, A. A., & Groom, J. R. (2020). Transcription tipping points for T follicular helper cell and T-helper 1 cell fate commitment. *Cellular & Molecular Immunology 2020 18:3*, *18*(3), 528–538. https://doi.org/10.1038/s41423-020-00554-y

Snook, J. P., Kim, C., & Williams, M. A. (2018). TCR signal strength controls the differentiation of CD4+ effector and memory T cells. *Science Immunology*, *3*(25). https://doi.org/10.1126/SCIIMMUNOL.AAS9103

Spiotto, M. T., Yu, P., Rowley, D. A., Nishimura, M. I., Meredith, S. C., Gajewski, T. F., Fu, Y. X., & Schreiber, H. (2002). Increasing Tumor Antigen Expression Overcomes "Ignorance" to Solid Tumors via Crosspresentation by Bone Marrow-Derived Stromal Cells. *Immunity*, *17*(6), 737–747. https://doi.org/10.1016/S1074-7613(02)00480-6

Sprent, J., & Surh, C. D. (2003). T Cell Memory. *Https://Doi.Org/10.1146/Annurev.Immunol.20.100101.151926*, *20*, 551–579. https://doi.org/10.1146/ANNUREV.IMMUNOL.20.100101.151926

Stamm, A., Valentine, L., Potts, R., & Premenko-Lanier, M. (2012). An intermediate dose of LCMV clone 13 causes prolonged morbidity that is maintained by CD4+ T cells. *Virology*, *425*(2), 122. https://doi.org/10.1016/J.VIROL.2012.01.005

Stemberger, C., Huster, K. M., Koffler, M., Anderl, F., Schiemann, M., Wagner, H., & Busch, D. H. (2007). A Single Naive CD8+ T Cell Precursor Can Develop into Diverse Effector and Memory Subsets. *Immunity*, *27*(6), 985–997. https://doi.org/10.1016/J.IMMUNI.2007.10.012/ATTACHMENT/F6B328FB-71AE-4A68-8061-04A76CDD422F/MMC1.PDF

Sum, E., Rapp, M., Dürr, H., Mazumdar, A., Romero, P. J., Trumpfheller, C., & Umaña, P. (2022). The tumor-targeted CD40 agonist CEA-CD40 promotes T cell priming via a dual mode of action by increasing antigen delivery to dendritic cells and enhancing their activation. *Journal for Immunotherapy of Cancer*, *10*(3), 3264. https://doi.org/10.1136/JITC-2021-003264

Szabo, S. J., Kim, S. T., Costa, G. L., Zhang, X., Fathman, C. G., & Glimcher, L. H. (2000). A novel transcription factor, T-bet, directs Th1 lineage commitment. *Cell*, *100*(6), 655–669. https://doi.org/10.1016/S0092-8674(00)80702-3

Bibliography

Taniuchi, I. (2018). CD4 Helper and CD8 Cytotoxic T Cell Differentiation. *Annual Review of Immunology*, *36*, 579–601. https://doi.org/10.1146/ANNUREV-IMMUNOL-042617-053411

Tao, X., Grant, C., Constant, S., & Bottomly, K. (1997). Induction of IL-4-producing CD4+ T cells by antigenic peptides altered for TCR binding. *The Journal of Immunology*, *158*(9).

Tubo, N. J., Fife, B. T., Pagan, A. J., Kotov, D. I., Goldberg, M. F., & Jenkins, M. K. (2016). Most Microbe-specific Naïve CD4+ T Cells Produce Memory Cells During Infection. *Science (New York, N.Y.)*, *351*(6272), 511. https://doi.org/10.1126/SCIENCE.AAD0483

Tubo, N. J., & Jenkins, M. K. (2014). TCR signal quantity and quality in CD4+ T cell differentiation. *Trends in Immunology*, *35*(12), 591. https://doi.org/10.1016/J.IT.2014.09.008

Tubo, N. J., Pagán, A. J., Taylor, J. J., Nelson, R. W., Linehan, J. L., Ertelt, J. M., Huseby, E. S., Way, S. S., & Jenkins, M. K. (2013). Single Naive CD4+ T Cells from a Diverse Repertoire Produce Different Effector Cell Types during Infection. *Cell*, *153*(4), 785–796. https://doi.org/10.1016/J.CELL.2013.04.007

van Gassen, S., Callebaut, B., van Helden, M. J., Lambrecht, B. N., Demeester, P., Dhaene, T., & Saeys, Y. (2015). FlowSOM: Using self-organizing maps for visualization and interpretation of cytometry data. *Cytometry. Part A : The Journal of the International Society for Analytical Cytology*, *87*(7), 636–645. https://doi.org/10.1002/CYTO.A.22625

van Heijst, J. W. J., Gerlach, C., Swart, E., Sie, D., Nunes-Alves, C., Kerkhoven, R. M., Arens, R., Correia-Neves, M., Schepers, K., & Schumacher, T. N. M. (2009). Recruitment of antigen-specific cd8+ t cells in response to infection is markedly efficient. *Science*, *325*(5945), 1265–1269. https://doi.org/10.1126/SCIENCE.1175455/SUPPL_FILE/VANHEIJST.SOM.PDF

van Panhuys, N. (2016). TCR signal strength alters T-DC activation and interaction times and directs the outcome of differentiation. *Frontiers in Immunology*, *7*(JAN), 6. https://doi.org/10.3389/FIMMU.2016.00006/BIBTEX

Vella, L. A., Herati, R. S., & Wherry, E. J. (2017). CD4+ T Cell Differentiation in Chronic Viral Infections: The Tfh Perspective. *Trends in Molecular Medicine*, *23*(12), 1072–1087. https://doi.org/10.1016/J.MOLMED.2017.10.001

Viganò, S., Utzschneider, D. T., Perreau, M., Pantaleo, G., Zehn, D., & Harari, A. (2012). Functional Avidity: A Measure to Predict the Efficacy of Effector T Cells? *Clinical and Developmental Immunology*, *2012*, 14. https://doi.org/10.1155/2012/153863

Vignali, D. A. A., Collison, L. W., & Workman, C. J. (2008). How regulatory T cells work. *Nature Reviews Immunology 2008 8:7*, *8*(7), 523–532. https://doi.org/10.1038/nri2343

Vinuesa, C. G., Linterman, M. A., Yu, D., & Maclennan, I. C. M. (2016). *Follicular Helper T Cells*. https://doi.org/10.1146/annurev-immunol-041015-055605

Weiskopf, D., Bangs, D. J., Sidney, J., Kolla, R. v., de Silva, A. D., de Silva, A. M., Crotty, S., Peters, B., & Sette, A. (2015). Dengue virus infection elicits highly polarized CX3CR1+ cytotoxic CD4+ T cells associated with protective immunity. *Proceedings of the National Academy of Sciences of the United States of America*, *112*(31), E4256–E4263. https://doi.org/10.1073/PNAS.1505956112

Welsh, R. M., & Seedhom, M. O. (2008). LCMV: Propagation, quantitation, and storage. *Current Protocols in Microbiology*, *CHAPTER*(SUPPL. 8), Unit. https://doi.org/10.1002/9780471729259.MC15A01S8

Wherry, E. J., Puorro, K. A., Porgador, A., & Eisenlohr, L. C. (1999). High Levels of Epitope Are Attained Responses Rise Steadily Until Excessively Function of Increasing Epitope Expression: The Induction of Virus-Specific CTL as a. *J Immunol* , *3735*, 3735–3745. http://www.jimmunol.org/content/163/7/http://www.jimmunol.org/content/163/7/3735.full#ref-list-1

Wieczorek, M., Abualrous, E. T., Sticht, J., Álvaro-Benito, M., Stolzenberg, S., Noé, F., & Freund, C. (2017). Major histocompatibility complex (MHC) class I and MHC class II proteins: Conformational plasticity in antigen presentation. *Frontiers in Immunology*, *8*(MAR), 292. https://doi.org/10.3389/FIMMU.2017.00292/BIBTEX

Williams, L. M., & Rudensky, A. Y. (2007). Maintenance of the Foxp3-dependent developmental program in mature regulatory T cells requires continued expression of Foxp3. *Nature Immunology 2007 8:3*, *8*(3), 277–284. https://doi.org/10.1038/ni1437

Wolf, F. A., Angerer, P., & Theis, F. J. (2018). SCANPY: Large-scale single-cell gene expression data analysis. *Genome Biology*, *19*(1), 1–5. https://doi.org/10.1186/S13059-017-1382-0/FIGURES/1

Wooldridge, L., van den Berg, H. A., Glick, M., Gostick, E., Laugel, B., Hutchinson, S. L., Milicic, A., Brenchley, J. M., Douek, D. C., Price, D. A., & Sewell, A. K. (2005). Interaction between the CD8 coreceptor and major histocompatibility complex class I stabilizes T cell receptor-antigen complexes at the cell surface. *The Journal of Biological Chemistry*, *280*(30), 27491–27501. https://doi.org/10.1074/JBC.M500555200

Woronicz, J. D., Calnan, B., Ngo, V., & Winoto, A. (1994). Requirement for the orphan steroid receptor Nur77 in apoptosis of T-cell hybridomas. *Nature*, *367*(6460), 277–281. https://doi.org/10.1038/367277A0

Zehn, D., Lee, S. Y., & Bevan, M. J. (2009). Complete but curtailed T-cell response to very low-affinity antigen. *Nature 2009 458:7235*, *458*(7235), 211–214. https://doi.org/10.1038/nature07657

Zhou, X., Ramachandran, S., Mann, M., & Popkin, D. L. (2012). Role of Lymphocytic Choriomeningitis Virus (LCMV) in Understanding Viral Immunology: Past, Present and Future. *Viruses*, *4*(11), 2650. https://doi.org/10.3390/V4112650

Zhu, X., & Zhu, J. (2020). CD4 T Helper Cell Subsets and Related Human Immunological Disorders. *International Journal of Molecular Sciences 2020, Vol. 21, Page 8011*, *21*(21), 8011. https://doi.org/10.3390/IJMS21218011

8 Acknowledgement

This thesis would not have been possible without the enormous support from many people. I would first like to thank my supervisors, Veit Buchholz and Simon Graßmann, for creating an inspiring scientific environment to thrive in. The many discussions, suggestions, and their support were a major contribution to the success of this work. In this regard, I would also like to thank Lorenz Kretschmer for his mentoring, vast support, and supervision of the recruitment project. Furthermore, I would like to thank Dietmar Zehn and Dirk Busch for the scientific discussions, their interest in my projects, and their role as supervisors and mentors of my thesis.

I would also like to express my gratitude towards my collaborators and their contributions to this work. I want to thank all Buchholz and Busch group members for their continuous support. Especially, my gratitude goes to, Simon Graßmann, Sophie Flommersfeld, Sebastian Jarosch, Inge Hensel, Tomas Müller, Fabian Mohr, Anton Mühlbauer, Julian Hönninger, Immanuel Andrä, Lorenz Kretschmer and Ludwig Pachmayer for their friendship and the special moments we shared in the last years. Furthermore, I would like to thank Thomas Müller, Kilian Schober, and Fabian Mohr for their expertise and support in the isolation of TCRs. Additionally, I want to express my gratitude to Sebastian Jarosch, Monika Hammel, and Anton Mühlbauer for their support and contributions to the sequencing experiments. Moreover, I want to thank the sorting facility and especially Immanuel Andrä for their support of the extensive cell sorting and speed enrichment experiments. Finally, I want to thank the students and apprentices that have contributed to these research projects, especially Madleen Biggel, Rosalie Amanze, Barzan Sarhan, Lisa-Marie Lippert and Franziska Graml.

Last but not least, my deepest gratitude goes to my fiancée and my family for their unconditional love and never-ending support. Without you, I would not be where I am today.

9 Attachments

Attached are the sequences of the isolated TCRs and their expression constructs. Lowercase letters encompass sequences added for cloning and the Kozak sequence. Uppercase letters denote the coding sequences. The constructs start with the TCR beta chain followed by a P2A element (bold) and the TCR alpha chain.

9.1 TCR 1

5'-
attagcggccgcgccaccATGGGCTCCAGACTCTTCTTTGTGGTTTTGATTCTCCTGTGTGCAAA
ACACATGGAGGCTGCAGTCACCCAAAGTCCAAGAAGCAAGGTGGCAGTAACAGGAGGA
AAGGTGACATTGAGCTGTCACCAGACTAATAACCATGACTATATGTACTGGTATCGGCA
GGACACGGGGCATGGGCTGAGGCTGATCCATTACTCATATGTCGCTGACAGCACGGAG
AAAGGAGATATCCCTGATGGGTACAAGGCCTCCAGACCAAGCCAAGAGAATTTCTCTCT
CATTCTGGAGTTGGCTTCCCTTTCTCAGACAGCTGTATATTTCTGTGCCAGCAGTGACC
GGGGACCCAACGAAAGATTATTTTTCGGTCATGGAACCAAGCTGTCTGTCCTGGAGGAT
CTGAGAAATGTGACTCCACCCAAGGTCTCCTTGTTTGAGCCATCAAAAGCAGAGATTGC
AAACAAACAAAAGGCTACCCTCGTGTGCTTGGCCAGGGGCTTCTTCCCTGACCACGTG
GAGCTGAGCTGGTGGGTGAATGGCAAGGAGGTCCACAGTGGGGTCAGCACGGACCCT
CAGGCCTACAAGGAGAGCAATTATAGCTACTGCCTGAGCAGCCGCCTGAGGGTCTCTG
CTACCTTCTGGCACAATCCTCGCAACCACTTCCGCTGCCAAGTGCAGTTCCATGGGCTT
TCAGAGGAGGACAAGTGGCCAGAGGGCTCACCCAAACCTGTCACACAGAACATCAGTG
CAGAGGCCTGGGGCCGAGCAGACTGTGGGATTACCTCAGCATCCTATCAACAAGGGGT
CTTGTCTGCCACCATCCTCTATGAGATCCTGCTAGGGAAAGCCACCCTGTATGCTGTGC
TTGTCAGTACACTGGTGGTGATGGCTATGGTAAGGAACAGG**GGCAGCGGCGCCACCA**
ACTTCAGCCTGCTGAAGCAGGCCGGCGACGTGGAAGAGAACCCCGGGCCCATGGAC
AAGATCCTGACAGCATCGTTTTTACTTCTAGGCCTTCACCTAGCTGGGGTGAGTGGCCA
GCAGGAGAAACGTGACCAGCAGCAGGTGAGACAAAGTCCCCAATCTCTGACAGTCTGG
GAAGGAGAGACCGCAATTCTGAACTGCAGTTATGAGAACAGTGCTTTTGACTACTTCCC
ATGGTACCAGCAGTTCCCTGGGGAAGGTCCCGCTCTCCTGATATCCATACTTTCAGTGT
CCGATAAAAAGGAAGATGGACGATTCACAATCTTCTTCAATAAAAGGGAGAAAAAGCTC
TCCTTGCACATTGCAGACTCTCAGCCTGGAGACTCAGCCACCTACTTCTGTGCAGCAGC
CAATAACTATGCCCAGGGATTAACCTTCGGTCTTGGCACCAGAGTATCTGTGTTTCCCT
ACATCCAGAACCCAGAACCTGCTGTGTACCAGTTAAAAGATCCTCGGTCTCAGGACAGC
ACCCTCTGCCTGTTCACCGACTTTGACTCCCAAATCAATGTGCCGAAAACCATGGAATC
TGGAACGTTCATCACTGACAAAACTGTGCTGGACATGAAAGCTATGGATTCCAAGAGCA
ATGGGGCCATTGCCTGGAGCAACCAGACAAGCTTCACCTGCCAAGATATCTTCAAAGAG
ACCAACGCCACCTACCCCAGTTCAGACGTTCCCTGTGATGCCACGTTGACTGAGAAAAG
CTTTGAAACAGATATGAACCTAAACTTTCAAAACCTGTCAGTTATGGGACTCCGAATCCT
CCTGCTGAAAGTAGCCGGATTTAACCTGCTCATGACGCTGAGGCTGTGGTCCAGTTGAg
aattcatta
-3'

9.2 TCR 5

5’-
attagcggccgcgccaccATGGGCTCCAGGCTCTTCTTCGTGCTCTCCAGTCTCCTGTGTTCAA
AACACATGGAGGCTGCAGTCACCCAAAGCCCAAGAAACAAGGTGGCAGTAACAGGAGG
AAAGGTGACATTGAGCTGTAATCAGACTAATAACCACAACAACATGTACTGGTATCGGC
AGGACACGGGGCATGGGCTGAGGCTGATCCATTATTCATATGGTGCTGGCAGCACTGA
GAAAGGAGATATCCCTGATGGATACAAGGCCTCCAGACCAAGCCAAGAGAACTTCTCC
CTCATTCTGGAGTTGGCTACCCCCTCTCAGACATCAGTGTACTTCTGTGCCAGCGGTGA
TGCTGGGGGGGCGGACCAAGACACCCAGTACTTTGGGCCAGGCACTCGGCTCCTCGT
GTTAGAGGATCTGAGAAATGTGACTCCACCCAAGGTCTCCTTGTTTGAGCCATCAAAAG
CAGAGATTGCAAACAAACAAAAGGCTACCCTCGTGTGCTTGGCCAGGGGCTTCTTCCCT
GACCACGTGGAGCTGAGCTGGTGGGTGAATGGCAAGGAGGTCCACAGTGGGGTCAGC
ACGGACCCTCAGGCCTACAAGGAGAGCAATTATAGCTACTGCCTGAGCAGCCGCCTGA
GGGTCTCTGCTACCTTCTGGCACAATCCTCGCAACCACTTCCGCTGCCAAGTGCAGTTC
CATGGGCTTTCAGAGGAGGACAAGTGGCCAGAGGGCTCACCCAAACCTGTCACACAGA
ACATCAGTGCAGAGGCCTGGGGCCGAGCAGACTGTGGGATTACCTCAGCATCCTATCA
ACAAGGGGTCTTGTCTGCCACCATCCTCTATGAGATCCTGCTAGGGAAAGCCACCCTGT
ATGCTGTGCTTGTCAGTACACTGGTGGTGATGGCTATGGTAAGGAACAGG**GGCAGCGG**
CGCCACCAACTTCAGCCTGCTGAAGCAGGCCGGCGACGTGGAAGAGAACCCCGGGC
CCATGCTCCTGGCGCTCCTCCCAGTGCTGGGGATACACTTTGTCCTGAGAGATGCCCA
AGCTCAGTCAGTGACACAGCCCGATGCTCGCGTCACTGTCTCTGAAGGAGCCTCTCTG
CAGCTGAGATGCAAGTATTCCTACTCTGCGACACCTTATCTGTTCTGGTATGTCCAGTAC
CCGCGGCAGGGGCTGCAGCTGCTCCTCAAGTACTATTCAGGAGACCCAGTGGTTCAAG
GAGTGAACAGCTTCGAGGCTGAGTTCAGCAAGAGTAACTCTTCCTTCCACCTGCAGAAA
GCCTCTGTGCACTGGAGCGACTCGGCTGTGTACTTCTGTGCTCTGAGTTCTGGGACTTA
CCAGAGGTTTGGAACTGGGACAAAACTCCAAGTCGTTCCAAACATCCAGAACCCAGAAC
CTGCTGTGTACCAGTTAAAAGATCCTCGGTCTCAGGACAGCACCCTCTGCCTGTTCACC
GACTTTGACTCCCAAATCAATGTGCCGAAAACCATGGAATCTGGAACGTTCATCACTGA
CAAAACTGTGCTGGACATGAAAGCTATGGATTCCAAGAGCAATGGGGCCATTGCCTGG
AGCAACCAGACAAGCTTCACCTGCCAAGATATCTTCAAAGAGACCAACGCCACCTACCC
CAGTTCAGACGTTCCCTGTGATGCCACGTTGACTGAGAAAAGCTTTGAAACAGATATGA
ACCTAAACTTTCAAAACCTGTCAGTTATGGGACTCCGAATCCTCCTGCTGAAAGTAGCC
GGATTTAACCTGCTCATGACGCTGAGGCTGTGGTCCAGTTGAgaattcatta

-3’

9.3 TCR 9

5’-
attagcggccgcgccaccATGAGAGTTAGGCTCATCTCTGCTGTGGTGCTGTGTTTCCTAGGAA
CAGGCCTTGTGGACATGAAAGTAACCCAGATGCCAAGATACCTGATCAAAAGAATGGGA
GAGAATGTTTTGCTGGAATGTGGACAGGACATGAGCCATGAAACAATGTACTGGTATCG
ACAAGACCCTGGTCTGGGGCTACAGCTGATTTATATCTCATACGATGTTGATAGTAACA
GCGAAGGAGACATCCCTAAAGGATACAGGGTCTCACGGAAGAAGCGGGAGCATTTCTC
CCTGATTCTGGATTCTGCTAAAACAAACCAGACATCTGTGTACTTCTGTGCTAGCAGTTT
AGCTGGGGGGGCGTCAGAAACGCTGTATTTTGGCTCAGGAACCAGACTGACTGTTCTC
GAGGATCTGAGAAATGTGACTCCACCCAAGGTCTCCTTGTTTGAGCCATCAAAAGCAGA
GATTGCAAACAAACAAAAGGCTACCCTCGTGTGCTTGGCCAGGGGCTTCTTCCCTGACC
ACGTGGAGCTGAGCTGGTGGGTGAATGGCAAGGAGGTCCACAGTGGGGTCAGCACGG
ACCCTCAGGCCTACAAGGAGAGCAATTATAGCTACTGCCTGAGCAGCCGCCTGAGGGT
CTCTGCTACCTTCTGGCACAATCCTCGCAACCACTTCCGCTGCCAAGTGCAGTTCCATG
GGCTTTCAGAGGAGGACAAGTGGCCAGAGGGCTCACCCAAACCTGTCACACAGAACAT
CAGTGCAGAGGCCTGGGGCCGAGCAGACTGTGGGATTACCTCAGCATCCTATCAACAA
GGGGTCTTGTCTGCCACCATCCTCTATGAGATCCTGCTAGGGAAAGCCACCCTGTATGC
TGTGCTTGTCAGTACACTGGTGGTGATGGCTATGGTAAGGAACAGG**GGCAGCGGCGCC**
ACCAACTTCAGCCTGCTGAAGCAGGCCGGCGACGTGGAAGAGAACCCCGGGCCCAT
GGACAAGATCCTGACAGCATTGTTTTTACTTCTAGGTCTTCACCTAGCTGGGGTGAGTG
GCCAGCAGGAGAAACATGACCAGCAGCAGGTGAGACAAAGTTCCCAATCTCTGACAGT
CTGGGAAGGAGAGACCGCAATTCTGAACTGCAGTTATGAGAACAGTGCTTTTGACTACT
TCCCATGGTACCAGCAGTTCCCTGGGGAAGGCCCTGCTCTCCTGATAGCCATACGTTC
AGTGTCCGATAAAAAGGAAGATGGACGATTCACAATCTTCTTCAATAAAAGGGAGAAAA
ATCTCTCCTTGCACATCAAAGACTCTCAGCCTGGAGACTCAGCCACCTACTTCTGTGCA
GCAAGTTCCGGAGGCTATAAAGTGGTCTTTGGAAGTGGGACTCGATTGCTGGTAAGCC
CTGACATCCAGAACCCAGAACCTGCTGTGTACCAGTTAAAAGATCCTCGGTCTCAGGAC
AGCACCCTCTGCCTGTTCACCGACTTTGACTCCCAAATCAATGTGCCGAAAACCATGGA
ATCTGGAACGTTCATCACTGACAAAACTGTGCTGGACATGAAAGCTATGGATTCCAAGA
GCAATGGGGCCATTGCCTGGAGCAACCAGACAAGCTTCACCTGCCAAGATATCTTCAAA
GAGACCAACGCCACCTACCCCAGTTCAGACGTTCCCTGTGATGCCACGTTGACTGAGA
AAAGCTTTGAAACAGATATGAACCTAAACTTTCAAAACCTGTCAGTTATGGGACTCCGAA
TCCTCCTGCTGAAAGTAGCCGGATTTAACCTGCTCATGACGCTGAGGCTGTGGTCCAGT
TGAgaattcatta

-3’

9.4 TCR 11

5’-
attagcggccgcgccaccATGGGCTCCAGGCTCTTCTTCGTGCTCTCCAGTCTCCTGTGTTCAA
AACACATGGAGGCTGCAGTCACCCAAAGCCCAAGAAACAAGGTGGCAGTAACAGGAGG
AAAGGTGACATTGAGCTGTAATCAGACTAATAACCACAACAACATGTACTGGTATCGGC
AGGACACGGGGCATGGGCTGAGGCTGATCCATTATTCATATGGTGCTGGCAGCACTGA
GAAAGGAGATATCCCTGATGGATACAAGGCCTCCAGACCAAGCCAAGAGAACTTCTCC
CTCATTCTGGAGTTGGCTACCCCCTCTCAGACATCAGTGTACTTCTGTGCCAGCGGTGA
TCTGGGGGGGGTTAACCAAGACACCCAGTACTTTGGGCCAGGCACTCGGCTCCTCGTG
TTAGAGGATCTGAGAAATGTGACTCCACCCAAGGTCTCCTTGTTTGAGCCATCAAAAGC
AGAGATTGCAAACAAACAAAAGGCTACCCTCGTGTGCTTGGCCAGGGGCTTCTTCCCTG
ACCACGTGGAGCTGAGCTGGTGGGTGAATGGCAAGGAGGTCCACAGTGGGGTCAGCA
CGGACCCTCAGGCCTACAAGGAGAGCAATTATAGCTACTGCCTGAGCAGCCGCCTGAG
GGTCTCTGCTACCTTCTGGCACAATCCTCGCAACCACTTCCGCTGCCAAGTGCAGTTCC
ATGGGCTTTCAGAGGAGGACAAGTGGCCAGAGGGCTCACCCAAACCTGTCACACAGAA
CATCAGTGCAGAGGCCTGGGGCCGAGCAGACTGTGGGATTACCTCAGCATCCTATCAA
CAAGGGGTCTTGTCTGCCACCATCCTCTATGAGATCCTGCTAGGGAAAGCCACCCTGTA
TGCTGTGCTTGTCAGTACACTGGTGGTGATGGCTATGGTAAGGAACAGG**GGCAGCGGC**
GCCACCAACTTCAGCCTGCTGAAGCAGGCCGGCGACGTGGAAGAGAACCCCGGGCC
CATGCTCCTGGCGCTCCTCCCAGTGCTGGGGATACACTTTGTCCTGAGAGATGCCCAA
GCTCAGTCAGTGACACAGCCCGATGCTCGCGTCACTGTCTCTGAAGGAGCCTCTCTGC
AGCTGAGATGCAAGTATTCCTACTCTGCGACACCTTATCTGTTCTGGTATGTCCAGTACC
CGCGGCAGGGGCTGCAGCTGCTCCTCAAGTACTATTCAGGAGACCCAGTGGTTCAAGG
AGTGAACAGCTTCGAGGCTGAGTTCAGCAAGAGTAACTCTTCCTTCCACCTGCAGAAAG
CCTCTGTGCACTGGAGCGACTCGGCTGTGTACTTCTGTGCTCTGAGCACTGGGACTTA
CCAGAGGTTTGGAACTGGGACAAAACTCCAAGTCGTTCCAAACATCCAGAACCCAGAAC
CTGCTGTGTACCAGTTAAAAGATCCTCGGTCTCAGGACAGCACCCTCTGCCTGTTCACC
GACTTTGACTCCCAAATCAATGTGCCGAAAACCATGGAATCTGGAACGTTCATCACTGA
CAAAACTGTGCTGGACATGAAAGCTATGGATTCCAAGAGCAATGGGGCCATTGCCTGG
AGCAACCAGACAAGCTTCACCTGCCAAGATATCTTCAAAGAGACCAACGCCACCTACCC
CAGTTCAGACGTTCCCTGTGATGCCACGTTGACTGAGAAAAGCTTTGAAACAGATATGA
ACCTAAACTTTCAAAACCTGTCAGTTATGGGACTCCGAATCCTCCTGCTGAAAGTAGCC
GGATTTAACCTGCTCATGACGCTGAGGCTGTGGTCCAGTTGAgaattcatta
-3’

9.5 TCR 14

5’-
attagcggccgcgccaccATGGGCTCCAGACTCTTCTTTGTGGTTTTGATTCTCCTGTGTGCAAA
ACACATGGAGGCTGCAGTCACCCAAAGTCCAAGAAGCAAGGTGGCAGTAACAGGAGGA
AAGGTGACATTGAGCTGTCACCAGACTAATAACCATGACTATATGTACTGGTATCGGCA
GGACACGGGGCATGGGCTGAGGCTGATCCATTACTCATATGTCGCTGACAGCACGGAG
AAAGGAGATATCCCTGATGGGTACAAGGCCTCCAGACCAAGCCAAGAGAATTTCTCTCT
CATTCTGGAGTTGGCTTCCCTTTCTCAGACAGCTGTATATTTCTGTGCCAGCAGTGGGG
AGAACGAAAGATTATTTTTCGGTCATGGAACCAAGCTGTCTGTCCTGGAGGATCTGAGA
AATGTGACTCCACCCAAGGTCTCCTTGTTTGAGCCATCAAAAGCAGAGATTGCAAACAA
ACAAAAGGCTACCCTCGTGTGCTTGGCCAGGGGCTTCTTCCCTGACCACGTGGAGCTG
AGCTGGTGGGTGAATGGCAAGGAGGTCCACAGTGGGGTCAGCACGGACCCTCAGGCC
TACAAGGAGAGCAATTATAGCTACTGCCTGAGCAGCCGCCTGAGGGTCTCTGCTACCTT
CTGGCACAATCCTCGCAACCACTTCCGCTGCCAAGTGCAGTTCCATGGGCTTTCAGAG
GAGGACAAGTGGCCAGAGGGCTCACCCAAACCTGTCACACAGAACATCAGTGCAGAGG
CCTGGGGCCGAGCAGACTGTGGGATTACCTCAGCATCCTATCAACAAGGGGTCTTGTC
TGCCACCATCCTCTATGAGATCCTGCTAGGGAAAGCCACCCTGTATGCTGTGCTTGTCA
GTACACTGGTGGTGATGGCTATGGTAAGGAACAGG**GGCAGCGGCGCCACCAACTTCA**
GCCTGCTGAAGCAGGCCGGCGACGTGGAAGAGAACCCCGGGCCCATGGACAAGATC
CTGACAGCATTGTTTTTACTTCTAGGTCTTCACCTAGCTGGGGTGAGTGGCCAGCAGGA
GAAACATGACCAGCAGCAGGTGAGACAAAGTTCCCAATCTCTGACAGTCTGGGAAGGA
GAGACCGCAATTCTGAACTGCAGTTATGAGAACAGTGCTTTTGACTACTTCCCATGGTA
CCAGCAGTTCCCTGGGGAAGGCCCTGCTCTCCTGATAGCCATACGTTCAGTGTCCGAT
AAAAAGGAAGATGGACGATTCACAATCTTCTTCAATAAAAGGGAGAAAAATCTCTCCTTG
CACATCAAAGACTCTCAGCCTGGAGACTCAGCCACCTACTTCTGTGCAGCAAGTTTCGG
TAACAACAATGCCCCACGATTTGGAGCGGGAACCAAATTATCAGTAAAACCAAACATCC
AGAACCCAGAACCTGCTGTGTACCAGTTAAAAGATCCTCGGTCTCAGGACAGCACCCTC
TGCCTGTTCACCGACTTTGACTCCCAAATCAATGTGCCGAAAACCATGGAATCTGGAAC
GTTCATCACTGACAAAACTGTGCTGGACATGAAAGCTATGGATTCCAAGAGCAATGGGG
CCATTGCCTGGAGCAACCAGACAAGCTTCACCTGCCAAGATATCTTCAAAGAGACCAAC
GCCACCTACCCCAGTTCAGACGTTCCCTGTGATGCCACGTTGACTGAGAAAAGCTTTGA
AACAGATATGAACCTAAACTTTCAAAACCTGTCAGTTATGGGACTCCGAATCCTCCTGCT
GAAAGTAGCCGGATTTAACCTGCTCATGACGCTGAGGCTGTGGTCCAGTTGAgaattcatta
-3’

9.6 TCR 15

5’-
attagcggccgcgccaccATGGGCTCCAGACTCTTCTTTGTGGTTTTGATTCTCCTGTGTGCAAA
ACACATGGAGGCTGCAGTCACCCAAAGTCCAAGAAGCAAGGTGGCAGTAACAGGAGGA
AAGGTGACATTGAGCTGTCACCAGACTAATAACCATGACTATATGTACTGGTATCGGCA
GGACACGGGGCATGGGCTGAGGCTGATCCATTACTCATATGTCGCTGACAGCACGGAG
AAAGGAGATATCCCTGATGGGTACAAGGCCTCCAGACCAAGCCAAGAGAATTTCTCTCT
CATTCTGGAGTTGGCTTCCCTTTCTCAGACAGCTGTATATTTCTGTGCCAGCAGTGACC
ACCAAGACACCCAGTACTTTGGGCCAGGCACTCGGCTCCTCGTGTTAGAGGATCTGAG
AAATGTGACTCCACCCAAGGTCTCCTTGTTTGAGCCATCAAAAGCAGAGATTGCAAACA
AACAAAAGGCTACCCTCGTGTGCTTGGCCAGGGGCTTCTTCCCTGACCACGTGGAGCT
GAGCTGGTGGGTGAATGGCAAGGAGGTCCACAGTGGGGTCAGCACGGACCCTCAGGC
CTACAAGGAGAGCAATTATAGCTACTGCCTGAGCAGCCGCCTGAGGGTCTCTGCTACC
TTCTGGCACAATCCTCGCAACCACTTCCGCTGCCAAGTGCAGTTCCATGGGCTTTCAGA
GGAGGACAAGTGGCCAGAGGGCTCACCCAAACCTGTCACACAGAACATCAGTGCAGAG
GCCTGGGGCCGAGCAGACTGTGGGATTACCTCAGCATCCTATCAACAAGGGGTCTTGT
CTGCCACCATCCTCTATGAGATCCTGCTAGGGAAAGCCACCCTGTATGCTGTGCTTGTC
AGTACACTGGTGGTGATGGCTATGGTAAGGAACAGG**GGCAGCGGCGCCACCAACTTC**
AGCCTGCTGAAGCAGGCCGGCGACGTGGAAGAGAACCCCGGGCCCATGGACAAGAT
CCTGACAGCATCGTTTTTACTCCTAGGCCTTCACCTAGCTGGGGTGAGTGGCCAGCAG
CAGGAGAAACATGACCAGCAGCAGGTGAGACAAAGTCCCCAATCTCTGACAGTCTGGG
AAGGAGAGACAGCAATTCTGAACTGCAGTTATGAGGACAGCACTTTTGACTACTTCCCA
TGGTACCATCAGTTCCCTGGGGAAAGCCCTGCACTCCTGATAGCCATACGTCCAGTGTC
CAATAAAAAGGAAGATGGACGATTCACAATCTTCTTCAATAAAAGGGAGAAAAAGTTCTC
CTTGCACATCGCAGACTCTCAGCCTGGAGACTCAGCCACCTACTTCTGTGCAGCAAGTG
GAAACAACAATGCCCCACGATTTGGAGCGGGAACCAAATTATCAGTAAAACCAAACATC
CAGAACCCAGAACCTGCTGTGTACCAGTTAAAAGATCCTCGGTCTCAGGACAGCACCCT
CTGCCTGTTCACCGACTTTGACTCCCAAATCAATGTGCCGAAAACCATGGAATCTGGAA
CGTTCATCACTGACAAAACTGTGCTGGACATGAAAGCTATGGATTCCAAGAGCAATGGG
GCCATTGCCTGGAGCAACCAGACAAGCTTCACCTGCCAAGATATCTTCAAAGAGACCAA
CGCCACCTACCCCAGTTCAGACGTTCCCTGTGATGCCACGTTGACTGAGAAAAGCTTTG
AAACAGATATGAACCTAAACTTTCAAAACCTGTCAGTTATGGGACTCCGAATCCTCCTGC
TGAAAGTAGCCGGATTTAACCTGCTCATGACGCTGAGGCTGTGGTCCAGTTGAgaattcatt
a
-3’